

Connectivity motifs underlying neuronal computations in the adult OB

**Inauguraldissertation
zur Erlangung der Doktorwürde
vorgelegt der
Philosophisch-Naturwissenschaftlichen Fakultät
der Universität Basel
von**

Presented by

Tafheem Ahmad Masudi

From

Srinagar, India

Basel, 2016

Originaldokument gespeichert auf dem Dokumentenserver der Universität Basel
edoc.unibas.ch

Genehmigt von der Philosophisch-Naturwissenschaftlichen Fakultät auf

Antrag von:

Prof. Rainer W. Friedrich, FMI

(Dissertationsleiter und Fakultätsverantwortlicher)

Prof. Peter Scheiffele, Biozentrum

Basel

22.03.2016

The work presented in this thesis was carried out at the Friedrich Miescher Institute for Biomedical Research, Basel, Switzerland, under the supervision and in the laboratory of Prof. Rainer W. Friedrich. The results of this study will be published soon.

Acknowledgements

I would like to thank Prof. Rainer Friedrich for providing me the opportunity to work in his laboratory and also to all members of the Friedrich group for their constant support. To name a few, Adrian Wanner for his support throughout the project and valuable help during data acquisition. Peter Rupprecht, Anastasios Moressis, Gilad Jacobson, Lea Siksou, Iori Namekawa, Nila Moenig and Chie Satou for their valuable suggestions, both professionally and personally. Also thanks to Martin Naegeli and Estelle Arn for maintaining the fish facility and lab requirements.

Thank you to Prof. Filippo Rijli and Prof. Peter Scheiffele for taking part in my thesis committee and for all those valuable inputs, which shaped the project in the right direction. Again special thanks to Prof. Rainer Friedrich for giving me the opportunity to study projects related to olfactory bulb functionality and connectivity in his laboratory of which I had no prior experience.

Sincere thanks to Prof. K VijayRagavan and Dr. Ajeet Singh, who gave strong support to my application of FMI, and who continue to provide valuable guidance.

Many thanks to all the colleagues at FMI especially 4th floor neurobiologists. I would have not been able to enjoy so much of the stimulating environment, excellent research, and fantastic scientific discussions and company.

Many thanks to the Basel cricket club for a lot of fun during my PhD years in Basel.

Last but not the least, shukriya to my family for their dua, restless support and belief.

Contents

| | |
|---------------|---|
| Abbreviations | 6 |
| Abstract | 7 |
| Figures | 8 |

Introduction

| | |
|--|----|
| 1.1 The olfactory system and information processing | 10 |
| 1.2 Detailed architecture of the olfactory system | 12 |
| 1.3 Direct vs. indirect sensory input to mitral cells | 17 |
| 1.4 Reciprocal connectivity in the olfactory bulb | 19 |
| 1.5 Computational consequences of reciprocal connectivity | 22 |
| 1.6 State of the art in 3D EM for dense circuit reconstruction | 26 |
| 1.7 Zebrafish as a vertebrate model organism | 27 |
| 1.8 Aim of this study | 28 |

Methods

| | |
|--|----|
| 2.1 Zebrafish adult brain explant preparation | 30 |
| 2.2 Two photon calcium imaging and odor stimulation | 30 |
| 2.3 Staining tissue for electron microscopy | 32 |
| 2.4 Tissue preparation for serial block face electron microscopy | 34 |
| 2.5 Serial block face 3D electron microscope | 35 |
| 2.6 Image processing | 37 |
| 2.7 Neuronal skeleton tracing and synapse detection | 38 |

Results

| | |
|---|----|
| 3.1 Measuring granule cell sparseness in OB by two-photon imaging | 40 |
| 3.2 A small scale study to explore SBEM methods | 43 |
| 3.3 Large scale detailed SBEM imaging of adult olfactory bulb | 46 |
| 3.4 Detailed analysis from the adult olfactory bulb SBEM dataset | 49 |
| 3.5 Reconstruction of mitral cells in olfactory bulb | 58 |
| 3.6 Synapse identification and labelling | 62 |

Discussion

| | |
|---|----|
| 4.1 Reconstruction of neurons and synapses in volumetric EM data | 73 |
| 4.2 Mitral cells receive direct input from olfactory sensory axons | 73 |
| 4.3 Two photon calcium imaging reveals dense granule cell responses | 75 |
| 4.4 Reciprocal synapses show weak compartmentalization | 75 |
| 4.5 Reciprocal connectivity induces variance balancing | 76 |
| 4.6 Limitations of the study and outlook | 77 |

| | |
|------------|----|
| References | 81 |
|------------|----|

Abbreviations

| | |
|------------|--|
| ACSF | Artificial cerebrospinal fluid |
| ET: | External tufted cell |
| GC: | Granule cell |
| GCL: | Granule cell layer |
| GL: | Glomerular layer |
| HuC-YC: | Yellow cameleon fluorescent protein expressed under the Huc promotor |
| JG: | Juxtglomerular cells |
| MC: | Mitral cell |
| NMDA: | N-methyl-D-aspartate |
| OB: | Olfactory bulb |
| ORN: | Olfactory receptor neuron |
| OSN: | Olfactory sensory neuron |
| PG: | Periglomerular cell |
| PL: | Plexiform layer |
| PSD: | Position sensitive detector |
| Rhod-2-AM: | Rhodamine-2- acetoxymethyl |
| ROTO: | Reduced OsO ₄ – thiocarbohydrazide – OsO ₄ |
| SA: | Short axon cell |
| SBEM: | Serial block face electron microscope |
| SIR: | Sparse incomplete representation |
| TDCa: | Temporally deconvolved calcium imaging |
| VBS: | Variance balanced state |

Abstract

One of the great challenges in neuroscience is to explain the function of neuronal circuits as a consequence of the connections and interactions between large numbers of neurons. To understand the dynamics of small microcircuits, it is indispensable to study the connectivity between neurons and its influence on the function of the intact system. However, for most neural circuits the detailed wiring diagram is unknown. The zebrafish is an excellent model system to address these questions because it is small in size, facilitating large-scale neuronal reconstructions, and because a variety of established tools can be combined to identify neurons and measure neuronal activity patterns. The olfactory bulb (OB) is the first stage of information processing in the olfactory system and has become a model for studies of neural circuit structure and function in the intact brain. We used serial block face electron microscopy to obtain a large high-resolution anatomical dataset from the adult olfactory bulb. Focused reconstruction from a small subset of neurons revealed the complete structure of mitral cells. Synapse mapping revealed their complete synaptic map. In higher vertebrates an excitatory interneuron, external tufted cell, has been shown to receive direct synaptic input and then relay the information to the mitral cells. We observed that mitral cells in adult zebrafish receive direct synaptic inputs from the olfactory receptor neurons. Both these scenarios of information transfer can have different computational consequences in the OB.

Two recent computational studies focused on reciprocal connectivity in the OB between mitral cells and granule cells. One model predicts that granule cells activity is ultra-sparse and mitral cell activity is sparse, and that this type of reciprocal circuit helps to perform decorrelation in the OB. Another computational model used the same mathematical approach but comes with different predictions. It puts no constraints on the sparseness of MC and GC cells. It further predicts that the reciprocal circuit performs contrast normalization and brings the OB into a variance-balanced state. We tested both these models experimentally and saw indeed that the granule cell activity was not sparse, thereby showing that the first model is not biologically plausible in the OB. The fraction of reciprocal synapses out of all the input synapses on the mitral cells was significant. With this fraction the olfactory circuit still performs strong contrast normalization thereby showing that the second model is biologically plausible.

Figures

- Fig. 1: Simplified diagram of the olfactory system in zebrafish
- Fig. 2: Interneuron subtypes in the OB
- Fig. 3: Disynaptic pathway including ET cells
- Fig. 4: Reciprocal dendro-dendritic synapse
- Fig. 5: Feedback and Lateral inhibition
- Fig. 6: SIR and VBS models
- Fig. 7: Two-photon calcium imaging and odor stimulation
- Fig. 8: Embedding and resizing of the sample
- Fig. 9: Operation of the automated microtome in the vacuum chamber
- Fig. 10: PyKnossos
- Fig. 11: Granule cell responses to odors
- Fig. 12: Responses and density of granule cells
- Fig. 13: Overview of the adult OB
- Fig. 14: Neuron reconstruction
- Fig. 15: Large stack overview
- Fig. 16: Edge distortions
- Fig. 17: Extracellular space
- Fig. 18: Somata in the large stack
- Fig. 19: Layers in the olfactory bulb
- Fig. 20: GL, Plexiform, GC layer
- Fig. 21: Micro glomerular structures
- Fig. 22: Sensory axon bundles
- Fig. 23: Reconstructed of a mitral cell
- Fig. 24: Group of sister mitral cells
- Fig. 25: Presumptive interneuron
- Fig. 26: Four synapse classes

- Fig. 27: Synapse distribution of MC 1479
- Fig. 28: 2D dendrogram
- Fig. 29: Synapse numbers of MC 1483
- Fig. 30: 2D dendrogram
- Fig. 31: Synapse distribution, MC 1477
- Fig. 32: 2D dendrogram
- Fig. 33: Pooled synapses numbers
- Fig. 34: Fraction of reciprocal synapses in VBS model

INTRODUCTION

1.1 The olfactory system and information processing

The olfactory bulb is a telencephalic brain area that receives direct input from olfactory receptor neurons (ORNs) in the nose and has been proposed to share functional principles with cortical circuits (Haberly, 2001). Each ORN expresses a single odorant receptor out of a repertoire of approximately 1000 different receptors in rodents and about 300 in teleosts (Shepherd 1997, Mombaerts 1999, Alioto et al., 2005). ORNs expressing one specific receptor are scattered throughout the nasal epithelium, but their axons converge in the OB onto one or a few discrete glomeruli (Buck, 2000). The total number of glomeruli is approximately 2000 in mice and 200-300 in zebrafish (Mombaerts, 1999; Braubach et al., 2012). Within glomeruli, ORN axons form synapses with the principal cells of the OB, the mitral cells (MC), and with inhibitory interneurons.

Within the OB, mitral cells interact with three main classes of inhibitory interneurons: the periglomerular cells, the short-axon cells and the granule cells. The latter are located in the deep layers of the OB. The output of the OB is conveyed by mitral cells to multiple higher brain areas including the olfactory cortex. Each odorant receptor can bind multiple different odor molecules, and each odorant is recognized by multiple types of odorant receptors. Consequently, a given odor molecule is initially represented in the OB by the activation of a specific combination of glomeruli (Friedrich and Korsching, 1997; Rubin and Katz, 1999; Wachowiak and Cohen, 2001).

At the level of mitral cells, odors are also represented combinatorially. However, activity patterns across mitral cells change dynamically during the initial phase of a response, which reflects multiple computations. Initially, mitral cells activity patterns evoked by odors of the same chemical category overlap and are often very similar to each other. Subsequently, however, patterns evoked by different odors diverge and become more distinct (Friedrich and Laurent, 2001; Niessing and Friedrich, 2010).

This decorrelation facilitates the discrimination between odor representations by a simple classifier and may be necessary for storage of odor representations by auto-associative networks. However, the mechanisms underlying pattern decorrelation are, however, only beginning to be understood. One possibility is that pattern decorrelation emerges from neuronal nonlinearities and is amplified by recurrent connectivity (Wiechert et al., 2010). Computations such as pattern decorrelation depend on network interactions between mitral cells and interneurons. Most interglomerular interactions between mitral cells are mediated via interneurons that are inhibitory in nature.

Another computation performed by the olfactory bulb is pattern equalization, which stabilizes mitral cell activity patterns against variations in stimulus intensity (Zhu et al., 2013). Equalization is mediated, at least in part, by short-axon cells that are depolarized by sensory input and provide output to mitral cells via electrical and GABAergic synapses. Weak sensory input results in a depolarization of mitral cells that is transmitted via gap junctions while strong inputs hyperpolarize mitral cells via GABAergic inhibition. As a consequence, short-axon cells boost mitral responses to weak input but attenuate mitral cells responses to strong inputs. These and other mechanisms maintain both the mean and the variance of odor-evoked activity patterns across the mitral cell population within a narrow range and thereby help establish concentration-invariant representations of odor identity.

Testing models of neuronal computations in the olfactory bulb and other brain areas often requires more detailed insights into the connectivity between individual neurons and their computational consequences. Many synaptic contacts between mitral cells and interneurons (particularly granule cells) are reciprocal dendro-dendritic synapses: an excitatory mitral cell-to-interneuron synapse occurs in close proximity to an inhibitory interneuron-to-mitral cell synapse between the same neurons (Rall et al., 1966; Reese and Brightman 1966, Pinching and Powell, 1971, Isaacson and Strowbridge, 1998; Urban and Sakmann, 2002). It is therefore thought that interneurons, particularly granule cells, mediate mutual lateral inhibition between mitral cells. Besides this striking symmetry of connectivity at fine spatial scales, it is, however, unknown

whether connectivity between mitral cells and interneurons exhibits non-random structure at larger scales.

In other words, the topology of connections in the OB is largely unknown. For example, it is known that connectivity between mitral and granule cells is sparse and that connection probability decreases with distance (Egger and Urban, 2006; Fantana et al., 2008; Wiechert et al., 2010) but the precise neuron-to-neuron connectivity matrix is unknown. The reason for this lack of knowledge is that conventional approaches to determine connectivity such as stains of individual neurons, viral tracing of synaptically connected neuronal ensembles, or paired electrophysiological recordings provide only first-order statistical information on connection probability.

1.2 Detailed architecture of the olfactory system

The neuronal organization of the olfactory bulb is largely preserved throughout the vertebrate classes and exhibits similarities also to the first olfactory processing center in insects, the antennal lobe. The olfactory bulb and the antennal lobe both receive direct input from olfactory sensory neurons through an array of anatomically distinct glomeruli, encode odor information in a combinatorial fashion, and process odor-evoked activity patterns by interneuron networks that are coupled to output neurons via GABAergic synapses and gap junctions. However, the antennal lobe contains much fewer interneurons and, contrary to the olfactory bulb receives very few top-down projections. Moreover, the insect antennal lobe has only two projection targets, the mushroom body and the lateral horn, while the olfactory bulb has more projection targets (Hildebrand and Shepherd, 1997). Hence, some aspects of olfactory processing may differ between vertebrates and insects. We focused on the olfactory bulb of zebrafish, which is described in more detail below.

Olfaction in zebrafish

Zebrafish can detect molecules in aqueous solution like amino acids, nucleotides, steroids and bile acids. Some of these odorants or their mixtures elicit specific physiological responses or behaviors in zebrafish such as feeding, swimming, chemosensory, reproductive behaviors (Kyle 1983, Vogt, 2004, Zielinski, 2007). The noses of the zebrafish are a paired structure. Each nose has an inflow and an outflow opening through which water flows unidirectionally. Unlike rodents and other mammals, zebrafish do not sniff rhythmically. Water flow through the nose is generated by constantly beating cilia of supporting cells and by swimming (Zielinski, 2005; Zielinski, 2007).

Olfactory Sensory Neurons

ORNs are the primary sensory neurons in the nose (Shepherd, 1997). Zebrafish ORNs comprise three distinct cell types: ciliated cells, microvillous neurons and crypt cells (Hansen and Zielinski, 2005). Somata of these three different cell types are located at different depths in the olfactory epithelium. ORNs are constantly renewed by division of stem cells in the deep layers of the olfactory epithelium (Cancalon, 1982; Julliard, 1996).

The Zebrafish Olfactory Bulb

OB can be primarily divided into three layers, the glomerular layer (GL), the plexiform layer (PL) and the granule cell layer (GCL). (Fig. 1).

1) Glomerular layer. This layer contains glomerular neuropil units as well as somata of two types of output neurons, the mitral cells and ruffed cells. In addition, the GL contains somata of subsets of interneurons, including short-axon cells and periglomerular cells (Byrd et al., 2005; Fuller et al., 2006, Braubach et al., 2012). In mammals, an additional juxtglomerular cell type, the external tufted cell (ET), has been described (Hayar et al., 2004). While short-axon and periglomerular cells are GABAergic, external tufted cells are glutamatergic.

2) Plexiform layer. This neuropil layer consists mainly of dendrites of mitral cells and different types of interneurons. Only few somata can be found.

3) Granule cell layer. This layer contains a high density of interneuron somata. The largest population of interneurons is granule cells (Michel et al., 2002). Additional smaller populations of interneurons may include deep short axon cells, which have been described in other vertebrate species (Schneider and Macrides, 1978).

The Glomerulus

The zebrafish glomerular layer contains approximately 140 distinct glomeruli and a region containing additional, small glomerular structures that have not been delineated precisely. Subsets of these glomeruli are large and unambiguously identifiable between individuals (Braubach et al., 2012). Moreover, anatomically and molecularly defined clusters of glomeruli can be found consistently in different individuals.

Glomeruli represent the sites of convergence of ORNs expressing the same odorant receptor as well as the sites of convergence of the dendrites of a small number of mitral cells. Anatomically, the glomerulus comprises a shell and a core. The shell is comprised of a heterogeneous population of periglomerular and short-axon cells, which are collectively referred to as juxtglomerular cells (Kosaka et al., 1998). The core contains neuropil that contains ORN terminals, mitral cell dendrites and processes of juxtglomerular cells (Pinching and Powell, 1971).

Principal neurons

Mitral cells and ruffed cells are the principal neurons of the teleost olfactory bulb (Fig. 1). There are about 1500 mitral cells in adult zebrafish OB (Wiechert et al., 2010). The mammal olfactory bulb also contains two types of output neurons, the mitral cells and tufted cells, but it remains unclear whether tufted cells in mammals correspond to ruffed cells in teleosts.

Juxtglomerular cells

Juxtglomerular cells comprise of short axon cells (SA) periglomerular cells (PG) and external tufted cells (ET) (Cajal, 1911; Powell, 1971; Shepherd, 2004). Short axon interneurons have dendrites arborizing within and around the glomeruli without a dense apical tuft (Aungst et al., 2003; Shepherd et al., 2004; Shipley et al., 2010). Periglomerular cells (Fig. 2) have bushy dendrite

Introduction

arborization (Pinching and Powell, 1971a, c; Shepherd et al., 2004). External tufted cells are morphologically heterogeneous with a fan shaped apical dendritic tuft and arborize in a single glomerulus (Powell, 1971; Schneider, 1982; Hayar et al., 2004).

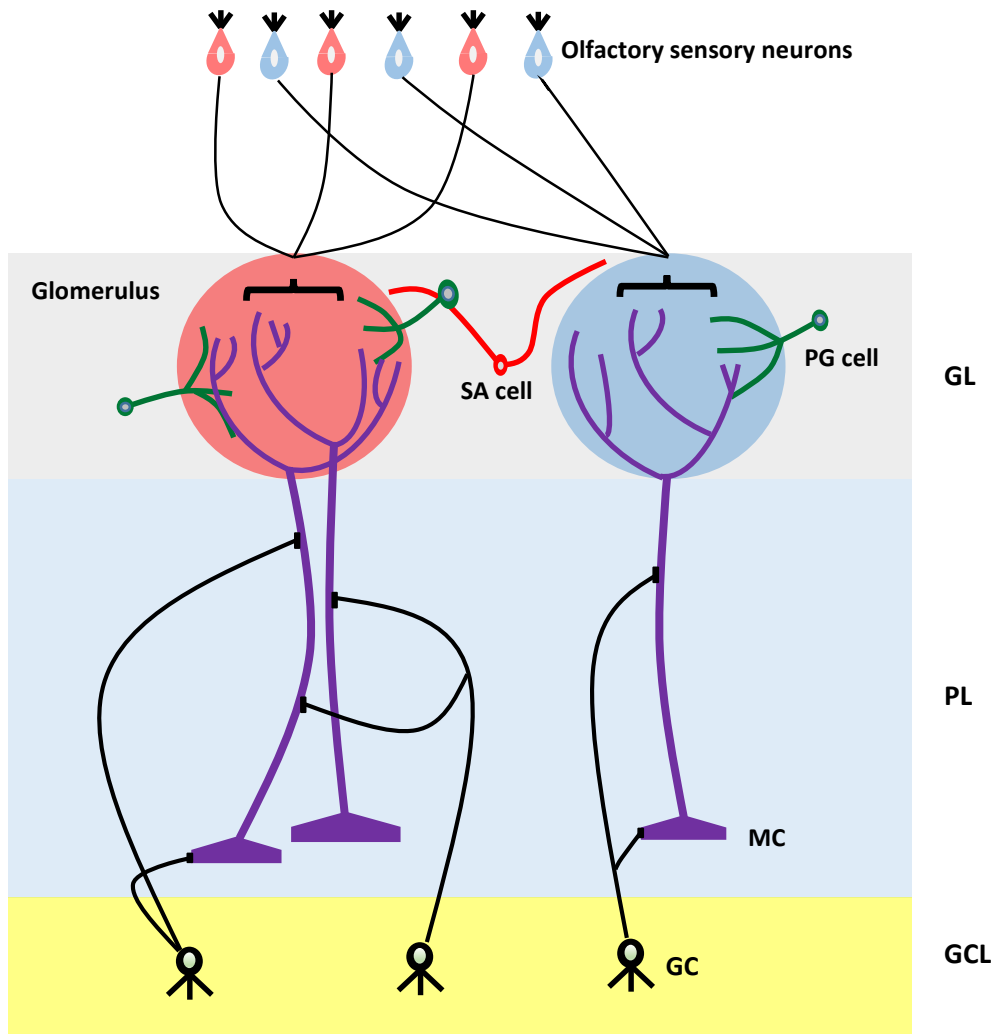


Fig. 1: Simplified diagram of the olfactory system in zebrafish.

The axons of olfactory receptor neurons make synapses in the glomerular layer (GL). Neurons surrounding glomeruli in the GL are juxtglomerular cells, consisting of three morphologically distinct interneuron cell types: periglomerular (PG) cells, external tufted (ET) cells (not shown), and superficial short-axon (SA) cells. There are two types of projection neurons, the mitral cells and the ruffed cells (not shown), which send their axons to the higher order brain centers/ downstream targets. Mitral cells project their primary dendrite into a glomerulus, where they are thought to receive synaptic inputs from the axons of olfactory receptor neurons and make reciprocal synapses with the dendrites of PG cells. Granule cells in GL are axon-less interneurons extending dendrites apically into the PL where they reciprocally synapse onto mitral cells.

Introduction

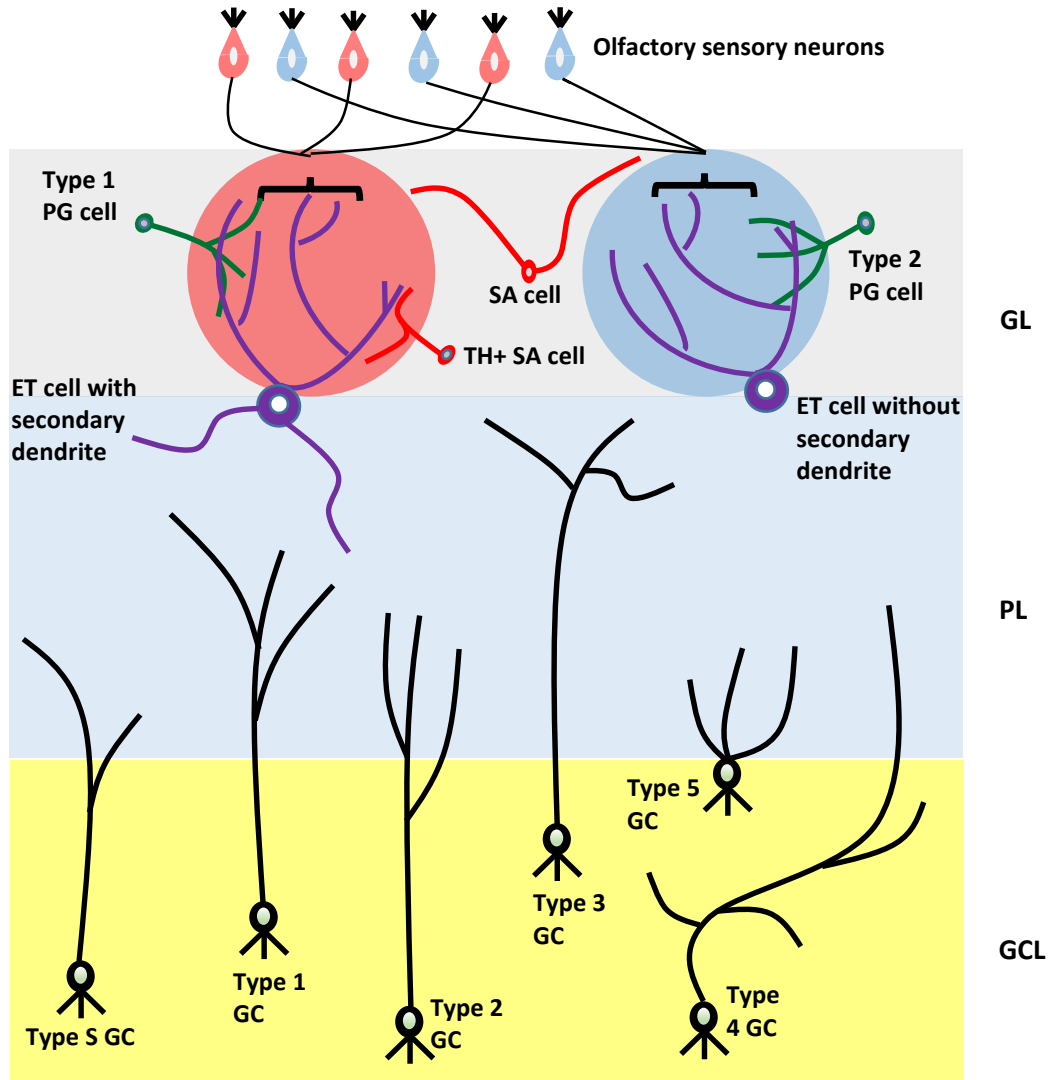


Fig. 2: Interneuron subtypes in the OB.

Schematic representations of different interneuron populations: periglomerular cells (green), short axon cells (red) and external tufted cells (purple). Two subtypes of PG cells are distinguished based on their synaptic connections. Type-1 PG cells receive synaptic inputs on their dendrites from both ORNs and neurons in the olfactory bulb. Type-2 PG cells only receive inputs from neurons in the olfactory bulb. SA cells have long processes. Subtypes of ET cells are determined by morphology: those without and those with secondary dendrites. Six subtypes of granule cells are distinguished based on the location (depth) of their cell somata in the GCL. Subtypes of deep SA cells (not shown) are also present in GCL. (Modified from Nagayama S and Imamura F, 2014).

External tufted cells

ET cells can be divided into two morphologically distinct subtypes: those with and those without secondary (basal) dendrites (Macrides and Schneider, 1982) (Fig. 2). These morphological differences are also correlated with physiological distinctions (Antal et al., 2006).

Thus basal-dendrite bearing and non-basal-dendrite-bearing ET cells may in principal be two (or more) separate populations. ET cells have long been considered glutamatergic. Recent studies suggest ET cells receive direct synaptic input from the terminals of olfactory receptor neurons. ET cells synapse onto mitral cells (Shipley et al., 2004; Schoppa et al., 2012).

Granule cells

Granule cells are a very large population of cells located in deep layers. Granule cells lack axons and extend dendrites to different depths of the plexiform layer (Fig. 2) (Golgi, 1875; Cajal, 1880). In mammals, GCs have been categorized into six types (superficial, intermediate and deep) based on their depth in OB (Mori et al., 1983; Mori et al., 1987; Orona et al., 1983; Naritsuka et al., 2009; Merkle et al., 2014). Granule cells form reciprocal dendro-dendritic synapses with mitral cells.

1.3 Direct vs. indirect sensory input to mitral cells

Classical anatomical studies concluded that mitral cells receive direct synaptic inputs from the olfactory receptor neurons (Pinching and Powell, 1971). These studies were based on transmission EM images from sections. Mitral cells were identified by the particular shape of their dendrites in the glomerular region. However, because it was not possible to follow the dendritic profile to the soma, the identification of mitral cells was tentative. The evidence that mitral cells receive direct sensory input was therefore considered convincing, albeit indirect.

Recent studies have challenged this conclusion and proposed that ORNs terminate on ET cells, which in turn provide synaptic input to MCs (Shipley et al., 2004; Schoppa et al., 2012). While physiological studies clearly support the conclusion that ET cells receive strong direct olfactory

receptor neuron input, and that MCs receive synaptic input from ET cells (Shipley et al., 2004). However, it is controversial whether MCs also receive direct sensory from ORNs.

Based on recent physiological results it has been proposed that such as direct synaptic pathway does not exist, and that all excitatory input from ORNs is transmitted to mitral cells by a disynaptic pathway via ET cells (Schoppa et al., 2012). However, this evidence is again indirect because it relies on extracellular stimulation and electrophysiological recordings. These methods cannot directly reveal synaptic connectivity. A disynaptic pathway between ORNs and MCs via ET cells could provide opportunities for additional processing between sensory input and output (De Saint Jan et al., 2009; Najac et al., 2011; Schoppa et al., 2012) (Fig. 3).

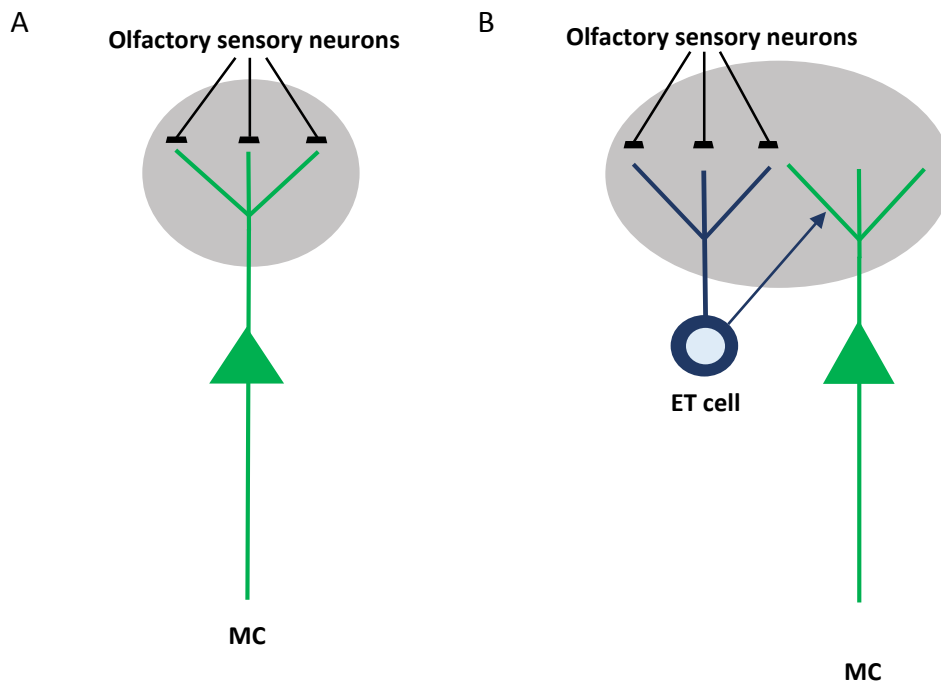


Fig. 3: Disynaptic pathway including ET cells.

(A) Schematic showing mitral cells receive direct input from the olfactory sensory axons. (B) Schematic of external tufted cells receiving direct olfactory sensory neuron input and then transfer the olfactory information to mitral cells in a disynaptic-step pathway.

1.4 Reciprocal connectivity in the olfactory bulb

Reciprocal synapses have been first reported in the olfactory bulb of rats (Fig. 4) (Hirata, 1964; Andres, 1965; Rall and Shepherd, 1968; Reese and Brightman 1966). In the olfactory bulb they have been observed frequently between glutamatergic mitral cells and interneurons, particularly GABAergic granule cells. Reciprocal synapses have also been found in other parts of the brain e.g. the hypothalamus (Giildner and Wolff 1974), superior colliculus (Lund et al., 1969) and retina (Dowling and Boycott 1966). Dendro-dendritic physiological properties were studied and first reported in rabbit OB. Further studies in turtle and salamander show that reciprocal synapses are functional in both directions (Phillips, 1963; Nicoll, 1969; Jahr and Nicoll, 1980; Nowycky et al., 1981; Wellis and Kauer, 1993; Isaacson and Strowbridge 1998; Schoppa et al., 1998).

Structurally, reciprocal synapses in the OB have been studied by electron microscopic reconstructions from single and serial sections. They consist of an asymmetric (excitatory) mitral cell to interneuron synapse and a close-by symmetric (inhibitory) interneuron to mitral cell synapse (Fig. 4). In mammalian granule cells, reciprocal synapses are located on large dendritic protrusions called gemmules that are similar to ordinary spines but larger (Rall et al., 1966; Rall and Shepherd, 1968; Price and Powell, 1970).

Functionally, a reciprocal structure efficiently generates feedback inhibition on the dendrites of mitral cells (Yokoi et al., 1995; Brennan and Keverne, 1997). Obviously, reciprocal connectivity can also generate lateral inhibition (Chen et al., 2000; Egger et al., 2003). Moreover, it has been argued that reciprocal connectivity supports synchronization of mitral cells (Kashiwadani et al., 1999; Mori et al., 1999; Schoppa et al., 2006).

NMDA receptors are highly expressed on granule cells and thought to play a major role in signaling at reciprocal synapses (Collingridge and Lester, 1989; Iverson et al., 1987). In brain slices, the activation of mitral cell to granule cell excitatory synapse can lead to a calcium influx through the NMDA receptor resulting in an increase in the calcium concentration in the granule cell gemmule. This in turn can trigger GABA release at the granule cell to mitral cell inhibitory synapse even in the absence of an action potential (Schoppa et al., 1998; Isaacson and

Strowbridge, 1998; Chen et al., 2000; Halabisky et al., 2000). This mechanism may mediate feedback inhibition of active mitral cells even when granule cell activity remains subthreshold.

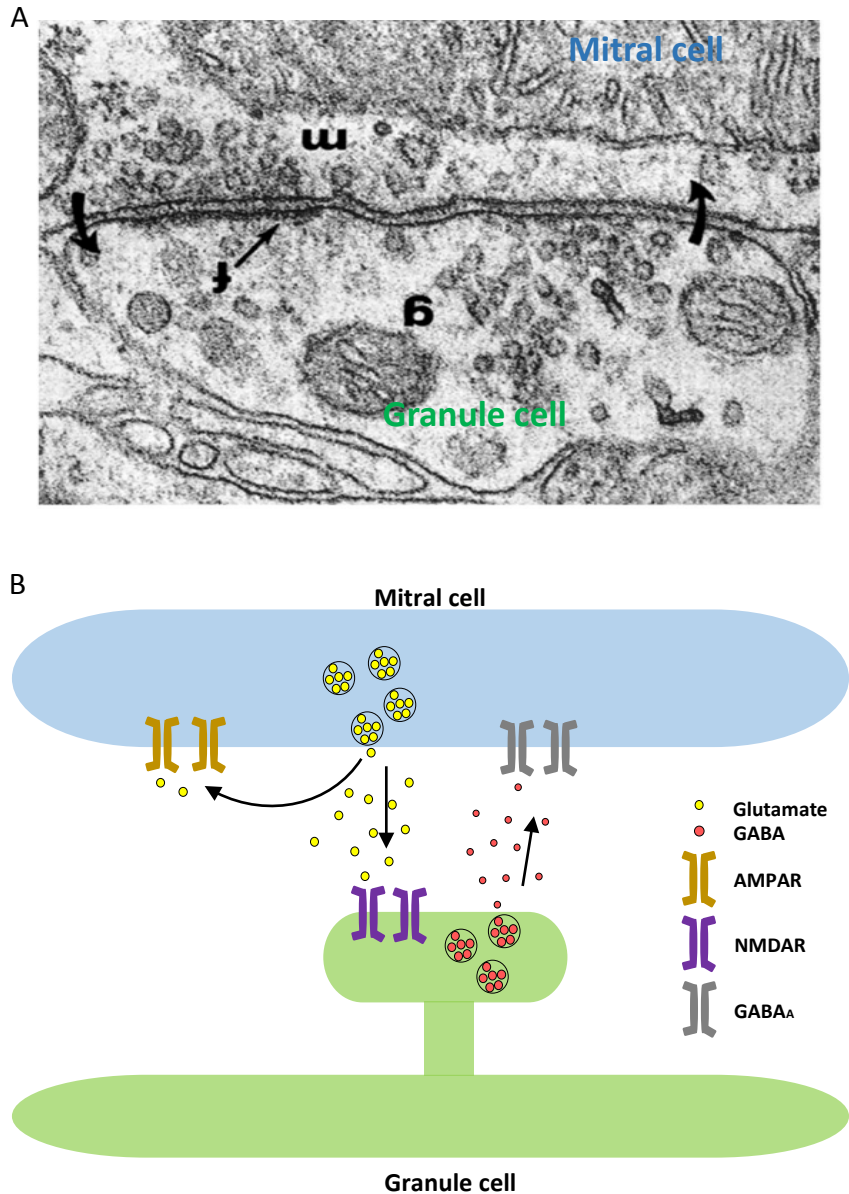


Fig. 4: Reciprocal dendro-dendritic synapse.

(A) Electron micrograph of a mitral secondary dendrite making a mitral-to-granule asymmetric synapse onto a granule cell spine, which makes a reciprocal granule-to-mitral symmetric synapse onto the same mitral cell dendrite (from Rall et al., 1966). (B) Illustration of reciprocal dendro-dendritic synapses between a mitral and granule cell in the OB. It consists of a glutamatergic mitral cell to granule cell excitatory synapse and a close-by granule cell to mitral cell GABAergic synapse.

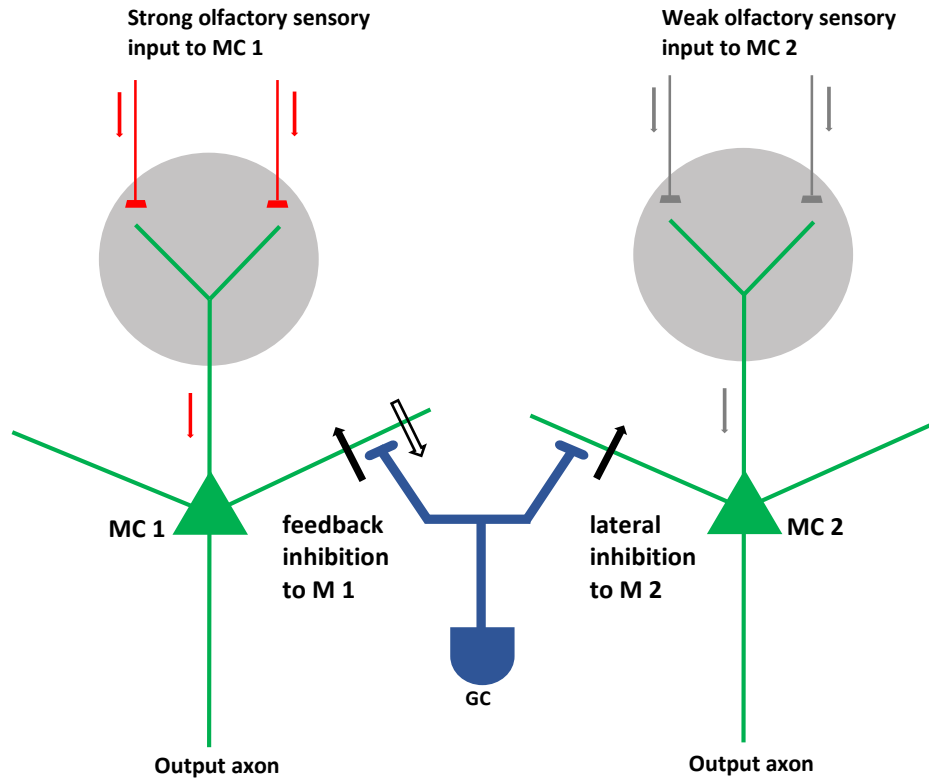


Fig. 5: Schematic illustration of feedback and lateral inhibition.

The scheme illustrates a hypothetical situation where mitral cell 1 receives strong ORN input and mitral cell 2 receives weak input. The granule cell shown forms reciprocal synapses with both mitral cells and receives sufficiently strong input, mainly from mitral cell 1, to generate an action potential. The granule cell therefore inhibits mitral cell 1, the main source of its excitatory input (feedback inhibition, black arrow), as well as mitral cell 2 (lateral inhibition, black arrow).

Strong excitatory input can induce an action potential in a granule cell which propagates throughout the dendritic tree, which is assumed to trigger GABA release at many synapses (Chen et al., 2000; Egger et al., 2003). The inhibition from granule cells to mitral cells is thus targeted to mitral cell involved in excitation but also to mitral cells which do not contribute in granule cell excitation, resulting in an effective lateral inhibition through reciprocal synapses (Fig. 5).

During an odor response, a substantial fraction of mitral cells rhythmically synchronize their action potentials at frequencies in the beta and gamma ranges. (Adrian, 1950; Rall and Shepherd

1968; Kashiwadani et al., 1999). The rhythmic activity of neurons in the OB can be recorded extracellularly as an oscillatory local field potential, and action potentials of mitral cells occur preferentially around a specific phase of the oscillation. Patch clamp recordings indicate that the timing of mitral cell action potentials depends on synaptic inhibition from granule cells (Schoppa et al., 2006) and it has been proposed that reciprocal connectivity between mitral and granule cells supports oscillatory synchronization.

1.5 Computational consequences of reciprocal connectivity

Most brain regions contain a majority of excitatory projection neurons whose activity is regulated by a smaller number of local inhibitory neurons. In the OB, however, inhibitory interneurons outnumber excitatory neurons by a factor of 100 or more (Aungst et al., 2007). The majority of olfactory bulb interneurons are granule cells (Mori et al., 1987; Shepherd et al., 2004) that form reciprocal synapses with the principal mitral cells. It has been proposed that reciprocal synaptic inhibition by olfactory bulb interneurons mediates gain control by feedback inhibition, contrast enhancement by lateral inhibition and synchronization of mitral cells. Conceivably, however, a strictly reciprocal connectivity between mitral cells and interneurons is not necessary for any of these computations.

Recently, two theoretical and computational studies examined computational consequences of reciprocal connectivity in more detail and arrived at different conclusions (Koulakov and Rinberg, 2011; Wiechert, 2015). The approaches used in these studies are based on the same simplified model that consists of principal neurons (“mitral cells”) and reciprocally connected inhibitory neurons (“granule cells”). However, the two studies differ in the mathematical analysis and made different simplifications.

The first study (Koulakov and Rinberg, 2011) suggests that sparse codes in the OB emerge as a result of the balance between mitral cell excitatory inputs and inhibition provided by the granule cells (Fig. 6 A). The model suggests that granule cells can form representations of the incoming olfactory stimuli in the inhibitory inputs that they return to the mitral cells. The pattern of

inhibitory synaptic input from granule cells will be then “removed” from the pattern of excitatory synaptic input from ORNs (or ET cells). An exact balance between the receptor neuron excitation and granule cell inhibition would completely eliminate mitral cell odor responses. However, because the granule cell population feedback cannot represent all possible mitral cell activity patterns, the set of granule cell odor representations is assumed to be “incomplete”. As a consequence, some residual mitral cell activity will not be cancelled out. This activity represents the mismatch between the sensory input and the granule cell feedback patterns and will be transmitted to higher brain areas.

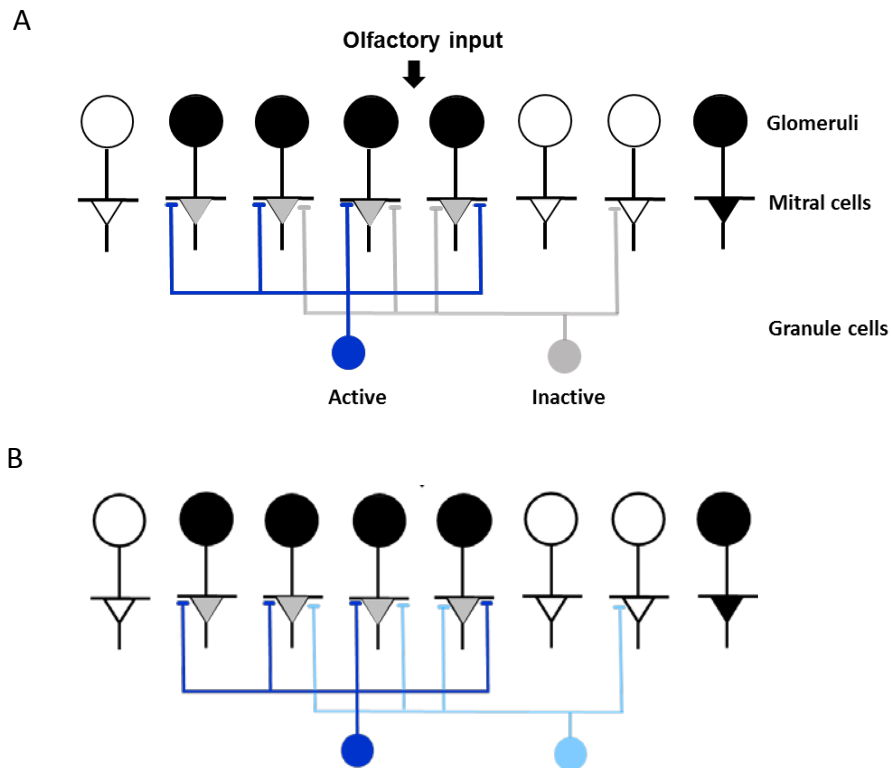


Fig. 6: Proposed computational consequences of reciprocal feedback: SIR and VBS models.

(A) SIR model: Strong olfactory inputs activate a subset of glomeruli (black circles), which in turn activate a specific subset of mitral cells. Active mitral cells excite granule cells via reciprocal synapses. The granule cell whose synaptic input pattern best matches the glomerular activity pattern (blue) will reach threshold first and provide reciprocal inhibition to the active MCs. As a consequence, most MCs will be nearly silenced (gray triangles). However, some mitral cells may escape silencing (black triangle) because the granule cell feedback pattern is incomplete. (B) VBS model: Reciprocal connectivity does not reorganize or sparsify mitral cell activity patterns but down-scales the entire pattern without reorganizing it and thereby normalizes pattern contrast.

This model will be referred to as the “sparse incomplete representation” (SIR) model and makes the following predictions (Koulakov and Rinberg, 2011):

- 1) Granule cell activity patterns should be very sparse. This is a strong prediction.
- 2) Granule cell feedback should decorrelate mitral cell activity patterns.
- 3) Granule cell feedback should sparsify mitral cell activity patterns.

The second study (Wiechert, 2015) arrived at the conclusion that reciprocal connectivity does not reorganize or sparsify mitral cell activity patterns (Fig. 6 B). This study found that the pattern of reciprocal feedback inhibition from the granule cell population mirrors the pattern of excitatory inputs and thereby down-scales the entire pattern without reorganizing it. The study demonstrates that this phenomenon holds also in “balanced state” networks, as discussed below, and results in a normalization of variance. It is therefore referred to as the “variance-balanced state” (VBS) model.

The balanced state is a theoretical model for neuronal networks in which each neuron receives constant excitatory and inhibitory inputs from other neurons in the network (Pare et al., 1998, Wolf et al., 2014). In a classical balanced state network, connectivity is assumed to be sparse and random, therefore inhibitory and excitatory currents are approximately uncorrelated. Classical balanced state networks can allow individual neurons to respond fast and reliably to specific stimuli while maintaining the mean firing rate of the population within a narrow range, even when the global input intensity fluctuates. However, this “normalizing” function works well only when the variance of activity across external inputs is relatively low. In reality, however, this variance can be high, particularly in sensory systems (Pare et al., 1998). In the OB, for example, an odor may provide inputs of very different strength to different glomeruli. The mathematical and computational analysis underlying the VBS model demonstrated that reciprocal connectivity can maintain a balanced state also when input variance varies over a wide range. This effect is a direct consequence of reciprocal connectivity and was found to be robust against variations of various model parameters (Wiechert, 2015).

Introduction

In a reciprocally connected network, excitatory and inhibitory inputs are therefore balanced not only on average but also in individual cells. As a consequence, input patterns are down-scaled when the variance of the input increases. It has therefore been proposed that reciprocal connectivity promotes contrast normalization in the OB, rather than contrast enhancement. Contrast normalization is a computation of high importance in many brain regions, particularly in sensory systems.

The VBS model makes predictions that are different from those of the SIR model:

1. Granule cell activity does not have to be extremely sparse.
2. Granule cell feedback does not decorrelate mitral cell activity patterns.
3. Granule cell feedback does not sparsify mitral cell activity patterns.

Both studies assume that a substantial fraction of mitral-granule cell synapses are reciprocal. Anatomical studies indicate that reciprocal synapses are indeed common in the OB but the exact degree of reciprocity has not been quantified. The VBS model suggests that a robust VBS requires approximately >20% of the synapses between mitral cells and interneurons to be reciprocal but the exact fraction may depend on synaptic strength (Wiechert, 2015).

How can the SIR and the VBS models be tested in the olfactory bulb? One approach would be to silence granule cells and analyze the density and correlation of mitral cell activity patterns in order to test predictions 2 and 3. However, this approach is technically difficult. Moreover, it may disrupt excitation/inhibition balance and thereby push the network into a qualitatively different state that would not allow for tests of the VBS model. Another approach is to examine whether granule cell activity is extremely sparse. This is a strong prediction of the SIR model. Hence, non-sparse activity across the granule cell population during an odor response would strongly argue against the SIR model and in favor of the VBS model. Previous studies indeed suggest that granule cell activity is not sparse (Tabor and Yaksi et al., 2004; Zhu et al., 2012). If so, further support for the VBS model could be obtained by determining the fraction of mitral cell-to-interneuron synapses that are reciprocal. If this fraction is >20%, this would provide further support for the VBS model.

1.6 State of the art in 3D EM for dense circuit reconstruction

One of the major challenges in neuroscience is to explain the function of neuronal circuits as a consequence of the connections and interactions between large numbers of neurons. To truly understand the dynamics of even small microcircuits, it is indispensable to study the detailed synaptic connectivity between neurons and its influence on the function of the intact system. One of the factors impeding progress in systems neurobiology has been the lack of appropriate methods to determine neuron-to-neuron connectivity in large networks.

Classical methods typically give information about the first-order statistics of neuronal connectivity, i.e. about the probability that defined cell types are connected to each other, and about the dependence of this probability on the distance between neurons. Higher-order topological motifs such as connected ensembles, however, are very difficult to identify using classical methods. The major challenge in understanding neuronal circuit function is therefore to obtain a detailed description of synaptic connections between most or all neurons in a circuit. Currently, this has not been achieved for any large neuronal circuit or ultimately for a complete nervous system with the exception of *C. elegans*, where connections were reconstructed from serial electron microscopic images through decades of manual labor (White et al., 1986).

The main challenge of exhaustive connectivity measurements by imaging methods has been to maintain a resolution of a few tens of nanometers, which is required to trace fine neuronal processes and identify synapses, throughout large volumes of tissue. Progress towards this goal has recently been made by novel developments in electron microscopy (EM) (Briggman and Denk, 2006). Serial block face scanning electron microscopy (SBEM) uses a microtome inside the vacuum chamber of a scanning EM to acquire series of EM images from the block face of a sample while successively cutting ultrathin sections (<30 nm) (Denk and Horstmann, 2004, Denk et al., 2012). This method is fully automated and can generate stacks of EM images from large blocks of tissue (hundreds of microns edge length).

Alternatively, a focused ion beam can be used to mill sections off the surface of the block (FIB-SBEM) (Knott et al., 2008). This method achieves higher resolution but is severely limited in

volume (tens of microns edge length). In a different strategy, serial sections are automatically cut, collected on tape, and transferred onto a silicon wafer. Subsequently, they may be imaged using an automated scanning EM. Unlike the block face methods, this approach allows for repeated imaging of the same sections but requires more elaborated image alignment to obtain 3-D stacks and may be more prone to problems associated with the preservation of sections.

Recent results have demonstrated that reconstructions of large circuits in the retina can be achieved by SBEM (Briggman et al., 2011). However sample charging in SBEM due to the electron beam on the sample can have severe effects such as improper cutting, reduced contrast and image distortions which limits the potential of SBEM (Mathieu, 1999; Denk and Horstmann, 2004; Titze and Denk, 2013). New methods which involve conductive embedding of the tissue samples reduce charging to great extent and therefore improve image quality and enable acquisition of large EM stacks (Wanner et. al, submitted).

Another challenge towards acquiring and understanding neuronal wiring diagrams is the reconstruction of individual neurons and their synaptic connections present in the EM data stack. Because the tracing of neuronal processes and the annotation of synapses in EM data stacks is very time-consuming, the physical size is currently a factor that constrains circuit reconstruction (Helmstaedter et al., 2013; Kim et al., 2014). Obviously, accuracy is important because reconstruction errors can result in incorrect wiring diagrams. Advancements in the interactive tracing and synapse detection software tools have allowed tracing neurons manually with high accuracy (Helmstaedter et al., 2011, Seung et al., 2014).

1.7 Zebrafish as a vertebrate model in systems neuroscience

The analysis of neuronal circuit functions underlying sensory processing and higher brain functions can be facilitated by the use of a small model organism. One of the popular model organisms is the zebrafish, a relatively small freshwater teleost species that is commonly found in still or slow waters such as rice fields of India, Bangladesh and Myanmar (Engeszer et al., 2007;

Spence et al., 2008). In addition, zebrafish are inexpensive to maintain in a facility, easy to breed and have a high reproduction rate.

The olfactory bulb of zebrafish is a particularly attractive circuit to study for multiple reasons. First, because since the OB is small (~400 um in diameter), neuronal population activity can be measured exhaustively with single cell resolution by using multiphoton calcium imaging (Denk et al., 1990). Moreover, activity can be manipulated with high spatial and temporal precision using optogenetic methods. Second, SBEM allows for (Denk et al., 2004; Denk et al., 2005) ultrastructural imaging of all layers of the OB. Third, computations in the OB have been studied extensively in adult zebrafish, providing a basis to relate neuronal circuit structure to function. Despite the smaller size of the OB, the developmental and organizational principles of the olfactory system in zebrafish are similar to those of other vertebrates (Wullimann and Mueller, 2004, Ache and Young, 2005; Sato et al., 2007, Friedrich et al., 2010).

1.8 Aim of the study

Large SBEM stack

The first goal of the project was to obtain a large high-resolution stack of EM images from the lateral part of the adult OB using SBEM. The stack should include both mitral cell and deep interneuron layers and the resolution should be sufficient to manually trace and reconstruct neurons and label individual synapses.

Principal cells in adult OB

To determine whether mitral cells receive direct input from ORNs, the second goal was to reconstruct individual mitral cells in the SBEM stack, map their synaptic inputs, and estimate the fraction of synaptic inputs from ORNs.

Sparseness of granule cell activity patterns

A third goal was to determine whether odor-evoked activity patterns across granule cells are extremely sparse in order to test the central prediction of the SIR model. It was expected that

the results provide a strong basis to compare the biological plausibility of the SIR model and the VBS model.

Mapping reciprocal connectivity

A fourth goal was to map reciprocal and other synapses onto the dendritic tree of mitral cells in 3D. The results should allow for a direct quantification of the fraction of reciprocal synapses made by mitral cells, which is important to assess the biological plausibility of the SIR and VBS models. Moreover, as little quantitative information about the number and subcellular distribution of synapses is available for mitral cells and most other cell types, these results were expected to provide novel insights into the synaptic organization of OB circuits.

METHODS

2.1 Zebrafish adult brain explant preparation

All experimental protocols on zebrafish were approved by the veterinary department of the Canton Basel-Stadt (Switzerland). The experiments were carried out on 4-6 month old adult zebrafish (*Danio rerio*). The fish were kept at 25-28°C on a 13 hour light/11 hour dark cycle in the FMI zebrafish facility. During experiments adult zebrafish were kept in the laboratory at 25–30°C. For the 2-photon experiments the recordings were performed on an explant preparation of adult (3-6 months old) zebrafish comprising of the nose and the entire brain, with the olfactory bulb remaining intact (Friedrich and Laurent, 2001; Zhu et al., 2012). Before the start of the experiment zebrafish were anesthetized by slowly cooling them down in fish water to approximately 4 degree C. Animals were then transferred to ACSF (artificial cerebrospinal fluid, Mathieson and Maler, 1988) and the head was decapitated from the rest of the body in the cold. Eyes along with lower jaw and bones were carefully removed to expose the two olfactory bulbs. For injection of a calcium indicator dye, the dura covering the OB was carefully removed with blunt forceps. For electron microscopy experiments the dura was kept intact for better preservation of the tissue during EM staining. For 2-photon imaging, the sample was then transferred to a custom-made holding chamber in the 2-photon microscope. Throughout the experiment a continuous perfusion of ACSF maintained (flow rate 1-5 mL/min). ACSF was aerated with carbogen (O₂: 95%, CO₂: 5%).

ACSF composition (NaCl = 124 mM, KCl = 2 mM, MgSO₄ = 1.6 mM, CaCl₂ = 2 mM, KH₂PO₄ = 1.25 mM, NaHCO₃ = 24 mM, Glucose = 22 mM).

2.2 Two photon calcium imaging and odor stimulation

In order to identify mitral cells in the olfactory bulb of adult zebrafish, a genetically modified line (HuC-YC) line was used that expresses the transgenic calcium indicator yellow cameleon

Methods

(YC) under the control of the HuC promoter (Miyawaki et al., 1997; Higashijima et al., 2003; Li et al., 2005). HuC drives panneuronal expression zebrafish larvae but more restricted expression in adults. In the adult OB, HuC drives expression selectively in mitral cells (Li et al., 2005). To label the bulbar neurons with a calcium indicator, a stock solution was made by dissolving 50 μg of Rhod-2-AM dye in 16 μl DMSO/Pluronic Acid F-127 (80/20). For each experiment 3 μl of the stock were diluted in a ratio 1:10 in oxygenized ACSF and 5 μl of the diluted dye solution were loaded into a customized glass injection pipette. The amino acid responsive, ventrolateral region (Yaksi et al., 2009) of the OB was located under the microscope using a position sensitive detector (PSD) that makes use of the transmitted light. Next, the injection pipette was brought close to this region. The first injection was done approximately 100 μm under the ventral surface of OB. 2-3 injections were then made in each plane and repeated in 3-4 planes to make sure the dye is homogeneously distributed throughout deep layers of the OB.

Amino acid odors (10^{-5} M; $\geq 99.0\%$ purity; Fluka, Neu-Ulm, Germany) were applied to the ipsilateral naris via a constant flow (Fig. 7). High-resolution two photon imaging of HuC-YC expression was carried out using a multiphoton microscope custom-built on an Olympus BX-51 body (Bundschuh et al., 2012). The microscope and related equipment were controlled by ScanImage and Ephus software (Pologruto et al., 2003; Suter et al., 2010).

Fluorophores were excited by two-photon excitation at 860 nm. Rhod-2 and YC signals were detected simultaneously through two channels separated by emission filters. The raw fluorescence values for acquired image series were converted pixel-wise into $\Delta F/F$ values and further analyzed. Regions corresponding to mitral cell and granule cell somata were marked manually based on the raw YC and Rhod-2 fluorescence images. Mean response amplitudes were calculated for the same time windows as the odor response maps.

Methods

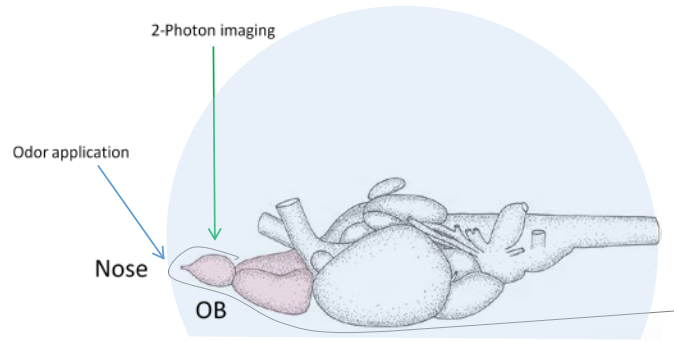


Fig. 7: Two-photon calcium imaging and odor stimulation.

Whole brain explant of zebrafish adult brain shown in the illustration. Olfactory bulb was injected with a calcium sensitive dye and odors were applied to the nose. The odor-evoked activity was measured using two-photon microscope. Drawing of brain is from Wullimann et al. (1996).

2.3 Staining tissue for electron microscopy

After brain explant preparation as described above, the entire adult zebrafish brain was removed from the head bones to further proceed to the EM staining procedure. Batches of five fish brains were stained in parallel. A total of 35 fish brains were stained with this procedure. All the 35 samples were carefully trimmed and imaged in serial block face EM to test the quality of the tissue. The best of the samples after staining and imaging were selected on the basis of tissue quality, hardness of the silver block, extent to which staining components have penetrated the tissue (by carefully analyzing acquired EM images from each sample) and the extent of damage to the sample which might have occurred during dissection or trimming of the sample. The step-by-step staining procedure is described below.

SBEM protocol with ROTO and en-bloc Walton's lead aspartate staining;

| No. | Steps in the protocol | Time | Total time |
|-----|--|------------|------------|
| 1. | Dissection: Dissect adult zebrafish to expose entire brain by removing head bones under constant perfusion of ACSF. | 15 minutes | 15 minutes |

Methods

| | | | |
|-----|--|------------|------------------------|
| 2. | Fixation: Immerse in 2% paraformaldehyde, 1% glutaraldehyde and 0.15M cacodylate buffer with 2mM calcium chloride, check pH 7.4. 1h at room temp. One hour on ice. | 2 hours | 2 hours and 15 minutes |
| 3. | Washing: Wash 5 x 3min in cold 0.15 M cacodylate buffer with 2 mM calcium chloride. | 15 minutes | 2 hours and 30 minutes |
| 4. | Post-fixation: Immerse in freshly prepared 3% $K_4[Fe(CN)_6]$ 0.3 M ice-cold cacodylate buffer with 4 mM calcium chloride and 4% aqueous OsO_4 . On ice. | 1 hour | 3 hours and 30 minutes |
| 5. | Washing: Wash with bidest H_2O 5 x 3min at room temperature. | 15 minutes | 3 hours and 45 minutes |
| 6. | Filter TCH solution through a 0.22 μm Millipore syringe filter and immerse sample in filtered solution at room temperature. | 30 minutes | 4 hours and 15 minutes |
| 7. | Washing: Rinse 5 x 3min in bidest dH_2O at room temperature. | 15 minutes | 4 hours and 30 minutes |
| 8. | Post fixation: Fix in 2% OsO_4 in bidest dH_2O at room temperature. | 45 minutes | 5 hours and 15 minutes |
| 9. | Washing: Wash 5 x 3min with bidest dH_2O at room temperature. | 15 minutes | 5 hours 30 minutes |
| 10. | Place in 1% uranyl acetate in bidest dH_2O | Overnight | Overnight |
| 11. | Washing: Wash sample 5 x 3min with bdH_2O . Put in a 60°C oven for 30min. | 45 minutes | 45 minutes |
| 12. | Immerse in freshly prepared lead aspartate solution in a 60°C oven. (Walton's lead aspartate preparation: 10ml bdH_2O at 60°C, 0.040g aspartic acid, 0.066g lead nitrate. Adjust pH to 5.5 (at 60°C) with 1M NaOH (~335ul). Place solution in a 60°C oven for 30min). | 1 hour | 1 hour 45 minutes |
| 13. | Washing: Wash sample 5 x 3min with bidest dH_2O at room temperature. | 15 minutes | 2 hours |
| 14. | Dehydrate in EtOH 6 x 5min (20%, 50%, 70%, 90%, 100%, and 100%). At room temperature. | 30 minutes | 2 hours and 30 minutes |
| 15. | Immerse samples in 50% Epon 50% EtOH. (Epon resin preparation: 9.25ml Glycid ether (11.1g), 6.25ml DDSA (6.19g), 5ml MNA (6.25g), mix very well 0.325ml BDMA. Mix & degas). | 30 minutes | 3 hours |
| 16. | Immerse samples in 100% Epon | 1 hour | 4 hours |
| 17. | Embed samples in Silver Conductive Resin | 4 hours | 8 hours |
| 18. | Place embedded samples in 60°C oven | 48 hours | 56 hours |

2.4 Tissue preparation for serial block face electron microscopy

Samples embedded in standard Epon are usually non-conductive and scanning them in EM leads to surface charging which could lead to adverse effects such as image distortions and improper cutting. In order to avoid these problems, we embedded the samples in conductive resin. The last step of the staining protocol (No. 17 above in protocol) is crucial. It must be ensured that the silver conductive resin is evenly distributed over the fish brain and that there are no air bubbles between the surface of the brain and the silver resin surrounding it. This is facilitated by first mixing the two component epoxy glue (Epo-Tek EE129-4) with silver particles in ratio of (A:B, 1.25:1) and then dipping the brain in the mixed resin multiple times, ensuring that all brain areas of interest are in direct contact with the conductive resin. The final sample obtained is a hard conductive opaque silver block, which needs to be further processed before it can be imaged.

First, the block has to be trimmed from all sides to remove unnecessary extra silver resin and also to remove the brain regions that are not of interest. It is desired to obtain a sample that is as small as possible. The block at the final stages therefore contained only the olfactory bulbs. The trimming of the sample involves multiple steps as described below (Fig. 8).

Step 1. Manual trimming of the sample was avoided as it might cause damage to the sample. Instead, freshly prepared glass knives with sharp edges were used in a microtome that can cut as thin as 0.5 μm . The silver block was labeled according to the position of the embedded brain inside. Trimming of the silver block then started from the caudal end.

Step 2. After loading the sample into the microtome, the caudal end was brought close to the edge of the knife. Positioning was controlled through the eyepiece of the attached microscope. Initially, thicker sections (5-10 microns) were cut. The glass knife was replaced after 20-30 steps to avoid rough and uneven cuts.

Step 3. Trimming started from the hindbrain and proceeded along the mid brain towards the telencephalon. As the olfactory bulbs were approached, step size was decreased to (1-2 μm)

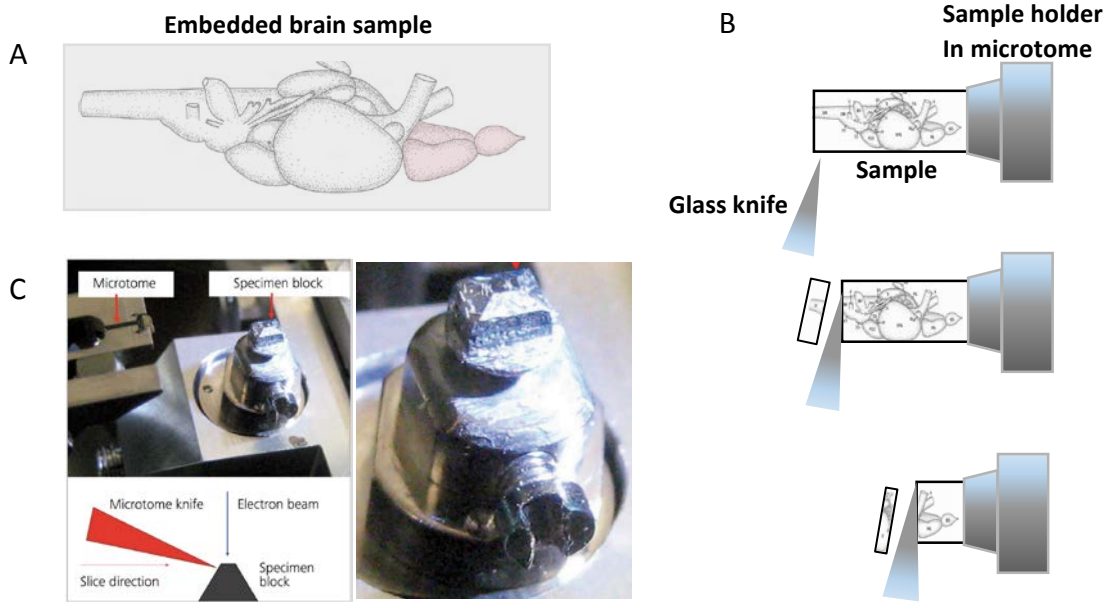


Fig. 8: Embedding and resizing of the sample.

(A) Embedding of the adult brain in silver conductive resin. The brain was positioned ventral side up. (B) Trimming was performed using a microtome with a sharp glass knives and proceeded from the caudal end of the brain. (C) After the trimming of the sample all the sides should have clean surfaces and should be shaped like a pyramid. (Source;http://www.zeiss.com/microscopy/en_de/products/scanning-electron-microscopes/merlin-life-science).

and the knife was changed more frequently. Trimming stopped after all of the telencephalon was cut.

Step 4. The block was trimmed on all six sides to remove extra silver resin, resulting in a pyramid-shaped sample block that contained only the two olfactory bulbs. Care was taken not to cut into any region of the OB. At the end all the trimmed sides should have clean surfaces and should be parallel. The sample should look pyramid shaped as shown below (Fig. 8).

2.5 Serial block face 3D electron microscope

Brain samples were imaged using an SEM. Two SEMs were used: an FEI QuantaFEG 200 or a Zeiss Merlin electron with a Gemini II column. The FEI QuantaFEG 200 is a variable-pressure microscope that can be operated either under standard high vacuum conditions, or with an adjustable low water pressure inside the vacuum chamber (low vacuum mode). In low vacuum,

Methods

charging of samples is reduced because the incoming electron beam ionizes water molecules which then remove charges from the sample surface as they are pumped out of the vacuum chamber. However, low vacuum conditions also degrade image contrast and beam focus by scattering of electrons.

The Zeiss Merlin can only be operated in high vacuum and therefore requires highly conductive samples. The Zeiss Merlin provided two important advantages: first, it contains technology that allows for very sharp focusing of the electron beam at very low landing energies (<2 keV). As such low landing energies are important for SBEM, this technology increases the effective resolution. Second, the Zeiss Merlin allowed for the acquisition of image data at 10 times higher speed (sampling rate: 2 MHz) than the FEI QuantaFEG 200 (sampling rate: 200 kHz).

Both microscopes were equipped in the vacuum chamber with an automated microtome (3View, Gatan) that cuts sections with a diamond knife (Diatome) (Denk and Horstmann., 2004). The microtome was controlled by the software package DigitalMicrograph® (Gatan; Fig. 9). Data acquisition was carried out using a data acquisition system that was also controlled by DigitalMicrograph® (Gatan). Backscattered electrons were detected by a silicon diode detector. The signal was amplified by a preamplifier and further amplified by a main amplifier (Gatan). Prior to a long acquisition, short series of images were acquired to ensure that thin sections could be obtained consistently (≤ 30 nm). In order stabilize the conditions in the recording chamber the sample was kept in the vacuum chamber overnight before starting a long-acquisition. To cover a large area, tiling was performed, which was controlled by DigitalMicrograph®. The overlap between adjacent tiles was approximately 10%.

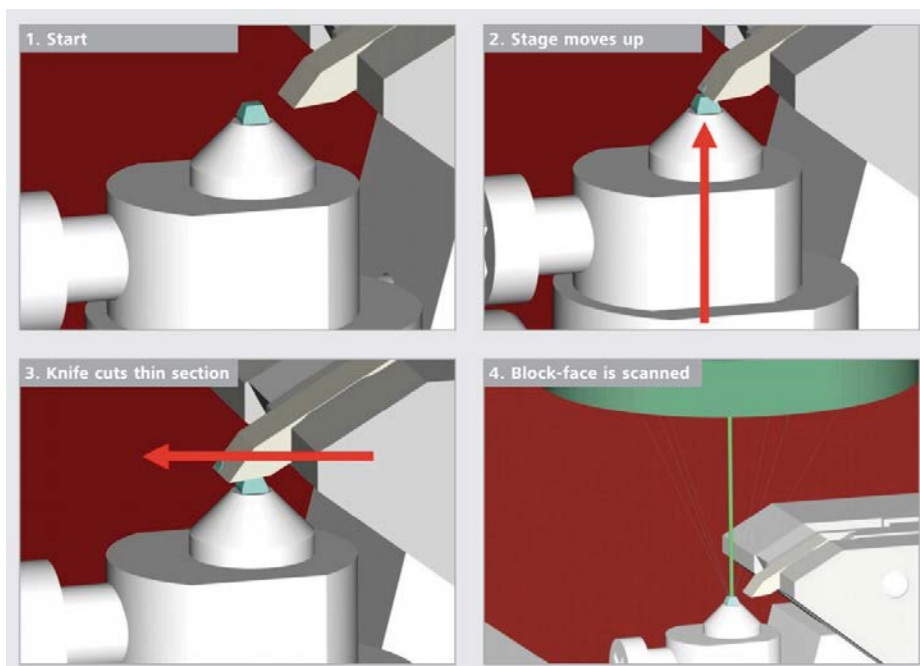


Fig. 9: Operation of the automated microtome in the vacuum chamber.

(1) The sample is moved up by a distance equal to the cutting thickness (usually 25 nm). (2) A section is removed from the sample surface by the automated microtome. (3) The knife proceeds beyond the sample to remove debris from the surface. (4) The block face is scanned by the electron beam to record an image. (Source; http://www.zeiss.com/microscopy/en_de/products/scanning-electron-microscopes/merlin-life-science).

2.6 Image processing

Stacks of raw 16 bit images were processed, registered and stitched using custom software tools in MATLAB written by Adrian Wanner that allowed for parallel batch processing of large datasets. For image registration, translational offsets between neighboring image tiles were calculated using an optimized reduced normalized cross-correlation procedure. The offsets were used to optimize the tile positions in a global total least square displacement sense. Image contrast was normalized by fitting a Gaussian distribution to the pixel intensity histogram and thresholding at 1.5 – 3 standard deviations around the peak of the Gaussian distribution to convert the images to 8 bit. After stitching, each section was inspected to identify artifacts that may have been caused by software errors or debris. The large stack consisted of 3918 sections, each with 40 tiles. In a total of >150,000 tiles, 70 corrupted tiles were identified and replaced by tiles from adjacent sections. Finally, image stacks were divided into cubes of 128 x 128 x 128 voxels for dynamic data loading in KNOSSOS or PyKNOSSOS.

2.7 Neuronal skeleton tracing and synapse detection

Tracing of neurites and synapse detection were performed using the freely available software package KNOSSOS (Helmstaedter et al., 2011) or PyKNOSSOS, a novel software package with extended functionality written in PYTHON (Wanner et. al., submitted). Both programs dynamically access small data cubes during user actions. This dynamic data loading strategy enables instantaneous seamless browsing and, in PyKNOSSOS, multi-scale zooming. In tracing mode, users can assign nodes and connections between nodes (edges) to define a skeleton representing the morphology of a neuron. Four different viewports are provided which allow the data to be seen in XY, YZ, XZ and orthogonal view and help in better visualization of the data (fig. 10). The reconstructed skeleton of the neurons can be further visualized in full 3D, as lines, points or tubes. Synapse detection was performed using PyKNOSSOS, which allows users to define synapses by two mouse clicks. Synapses were divided into four different categories and were given confidence levels ranging from 0 to 100% (Fig. 10). The previously traced skeleton of an individual neuron was navigated a second time for identification and labeling of individual synapses. An automated procedure was used to guide the user along all branches of the skeleton. Different synapse categories could be assigned different colors for ease of visualization. A synapse was defined by clicking on the synaptic cleft and then clicking again inside the partner neuron. At each click, a node was deposited, and the node on the synaptic cleft was automatically connected to the nearest node in the skeleton. Synapses were identified visually by vesicle clusters making contact with the plasma membrane.

Methods

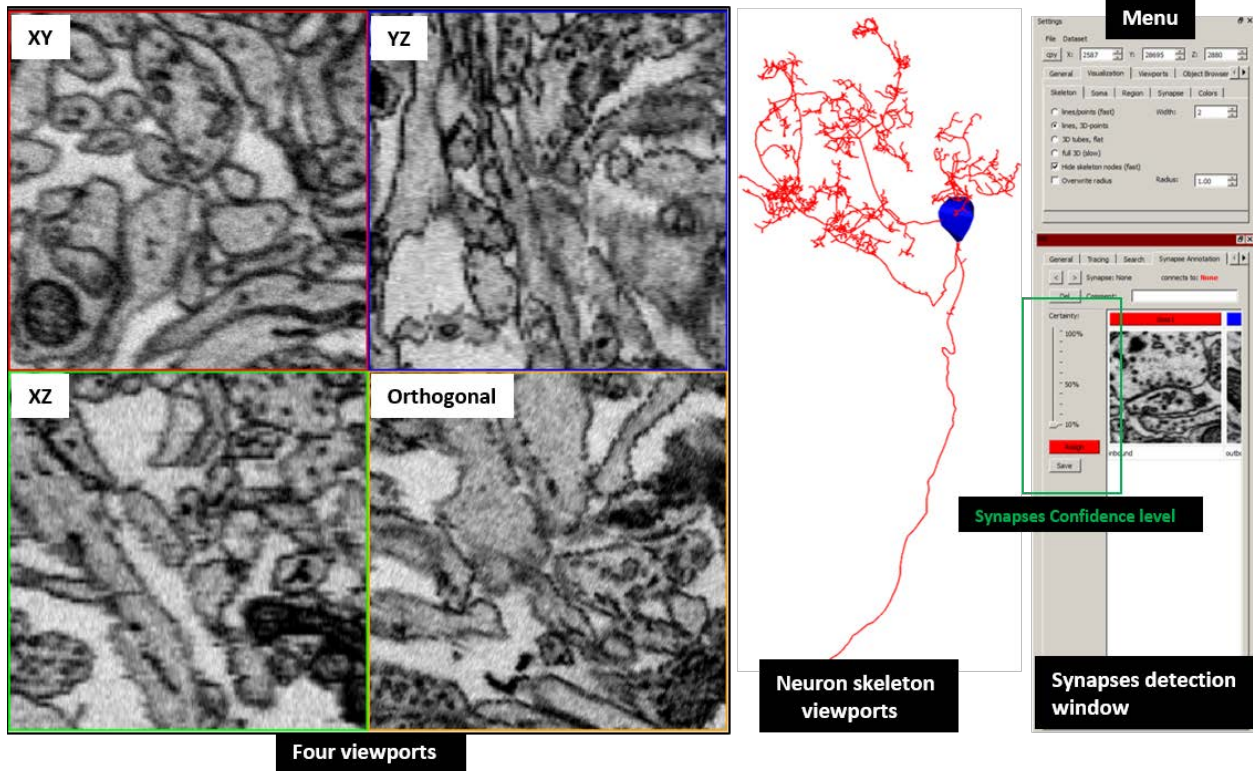


Fig. 10: PyKNOSSOS.

Overview of PyKNOSSOS. There are four viewports for data visualization: XY, YZ, XZ and orthogonal viewports. The skeleton viewport allows to visualize reconstructed neurons. Synapse detection mode: four synapse classes (Inbound, Outbound, Reciprocal and Sensory) were predefined. Each synapse was assigned to one of these classes and scored with a confidence level (certainty; green box).

RESULTS

3.1 Measuring granule cell sparseness in OB by two-photon imaging.

To determine whether odors evoke sparse activity in the population of granule cells, odor-evoked calcium signals were measured in an explant preparation of the adult zebrafish brain with intact nose (Zhu et al., 2012). Neurons in the olfactory bulb were loaded with rhod-2-AM, a red fluorescent calcium indicator, by bolus injection ($n = 4$ fish) (Brustein and Marandi, 2003; Stosiek and Garaschuk, 2003; Yaksi and Friedrich, 2006) and changes in rhod-2-AM fluorescence were measured by two-photon microscopy (Denk and Strickler, 1990). Wide range of odors like food odor and different amino acids were used to measure responses in granule cells (10^{-5} M; Fig. 11). Amino acids are natural odors for zebrafish with response thresholds in the nanomolar range and maximal concentrations within food sources in the millimolar range (Carr, 1988; Michel and Lubomudrov, 1995). HuC-YC, which is a yellow fluorescent transgenic marker, was used to identify mitral cells during imaging (Masino et al., 2003; Li and Mack, 2005).

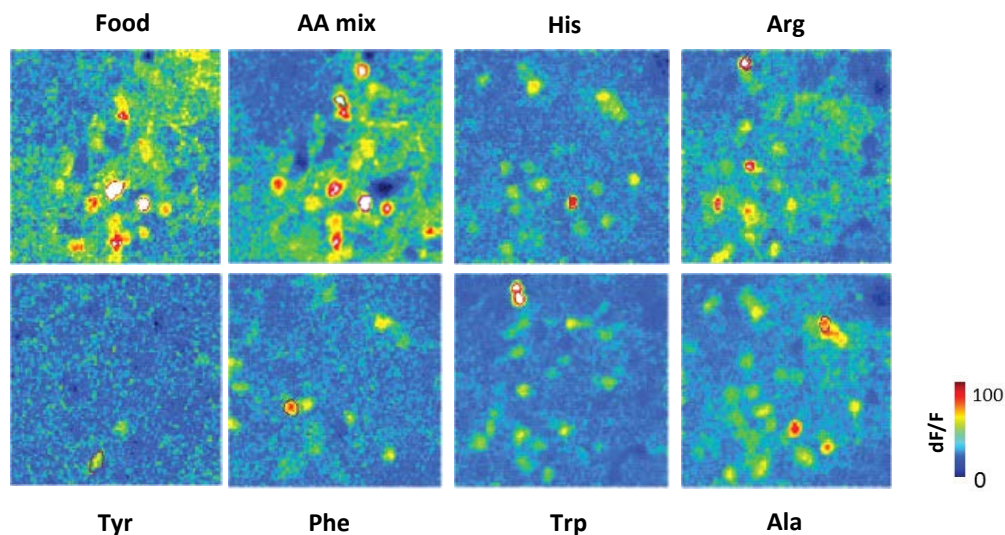


Fig. 11: Granule cell responses to odors.

Two-photon calcium imaging of neuronal odor responses in the granule cell layer. Each odor was applied twice in pseudo-random order and responses to the same odors were averaged. Concentration of amino acids was 10^{-5} M.

Density of granule cells responses

Two-photon calcium imaging showed that many neurons in the granule cell layer responded to odors ($n = 4$ fish). In order to quantify the density of responses in the granule cell layer we marked individual somata in the granule cell layer by regions of interest (ROIs) on the raw fluorescence images (Fig. 12). Relative changes in fluorescence intensity (dF/F) after odor stimulation were measured in all ROIs and plotted together for each fish. The results show that many granule cell responded to odor stimulation.

The density of granule cell responses was further analyzed by determining the fraction of cells that responded with $dF/F > 20\%$, which is a conservative threshold. 62% of cells in the granule cell layer showed responses with $dF/F > 20\%$. In addition, we determined the population sparseness (Vinie and Gallant, 2000), a measure that varies between 0 and 1. A population sparseness of zero indicates that all of the given cells are responding equally to different odors, while a population sparseness of 1 means that only one cell responds to each stimulus. We found the population sparseness to be 0.48. Together, these results show that odor responses in the granule cell layer are not sparse, contrary to the prediction of the “SIR” (Sparse incomplete representation) model (Koulakov and Rinberg, 2011).

Results

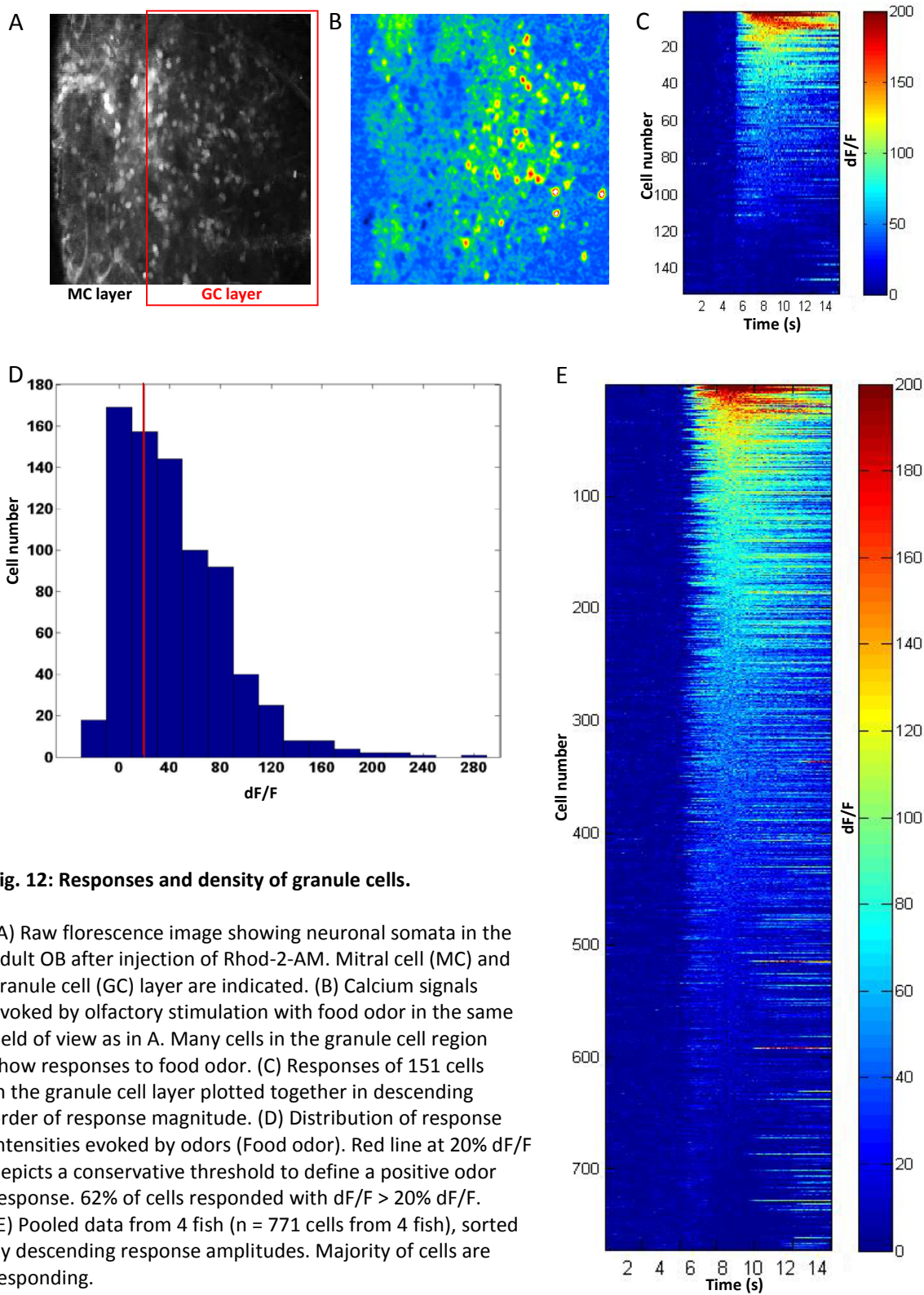


Fig. 12: Responses and density of granule cells.

(A) Raw fluorescence image showing neuronal somata in the adult OB after injection of Rhod-2-AM. Mitral cell (MC) and granule cell (GC) layer are indicated. (B) Calcium signals evoked by olfactory stimulation with food odor in the same field of view as in A. Many cells in the granule cell region show responses to food odor. (C) Responses of 151 cells in the granule cell layer plotted together in descending order of response magnitude. (D) Distribution of response intensities evoked by odors (Food odor). Red line at 20% dF/F depicts a conservative threshold to define a positive odor response. 62% of cells responded with $dF/F > 20\%$ dF/F. (E) Pooled data from 4 fish (n = 771 cells from 4 fish), sorted by descending response amplitudes. Majority of cells are responding.

3.2 A small scale study to explore SBEM methods

In order to test the imaging, staining and embedding methods for SBEM we acquired a small stack of EM images from the glomerular region of the OB using an FEI Quanta FEG-200 microscope. The QuantaFEG 200 offers options for low or high vacuum with an automated ultramicrotome inside the vacuum chamber. The adult zebrafish brain tissue was initially fixed, stained using the ROTO – Walton (reduced OsO₄ (osmium) – thio carbonylhydrazide – OsO₄) method with lead aspartate to contrast membranes (Tapia et al., 2012) and then embedded in epon resin. Various changes were made to the original protocol (Tapia et al., 2012, see Methods 2.3) to optimize penetration of reagents into the tissue. In particular, the incubation times of many steps were increased. A total of 35 samples were processed to select the best samples for further analysis. Criteria for sample selection were tissue stability, block strength, homogeneity of staining, orientation of sample in the block and the preservation of morphology inside the OB. Earlier samples (n = 22) that were embedded in epon without silver particles displayed signs of charging and image distortions as well as improper cutting of the tissue by automated knife during imaging. These issues were completely alleviated in samples embedded in resin containing silver particles.

A stack was obtained from the anterior region of the olfactory bulb in a sample embedded in silver-containing resin (Fig. 13). The field of view was 35 x 70 μm . The area of the stack was selected to contain glomerular neuropil. The stack was obtained over a period of one week during which the microscope was constantly imaging. Each image plane consisted of 2 tiles with 4096 x 4096 pixels and overlap of 10% between the tiles. A total of 1000 sections were obtained with slice thickness of 30 nm each, resulting in a volume of 35 x 70 x 30 μm^3 per section with a resolution desired for neuronal circuit reconstruction (11.3 x 11.3 nm^2).

To understand and visualize the general architecture of neurons in this stack it was essential to trace individual neurons. All the somata (n = 62) in the stack were identified and all the branches arising from these somata were traced using PyKnossos (Wanner et al., submitted). The total tracing length of all the neurons was 7.3 mm. Many of the 62 neurons had processes which did not branch profusely (Fig. 14). Synapses identification did not reveal synaptic connections

Results

between the traced neurons although they do have synapses with other unknown neurons. The average soma size was 6.5 ± 0.77 microns (mean \pm S.D.), which is smaller than the reported sizes of mitral cells (Pinching and Powell, 1971). These observations indicate that most or all of the 62 neurons were interneurons, presumably periglomerular and short-axon cells.

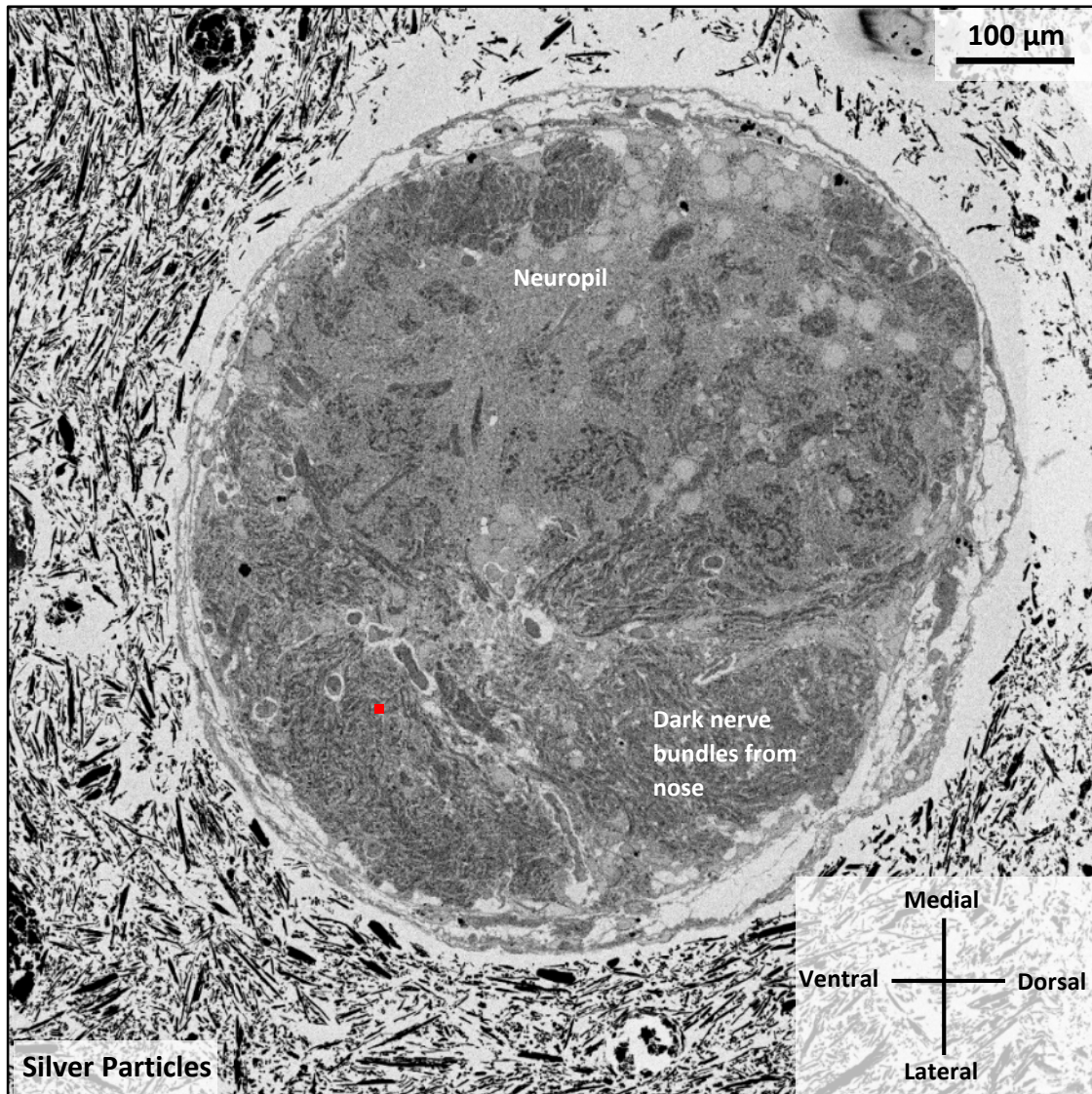


Fig. 13: Overview of the adult OB (left OB).

Low-magnification overview of an OB sample. Black objects in the resin outside the OB are silver particles. The red area indicates the ventro-lateral area from where the stack was imaged. The dura mater was left intact. Dark profiles inside the OB are olfactory nerve bundles coming from the nose. Light regions are the somata and neuropil of OB.

Results

In conclusion, the stack helped us to optimize the staining protocol, helped resolving technical issues during long acquisitions, and helped in choosing the best dimensions for the larger stack. The results demonstrated that a considerably larger volume was required to completely reconstruct mitral cells and determine the complete distribution of synapses on the dendrites of mitral cells. Ideally, the data should extend through both mitral and granule cells layers. To achieve this, we used another electron microscope (Zeiss Merlin) that can be operated only using high vacuum. It maintains a sharply focused beam and provides a large range of beam currents in the regime of very low E_L (<2 keV). This electron microscope allowed for faster data acquisition and also provided higher resolution for identification of synapses.

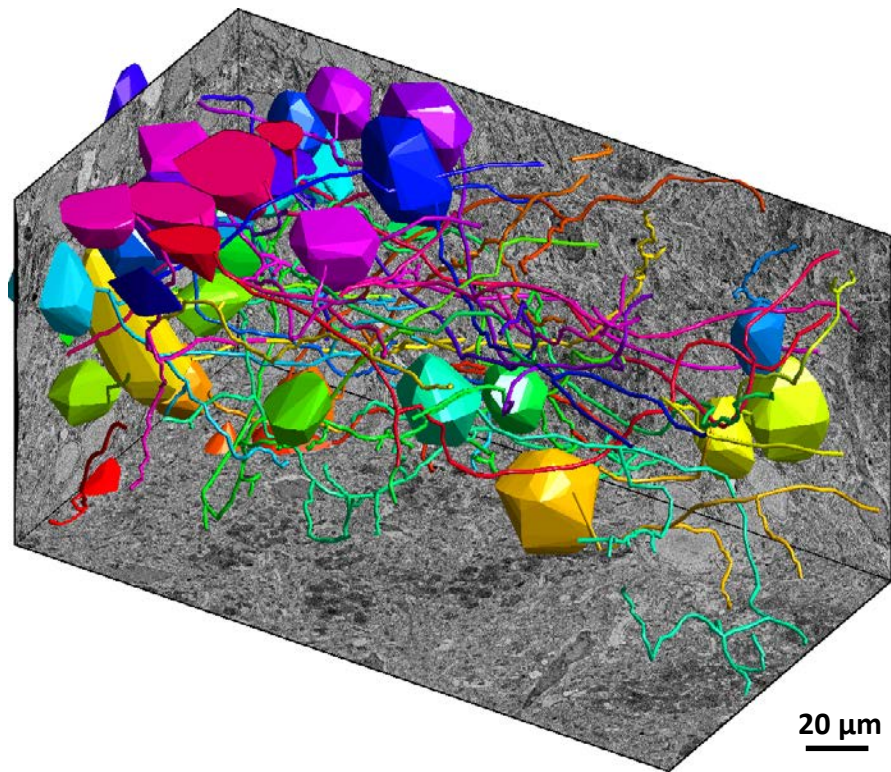


Fig. 14: Neuron reconstruction.

A total of 62 somata and branches of all these somata were reconstructed. Background shows the original EM data (stack covering a volume of $35 \times 70 \times 30 \mu\text{m}^3$; 1000 sections). Large structures represent somata; lines represent traced neurites. Different colors are given randomly to different neurons.

3.3 Large scale detailed SBEM imaging of adult olfactory bulb

In order to understand the detailed connectivity in the adult zebrafish olfactory bulb it is important to have a large dataset which encompasses both glomerular/mitral cell layer and interneuron layer (Fig. 15). To cover such a large volume we used an ultra-fast, high resolution, Zeiss Merlin electron microscope with a Gemini column with an automated microtome inside the vacuum chamber. This microscope can be operated only in high vacuum and maintains a highly coherent beam and provides a large range of beam currents in the regime of very low EL (<2 keV). The resolution and signal to noise ratio of the microscope are significantly higher. The speed of acquisition using Zeiss Merlin was 2 MHz. In the previous stack using Quanta microscope (Results 3.2) the speed of acquisition was 200 - 250 kHz.

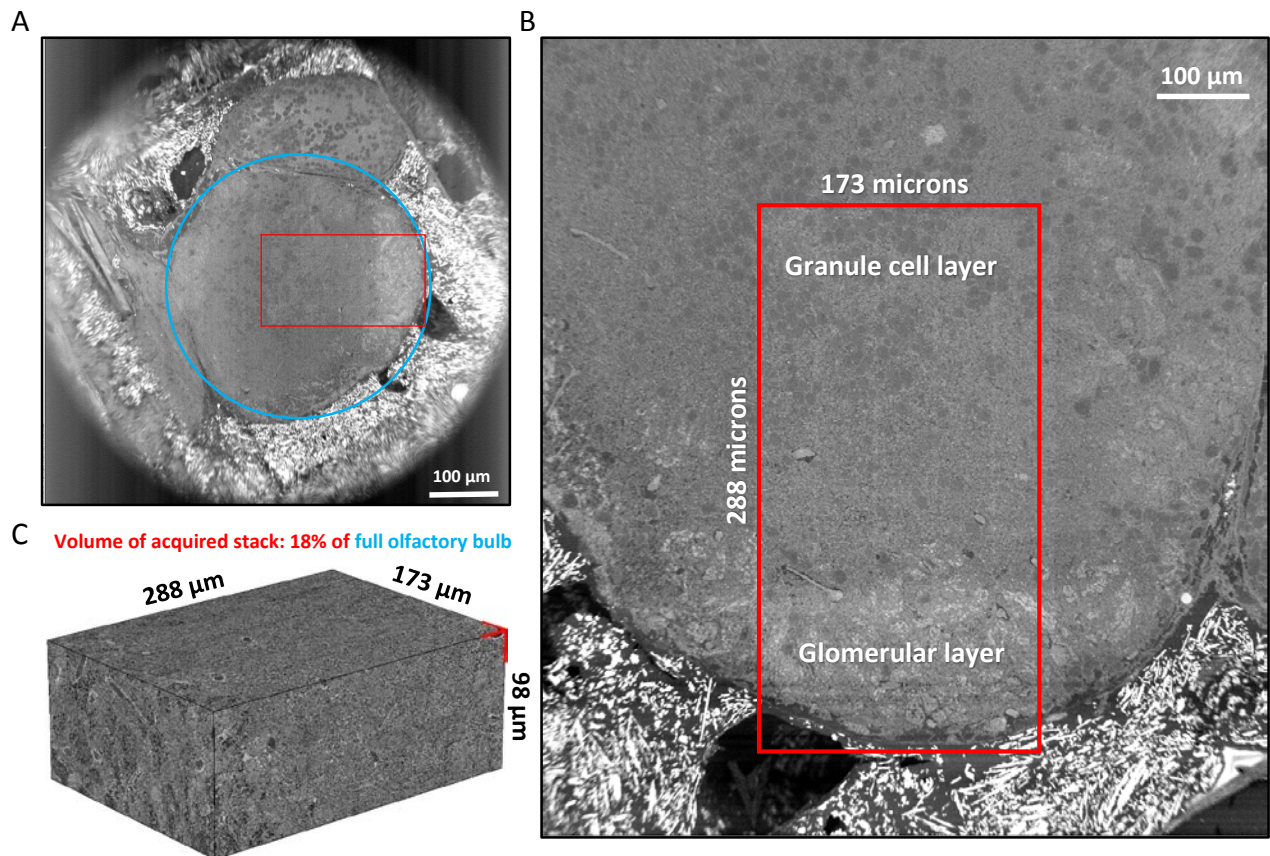


Fig. 15: Large stack from olfactory bulb: overview.

(A) EM overview of the OB. (B) The rectangular area shows area of the recorded stack. Glomerular/mitral cell and granule cell layers are present in the imaged area. Silver resin (detail in methods 2.4) is touching the OB. (C) Volume of the acquired stack. The total volume of the imaged stack is 18% of the entire OB.

Results

To image planes of a sufficiently large area, 40 tiles were combined into a large composite image in each plane with an overlap of 10%. Overlapping areas were exposed multiple times to the electron beam but this did not reduce the image quality. We initially choose tiles of 8192 x 8192 pixels but this caused mild edge distortions. We therefore reduced tile size to 4096 x 4096 pixels (Fig. 16). The complete stack was 288 x 173 x 98 μm^3 in volume. The total number of sections in the stack was 3918 with slice thickness of 25 nm. Voxel size in lateral directions was 9 x 9 nm^2 . This resolution was clearly sufficient to visually detect individual vesicles and label synapses. Landing energy was kept constant at 1.5 keV. The beam current initially used was 440 pA but was reduced to 412 pA after 1800 slices. Reduction in beam current had no effect on the quality of imaging and acquisition.

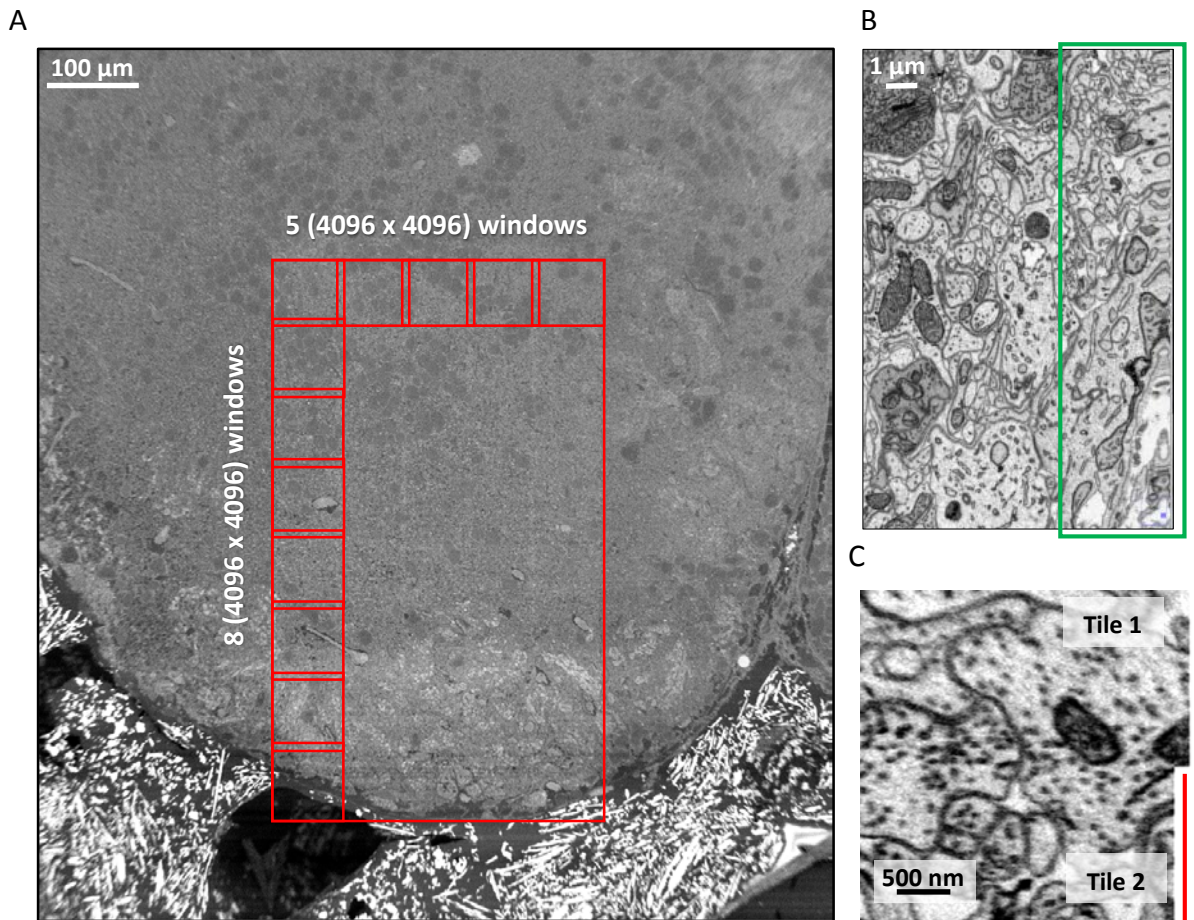


Fig. 16: Edge distortions.

(A) A total of 40 tiles with 4096 x 4096 pixels each were acquired with an overlap of 10% in each image plane. (B) Using 8096 x 8096 windows caused edge distortions (see area marked by green outline). (C) Overlap between adjacent 4096 x 4096 tiles did not affect image quality and synapse identification.

Results

The total time to image the stack was 32 days including overhead. The total data size was 6.4 TB unstitched at 16 bit/voxel and final size was 2.2 TB stitched at 8 bit/voxel. The total volume of the imaged stack covered ~18% of the entire OB (Fig. 15). After acquisition was complete and tiles were stitched in each plane, each of the 3918 sections was manually checked multiple times to detect any distortions, residual debris or other artifacts. 70 sections were either completely removed or corrupted tiles were replaced by tiles in preceding or following sections. The stack was then divided into small cubes of 128 x 128 x 128 voxels so that it could be dynamically loaded in PyKNOSSOS for further analysis (explained in methods 2.6).

We observe non-uniform extracellular space in the acquired data stack (Fig. 17). Extracellular space is abundantly present in the glomerular layer and the plexiform layer of the olfactory bulb. In the deeper layers of the olfactory bulb, there is less extracellular space. We did not find extracellular space in all the different samples we imaged. It is most likely an artifact which was caused during the staining of the tissue (Briggman et al., 2015).

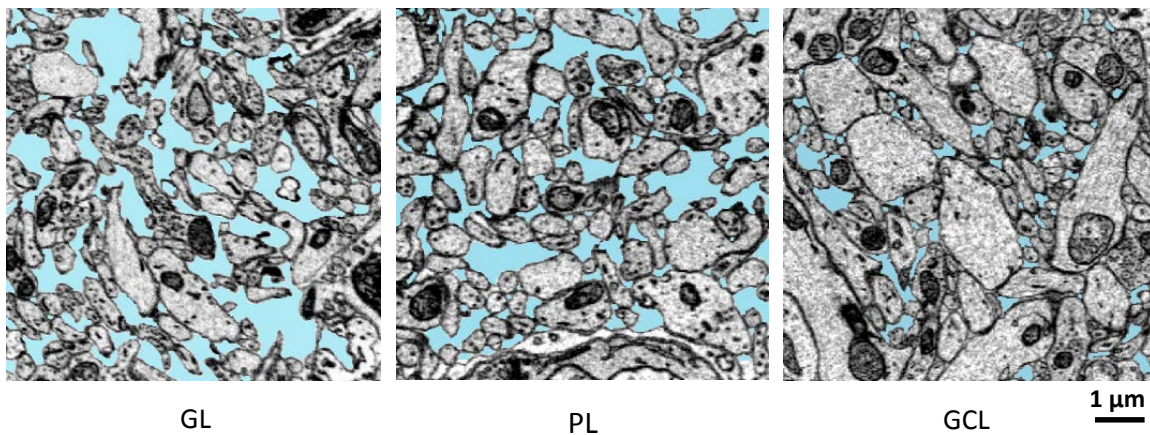


Fig. 17: Extracellular space.

In the GL and parts of the PL, but not in the GCL, considerable amount of extracellular space are visible. Extracellular space is shown in blue, manually labelled using Fiji.

3.4 Detailed analysis from the adult olfactory bulb SBEM dataset

3.4.1 Number of neurons in the dataset

In order to estimate the total number of neurons in the stack and their distribution we first labeled all somata using KNOSSOS (Helmstaedter et al., 2011). The total number of somata detected was 4892 (Fig. 18). The total number of mitral cells and interneurons in an adult OB has been estimated to be 1500 MCs and ~23,000 interneurons (Wiechert et al., 2010; Zhu et al., 2013). The number of detected somata in the stack is therefore consistent with the number expected for 18% of the OB volume.

In addition, we detected dark objects by thresholding gray levels. These are likely to mainly comprise mainly of blood vessels and sensory axons. Based on the distribution of somata and neuropil we distinguished three different layers in the OB: the superficial glomerular layer (GL), an underlying plexiform layer (PL), and the deep granule cell layer (GCL) (Fig. 18, 19).

Previous studies showed that the GL contains somata of two types of output neurons, mitral cells and ruffed cells and also has subpopulations of interneurons (Byrd et al., 2005; Fuller et al., 2006, Braubach et al., 2012; Zhu et al., 2013). The GL also contains abundant sensory axons that are stained darkly and have large axon terminals (Fig. 20 A). The neuropil in the PL mainly consists of dendrites of mitral cells and different types of interneurons. Somata are rare in this layer (Fig. 20 B). GCL are assumed to be dominated by granule cells but is likely to also contain other, rarer cell types such as deep short axon cells (Michel et al., 2002). Somata in the GCL appeared relatively homogeneous in their size and appearance, supporting the assumption that most of them are granule cells (Fig. 20).

Results

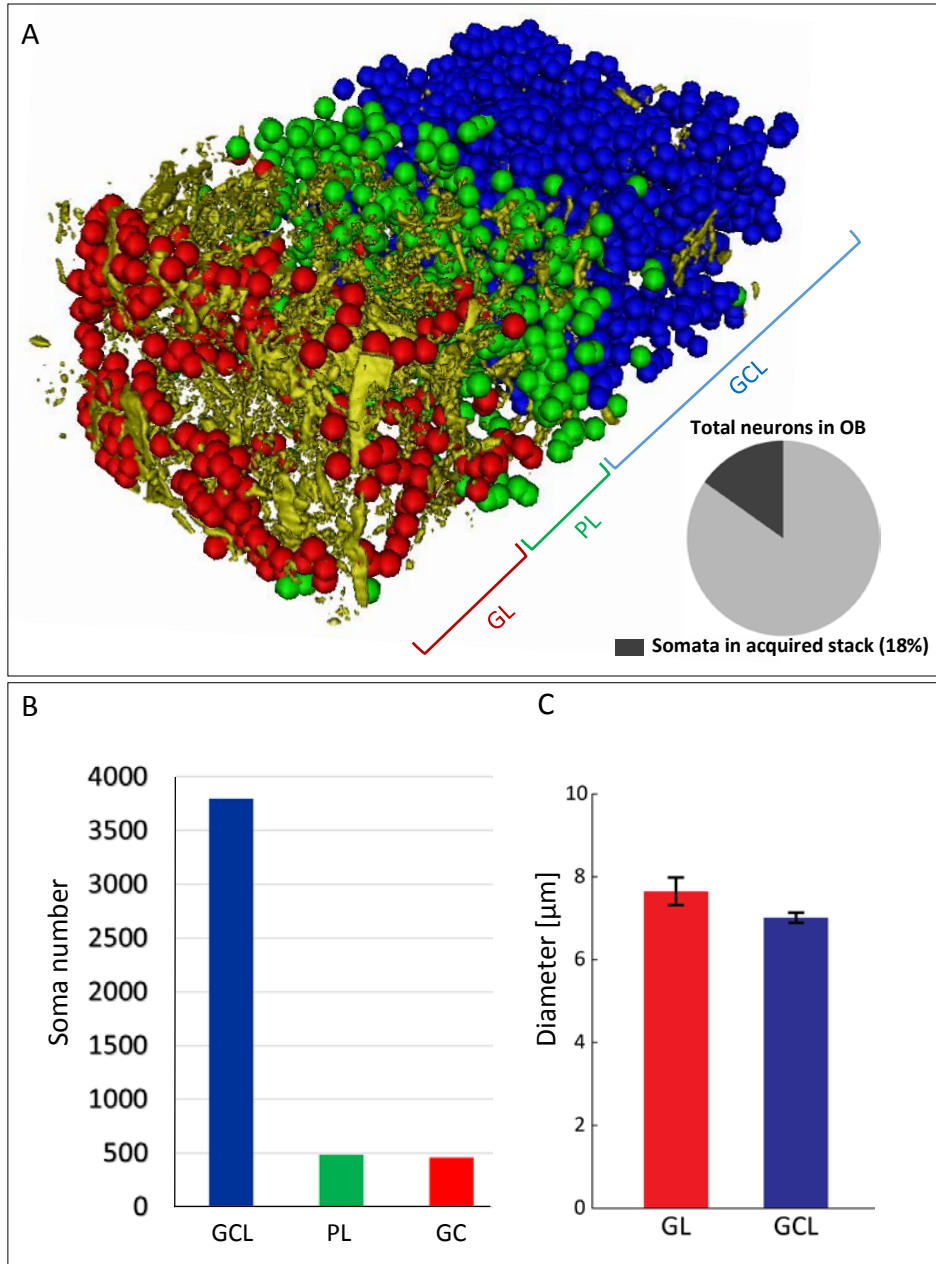
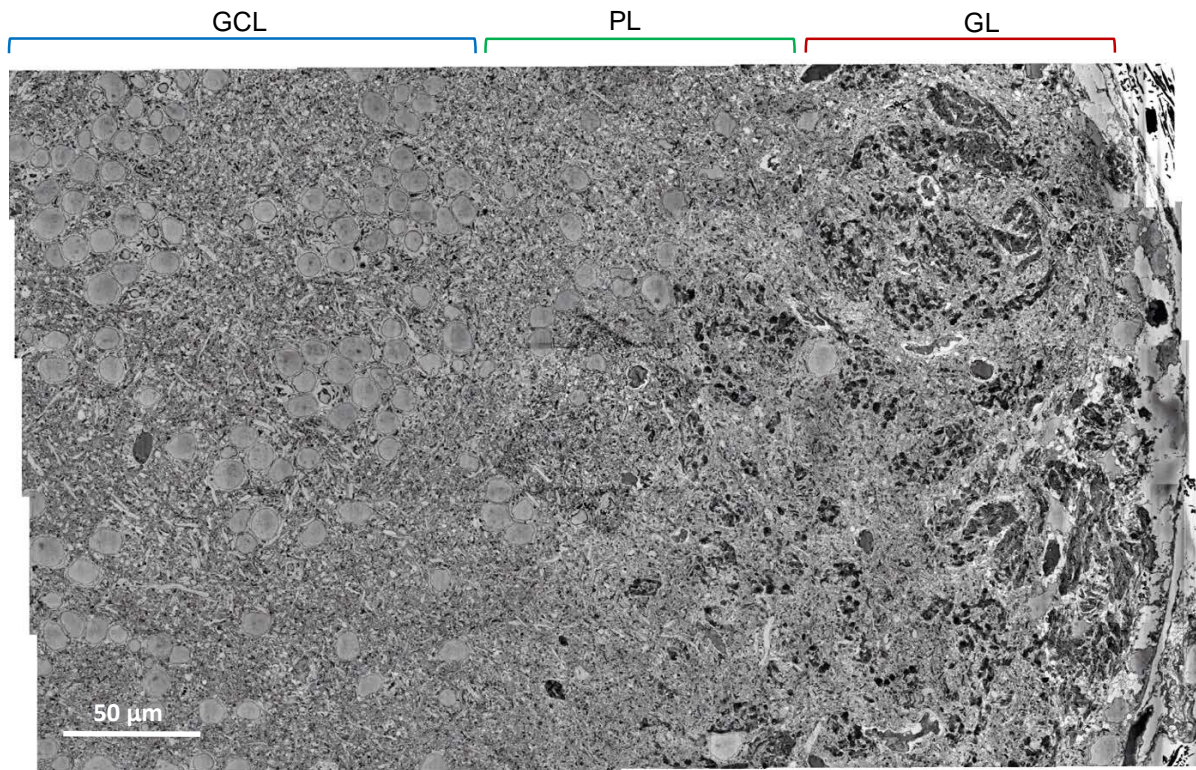


Fig. 18: Somata in the large stack.

(A) Distribution of somata ($n = 4892$) in the stack. Somata in different layers are labeled by different colors (red, green, blue). Dark objects, which are mainly sensory neurons and blood vessels, were identified by thresholding and are shown in yellow. (B) Number of somata detected in each layer. (C) Average soma diameter (μm) of 10 cells in the GL and 10 cells in the GCL. The mean soma diameter is not statistically different ($p = 0.16$) (student's t test).

Results

A



B

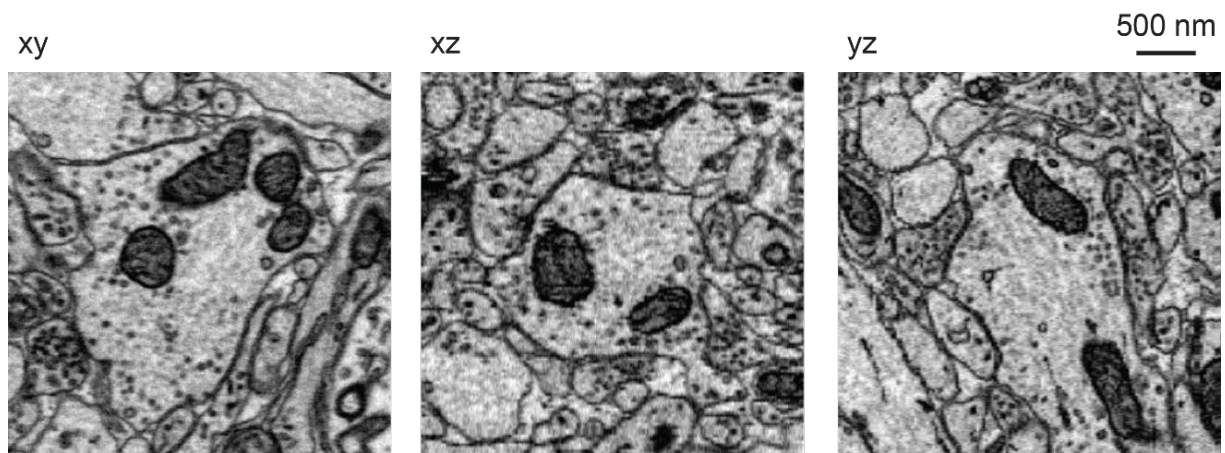
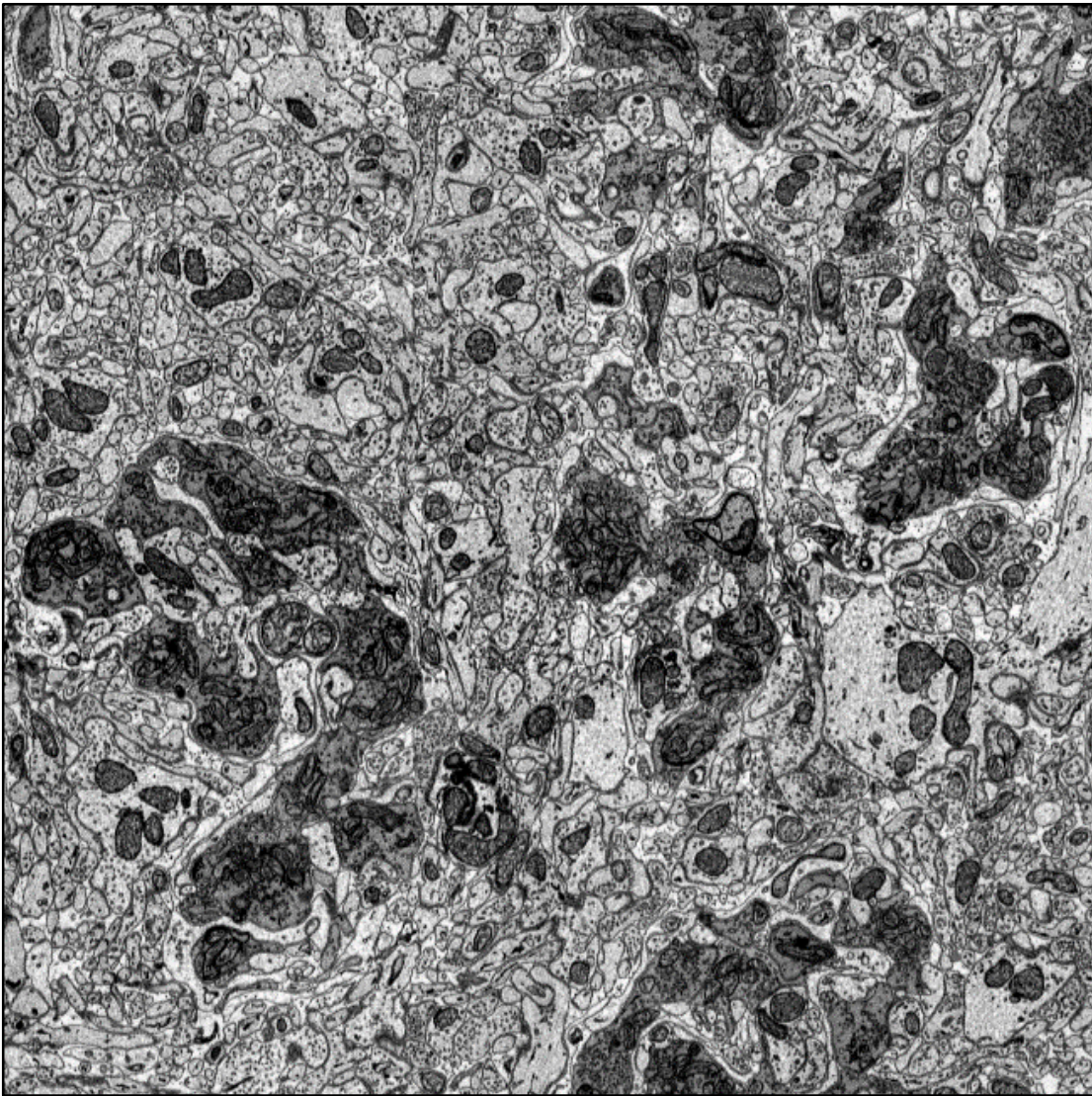


Fig. 19: Layers in the olfactory bulb.

(A) Section through the OB. Layers are indicated. (B) Inset images show re-slices at higher magnification. Resolution is clearly sufficient to identify synapses.

Glomerular layer

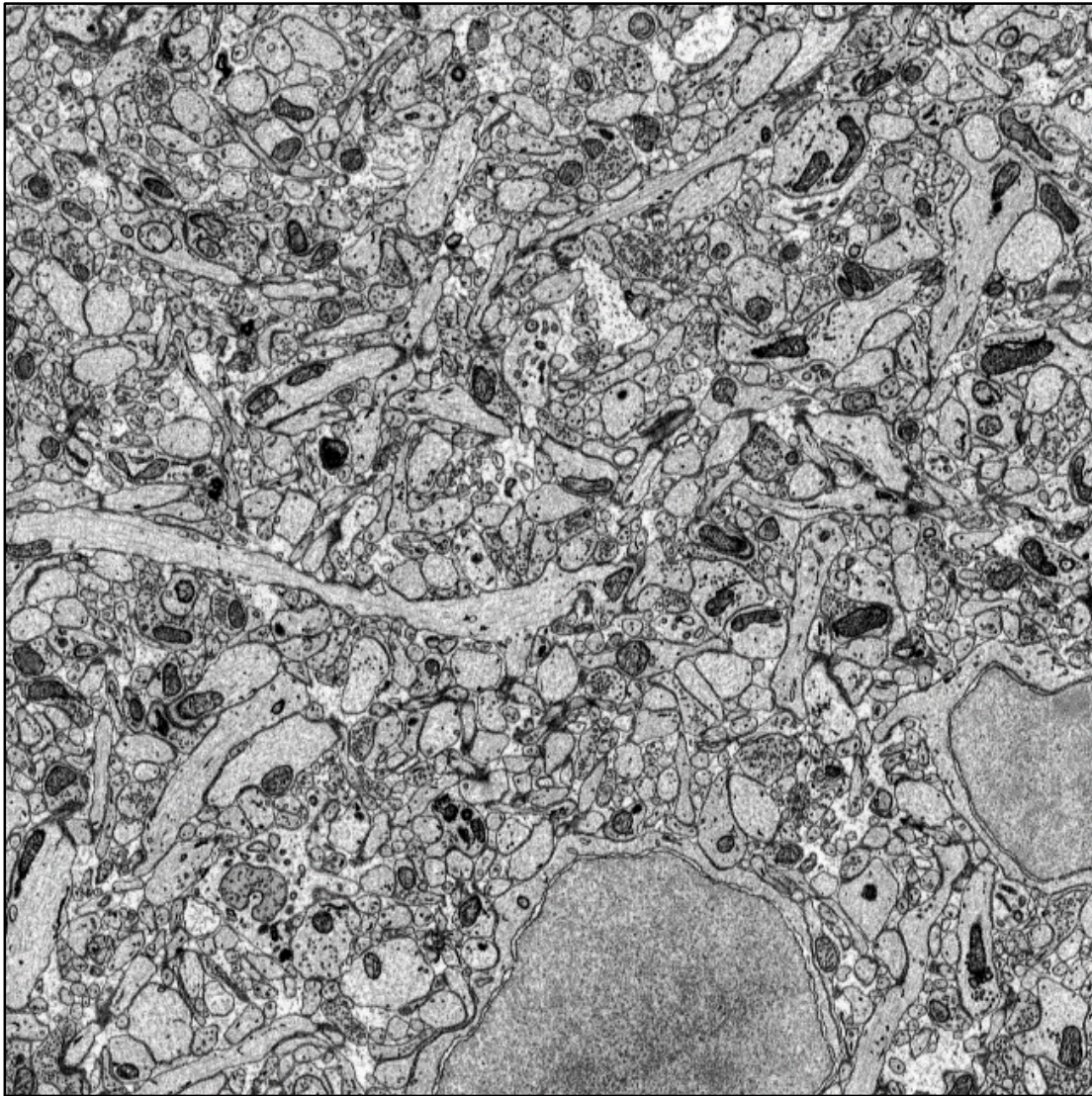


20 μ m

Fig. 20 A: GL layer.

The GL contains extensive neuropil including many sensory axons that are stained darkly and have large terminals. Somata are rare.

Plexiform layer

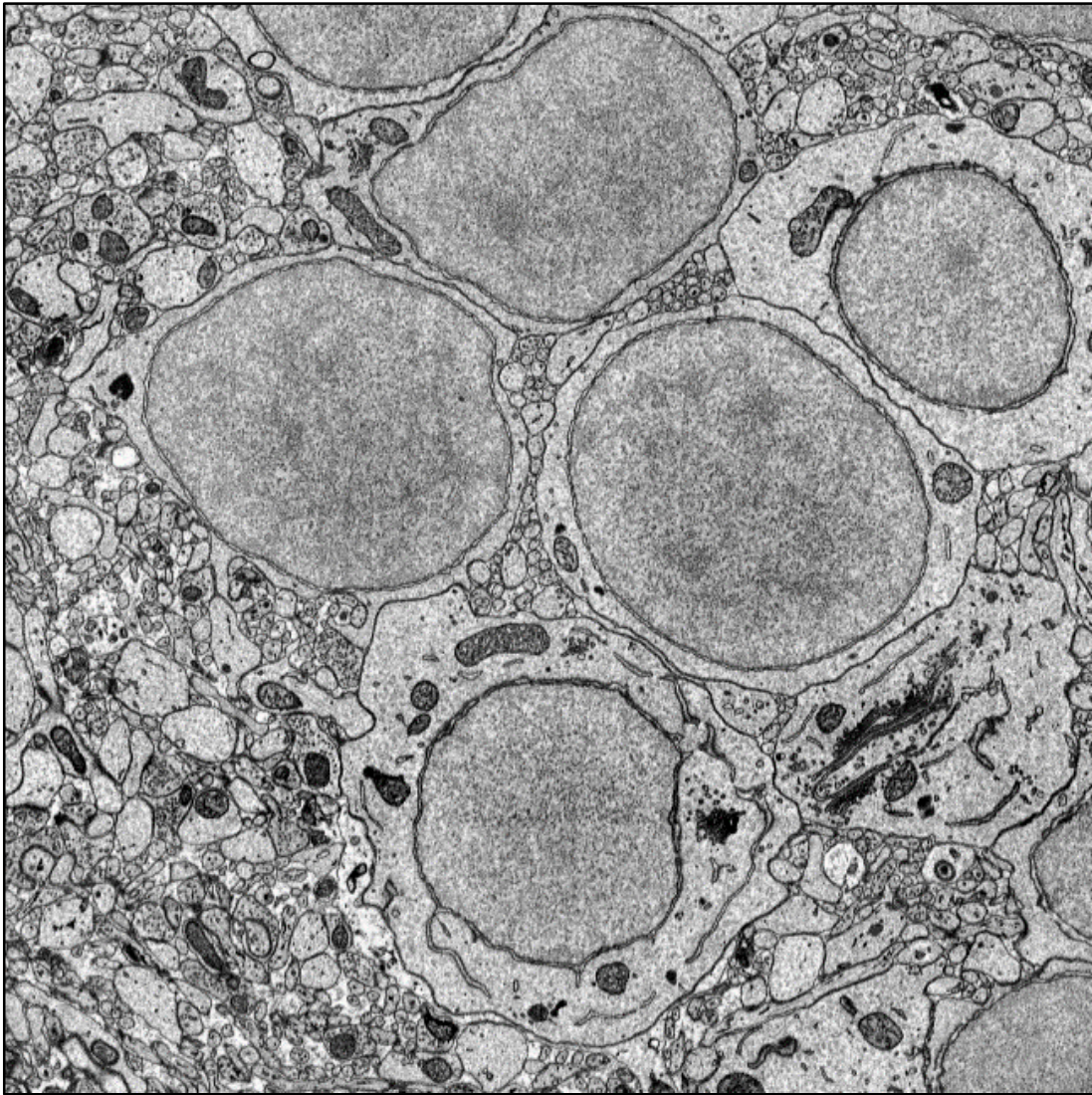


20 μ m

Fig. 20 B: PL layer.

The PL contains a high neuropil fraction but sensory axons are absent, indicating that neurites are contributed mainly by mitral cells, interneurons, and possibly centrifugal inputs. The density of somata is low.

Granule cell layer



20 μm

Fig 20 C. GC layer.

The GCL contains a high density of somata that are homogeneous in appearance and relatively small. Most of these somata are likely to be granule cells.

3.4.2 Glomerular structures

The zebrafish glomerular layer contains approximately 140 distinct glomeruli and a region containing additional, small glomerular structures that have not been delineated precisely (Braubach et al., 2012). Based on light microscopic studies, glomerular structures in adult zebrafish OB have been categorized and classified into different groups (Braubach et al., 2012). The size and number of glomeruli varies between regions of the OB (Braubach et al., 2012). The ventro-lateral region covered by our stack contains primarily small, densely packed glomerular structures that have not been analyzed in detail by light microscopy (Braubach et al., 2012). We term these structures “microglomeruli”. It is currently unknown whether individual microglomeruli are innervated by distinct subsets of ORN axons, indicating that they are independent functional units, or whether different microglomeruli are innervated by overlapping sets of ORN axons, indicating that they are subunits of a larger functional structure.

As the OB volume in our stack contained many microglomeruli we analyzed their anatomical organization in more detail. As in light microscopic studies (Braubach et al., 2012), microglomeruli were defined based on the organization of sensory axons and outlined manually. An aggregation of sensory axons was considered a microglomerulus if it was roughly spheroidal and connected to the olfactory nerve by a distinct stalk. The size and shape of microglomeruli varied substantially (Fig. 21).

In order to analyze the innervation pattern of microglomeruli we traced sensory axons which were identified by their dark cytoplasmic staining (Pinching and Powell., 1971). Outside glomeruli, sensory axons are usually organized in bundles. These bundles extend as a large group over long distances. Large bundles consist of several hundred axons and divide into successively smaller bundles before innervating a glomerulus (Fig. 22 A). Near a glomerulus, or within glomeruli, bundles separate into individual axons before axons make synapses onto postsynaptic cells.

Results

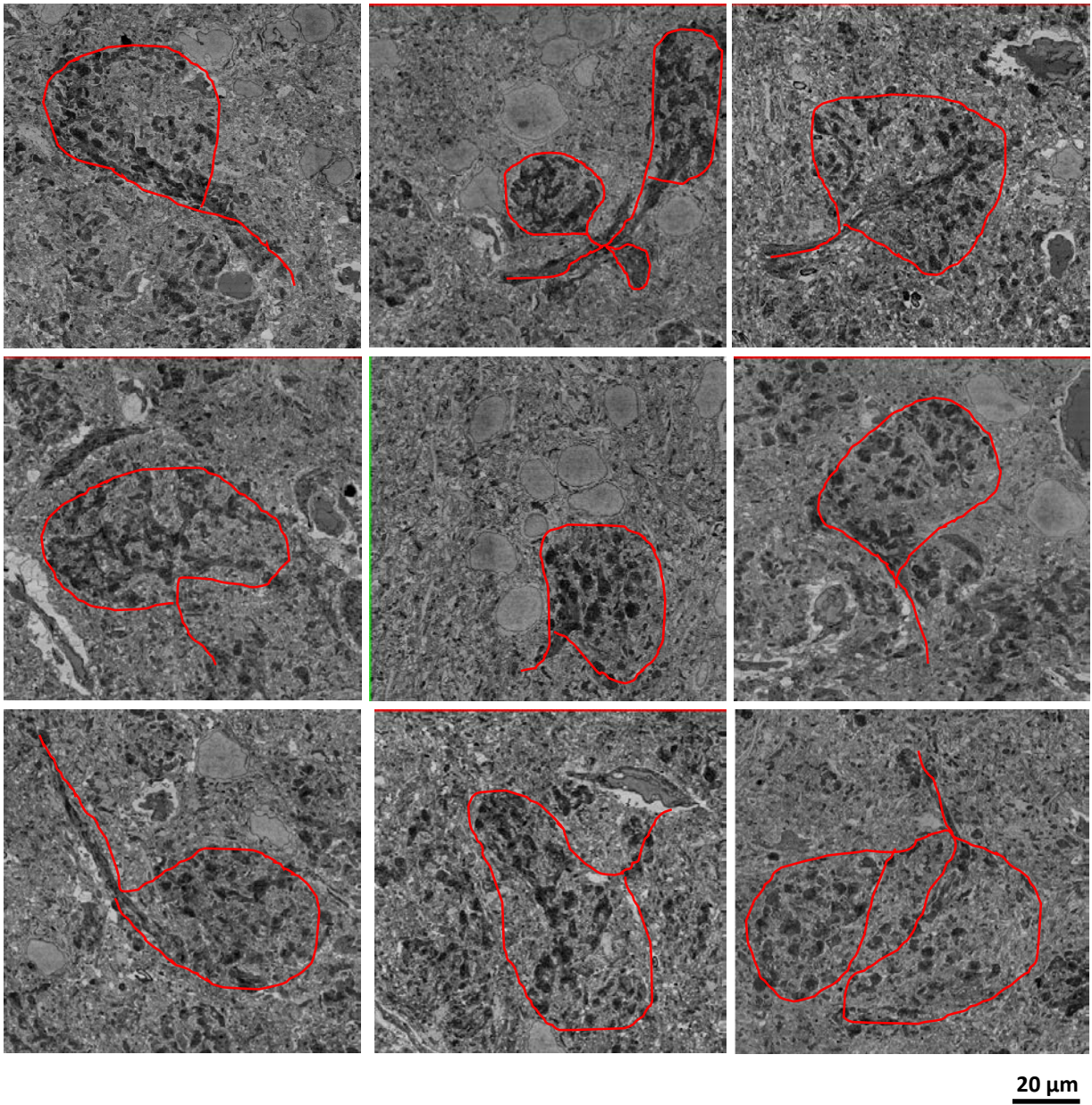


Fig. 21: Microglomeruli in the adult OB.

Outlined microglomeruli seen in the OB. The structures can be seen consistently in the GL layer. Here these microglomeruli structures have been manually outlined in red.

Results

Individual sensory neurons were traced by two approaches using PyKNOSSOS (Wanner et al., submitted):

First, sensory neuron tracing started from a synapse with a mitral cell that was reconstructed previously (Fig. 22 B) (see section 3.5 for MC reconstruction). The sensory neuron was then traced until it joined a large axon bundle. Second, sensory axons were selected randomly within a large axon bundle and traced into microglomeruli (Fig. 22 B). Using the two tracing approaches mentioned above we traced 30 sensory neurons. It was observed that sensory axons do not make branches in large bundles. Rather, individual sensory axons left large bundles as a whole. After leaving a bundle, axons did not project over long distances before innervating a microglomerulus. Branches were sparse, short and occurred near or within microglomeruli. These observations suggest that individual sensory axons innervate only one or at most a few neighboring microglomeruli.

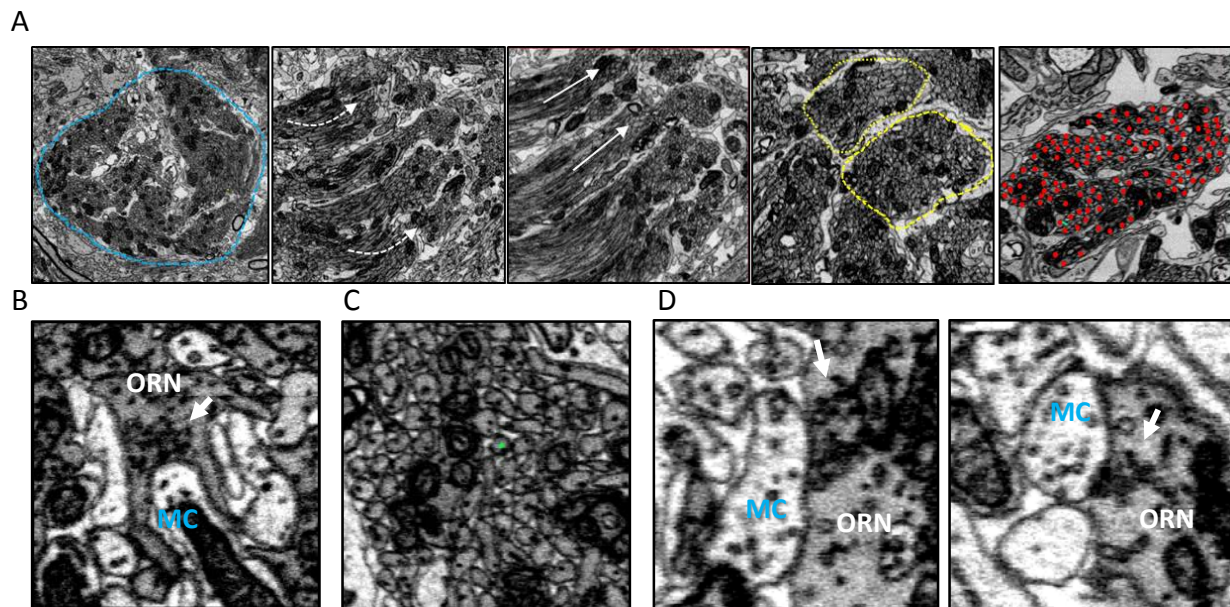


Fig. 22: Sensory axon bundles.

(A) First image shows large axon bundle (blue outline) consisting of several hundred sensory axons. Further, small bundles detach from the large axon bundle (white arrows, second and third image). After completely getting detached (yellow outlines, fourth image) these smaller bundles consist of fewer sensory axons (117 individual axons labelled in red, fifth image). (B) Sensory neuron tracing started from a typical synapses between olfactory receptor neuron and a mitral cell. A thick vesicle cluster at the site of synapse (white arrow). (C) A random axon was selected from an axon bundle (green) and traced till it enters a microglomeruli. (D) Same olfactory receptor neuron makes two synapses (white arrow) with the same post synaptic mitral cell in close proximity.

In order to annotate synapses of sensory axons, we followed all traced branches and identified locations where clusters of vesicles were present and touched the neuronal membrane. On average, we detected 15.2 ± 3.9 synapses per sensory axon (mean \pm S.D.; $n = 30$ axons). The average number of synapses per sensory axon is consistent with data from higher vertebrates (Greer et al., 1993). Moreover, we observed that synapses were usually large, containing a large number of synaptic vesicles.

As described below (section 3.5), five mitral cells were fully reconstructed. Three of these mitral cells were located in the same region as the reconstructed sensory axons. I determined the number of synapses that each sensory axon made with one of these mitral cells. The number ranged between 0 and 5, with a mean of 1.9 ± 1.4 synapses per mitral cell (mean \pm S.D.; $n = 30$ axons). Hence, sensory axons contacts the same mitral cell usually multiple times (Fig. 22 D). Moreover, each sensory axon targets multiple neurons. The identity of other post synaptic neurons which synapses with a sensory neuron is unknown. It has been reported that sub types of periglomerular cells present in the GL layer receive direct inputs from sensory neurons (Kosaka et al., 2005). Physiological studies have suggested that ET present in the glomerular layer also receive direct synaptic inputs from sensory neurons (Shipley et al., 2004).

3.5 Reconstruction of mitral cells in olfactory bulb

Two strategies were used to reconstruct mitral cells. First, processes postsynaptic to ORN axons were traced because mitral cells have been proposed to receive direct synaptic input from ORNs. However, synaptic input from ORNs is not a diagnostic feature of mitral cells because ORN axons also make synapses with interneurons. Moreover, recent studies suggested that mitral cells do not receive direct synaptic input from ORNs, although this view is debated (Shipley et al., 2004, Schoppa et al., 2012). The second strategy was to start tracing from somata near glomeruli. Because mitral cells cannot be identified based on somata alone, the identity of the cell cannot be predicted before the reconstruction. Both strategies therefore yielded reconstructions of mitral cells and interneurons. The identity of mitral cells was then established based on the presence of a myelinated axon, which does not occur in interneurons (Fig. 23).

We reconstructed 14 cells in total. Out of these, five cells had myelinated axons and were therefore classified as mitral cells. All five mitral cells had dense dendritic tufts innervating one or a few microglomeruli. This is consistent with previous descriptions of zebrafish mitral cells from light microscopy data (Byrd et al., 2006). Other neurons had small or no dendritic tuft and appeared to be axon-less which is consistent with light microscopic descriptions of interneurons, particularly short axon cells, in the zebrafish OB (Zhu et al., 2013).

The five mitral cells were analyzed further and had a total neurite length of 11.98 mm. Somata were large (7-8 microns) and myelinated axons travelled together in fascicles of 4-8 axons over long distances (Fig. 23). The somata of three mitral cells were adjacent to each other.

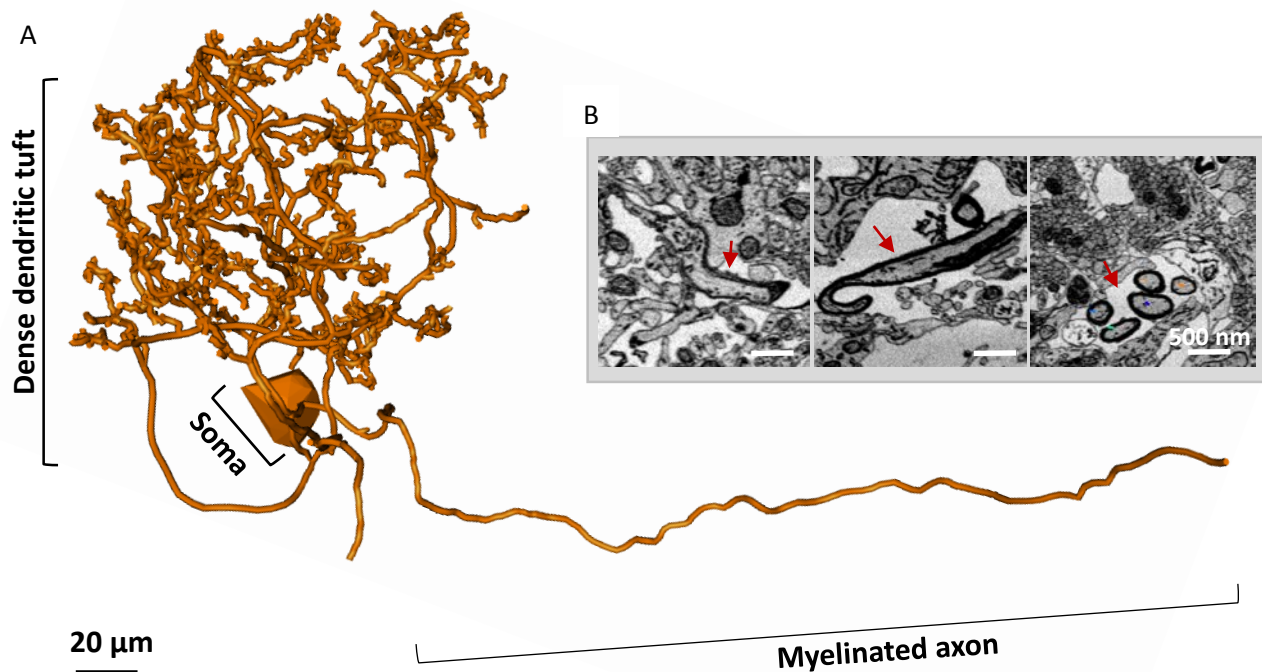


Fig. 23: Reconstruction of a mitral cell.

(A) Complete reconstruction of a mitral cell. A dense dendritic tuft, a soma (7.86 μm) and a myelinated axon can be seen. (B) Images show raw data along the axon with the traced skeleton. The first image shows the starting point (arrow) of myelination, which is apparent as a thick black layer around the axonal profile. The second image shows an axon completely myelinated. A fascicle containing five myelinated axons is seen in the last image.

Moreover, their dendrites innervated the same microglomeruli and their axons traveled in the same fascicle (Fig. 24). We therefore refer to these mitral cells as sister mitral cells. Somata of the other two MCs resided in a different location and innervated other glomeruli.

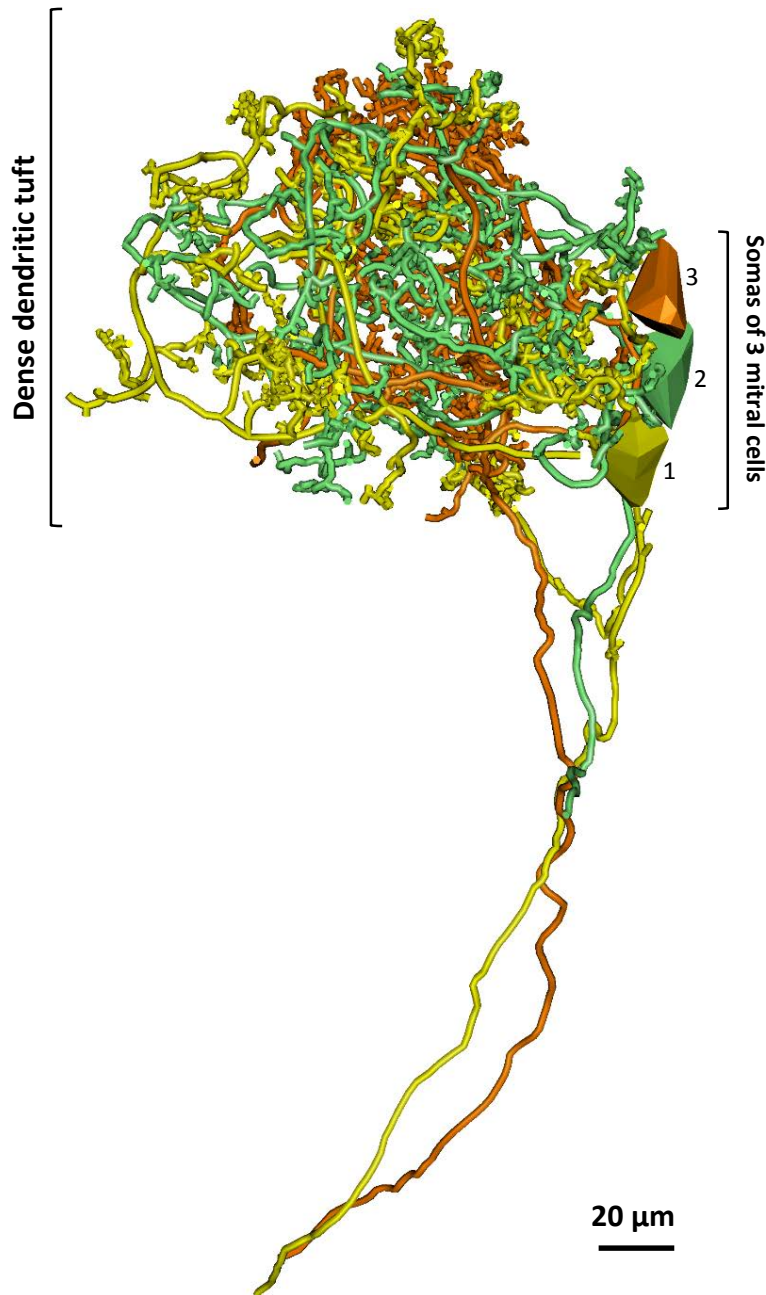


Fig. 24: Group of sister mitral cells.

Reconstruction of three sister mitral cells. All three cells have compact dendritic tufts innervating the same microglomeruli. All three have similar soma size, MC 1 (7.16 μm) MC 2 (7.42 μm) MC 3 (7.86 μm) and myelinated axons in the same fascicle.

Results

The identity of the nine cells that were not classified as mitral cells is unknown. Although not all of these neurons have been completely traced, it is obvious that these cells had neuronal morphologies. Moreover, none of them had a dense dendritic tuft, their somata were smaller than those of mitral cells, and no myelinated axons were detected, indicating that they were interneurons (Fig. 25).

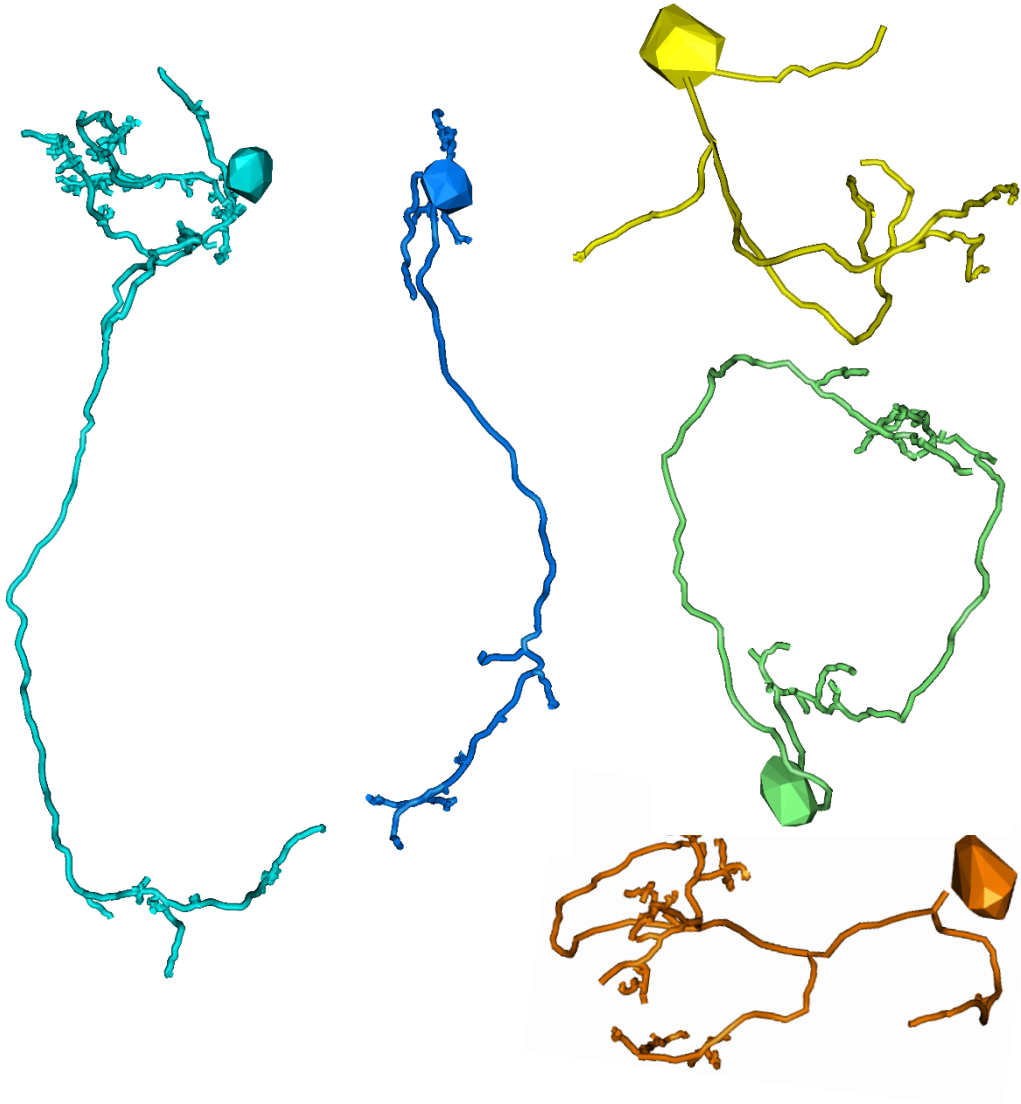


Fig. 25: Presumptive interneurons.

Incompletely reconstructed neurons that were not classified as mitral cells.

3.6 Synapse identification and labelling

An important aim of this study was to identify and label all the synapses of reconstructed mitral cells. Synapse labelling was done using PyKnossos (Wanner et al., submitted). In order to annotate synapses we followed all previously traced branches of mitral cells, identified locations where many vesicles were present, and searched for vesicle clusters touching the neuronal membrane. Sites that fulfilled these criteria were defined as synapses. The different synapses classes are described in detail below. Synapses were divided into four different classes:

Sensory synapses:

These synapses occur between ORN and dendritic branches of mitral cells (Fig. 26 A). Sensory axons could be identified because their cytoplasm is darkly stained (Pinching and Powell., 1971). Sensory synapses were usually large and contained many synaptic vesicles.

Inbound synapses:

A non-sensory synapse for which a mitral cell was postsynaptic is classified as an inbound synapse (Fig. 26 B). Most inbound synapses are assumed to be made by GABAergic interneurons.

Outbound synapses:

A synapse for which a mitral cell is presynaptic was classified as an outbound synapse (Fig. 26 C). As mitral cells are glutamatergic, outbound synapses are assumed to be excitatory.

Reciprocal synapses:

A pair of inbound and outbound synapses was classified as a reciprocal synapse when the synapses were between the same neurons and within a short distance from each other ($<1 \mu\text{m}$) (Fig. 26 D). Reciprocal synapses are known to occur between dendrites of mitral cells and interneurons (granule cell, periglomerular cell) in the OB. Reciprocal synapses are difficult to identify in single EM images because the two synapses are often not in the same image plane. In the 3D dataset, in contrast, reciprocal synaptic contacts are straightforward to detect.

Results

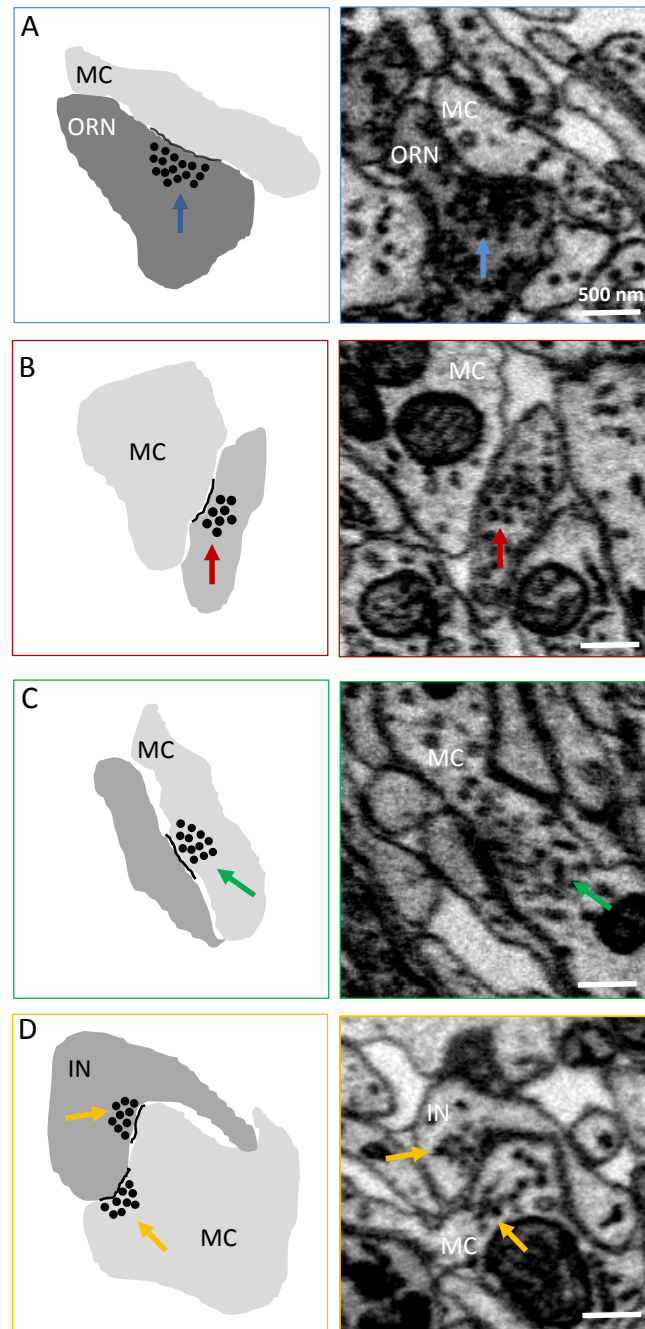


Fig. 26: Four synapses classes.

(A) A sensory synapse between an OSN and a mitral cell dendrite (blue). (B) An inbound synapse between an unknown neuron and a mitral cell (red). (C) An outbound synapse between a mitral cell and an unknown neuron (green). (D) A reciprocal synapse shown between a mitral cell and an unknown interneuron (yellow). Vesicle densities can be seen on both sides.

Synapse distribution (Mitral cell 1479)

Detailed synapse labelling and distribution is described below for three mitral cells (MC 1479, MC 1477, and MC 1483). Synapses were divided into four different categories as described above. Each traced branch in a mitral cell was visited at least once and each synapse was given a confidence level between 10% to 100% using PyKnossos (Wanner et al., submitted). The total tracing length of MC 1479 (arbitrary number for MC) was 2.48 mm and the total number of synapses annotated was 4582. The majority of the synapses labelled were sensory synapses (1478, 32%) followed by reciprocal synapses (1375, 30%). The total number of inbound synapses labelled were (1180, 26%) and the total number of outbound synapses labelled were (549, 12%). (Fig. 27).

In addition to the analysis of all synapses reported above, we also analyzed synapses near soma separately (Fig. 27 G) and found that no sensory synapses were present near the soma. Generally synapses near and around soma have smaller vesicle cluster, hence, more difficult to label compared to the synapses away from the soma. The relative abundance of the other synapse types was similar to the dendrite: inbound and reciprocal synapses were the most abundant types, followed by outbound synapses. These synapse numbers near soma were added to the final synapse count.

In order to facilitate visualization of the synapse distribution, labelled synapses were plotted on a dendrogram that represents the branching structure of the mitral cell dendrite in a 2D graph (Fig. 28). In MC 1479 we observed strong compartmentalization of sensory synapses (shown in blue) on the distal-most dendritic branches. Reciprocal synapses showed weak or no obvious compartmentalization and were scattered all along the mitral cell branches. Inbound and outbound synapses are also distributed all along the mitral cell branches. Synapses on the dendritic branches and synapses near the soma of a mitral cell often differ in size.

Results

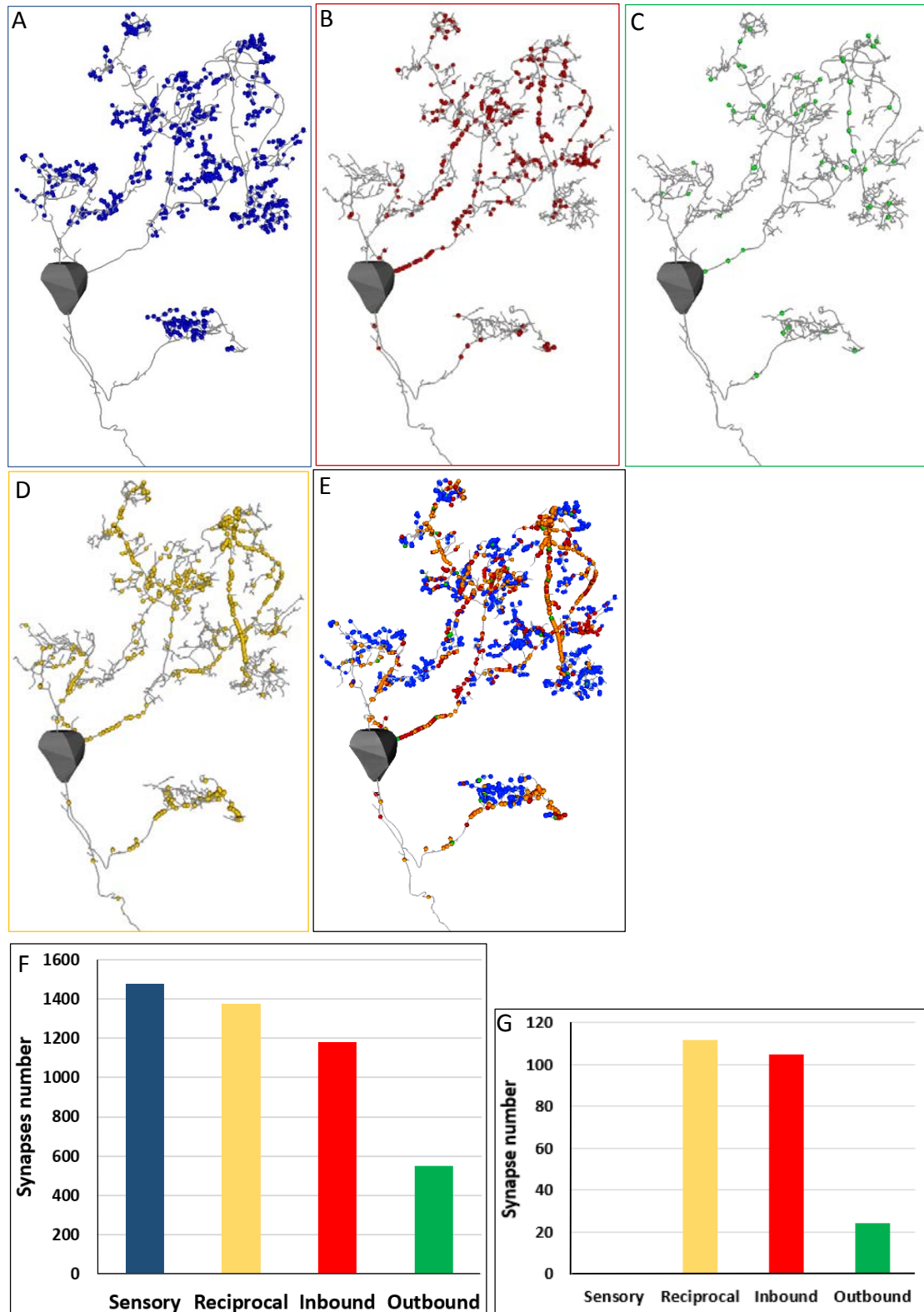


Fig. 27: Synapse distribution of mitral cell 1479.

Distribution of synapses on the branches of mitral cell 1479. (A) Sensory synapses are shown in blue. (B) Inbound synapses are shown in red. (C) Outbound synapses are shown in green. (D) Reciprocal synapses can be seen in yellow. (E) All synapses shown on the dendritic branches of the mitral cell. (F) Final synapse numbers. (G) Synapses numbers near soma.

Results

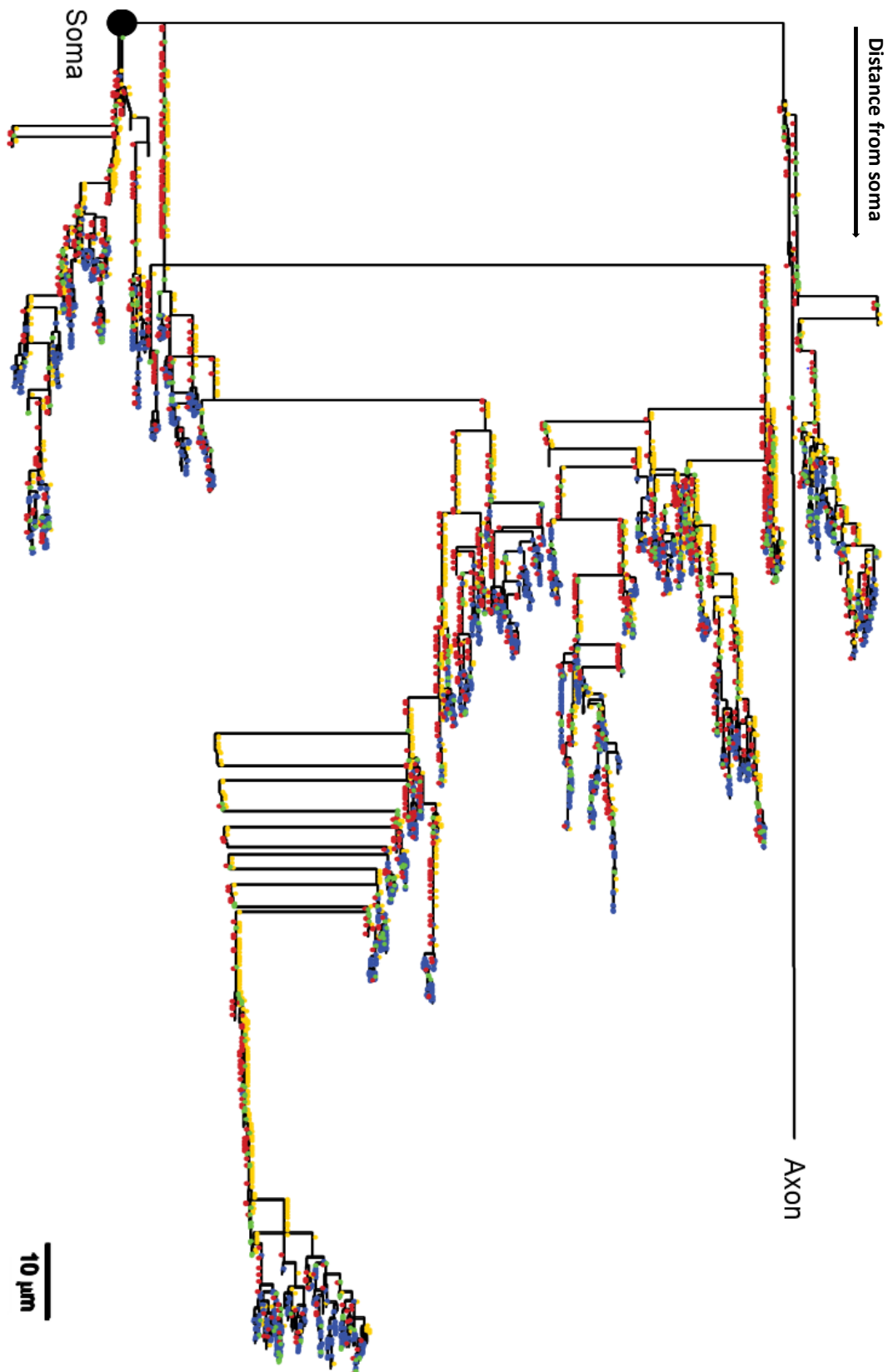


Fig. 28: 2D dendrogram.

Distribution of synapses in MC1479 shown in a 2D layout. Each small colored dot represents a synapse type. Sensory (blue), Reciprocal (yellow), Inbound (red) and outbound (green). The horizontal axis shows the distance from the soma and the vertical axis separates different branches.

Synapse distribution (Mitral cell 1483)

The complete skeleton reconstruction of mitral cell 1483 revealed the total tracing length to be 3.20 mm. We further labelled four classes of synapses in MC 1483. After synapses identification, the total number of synapses labelled were 3653. The majority of the synapses were sensory synapses (1223, 33%) and inbound synapses (1161, 32%). The number of reciprocal synapses were (835, 23%) and the number of outbound synapses were (434, 12%) (Fig. 29 A).

In order to visualize the synapse distribution in MC 1483, labelled synapses were plotted on a dendrogram that represents the branching structure of the mitral cell dendrite in a 2D graph (Fig. 30). There is a strong compartmentalization of sensory synapses (shown in blue) on the distal most dendritic branches of the mitral cell (Fig. 30). This is consistent with the results from mitral cell 1479. In MC 1483, Inbound and outbound synapses were distributed all along the mitral cell branches. There was no obvious compartmentalization of reciprocal synapses.

We labelled synapses around the soma and analyzed them separately. Reciprocal and inbound synapses were the most abundant near the soma followed by outbound synapses. No sensory synapses were seen as they are compartmentalized on the distal dendrites (Fig. 29 B). These synapse numbers near soma were added to the final synapse count.

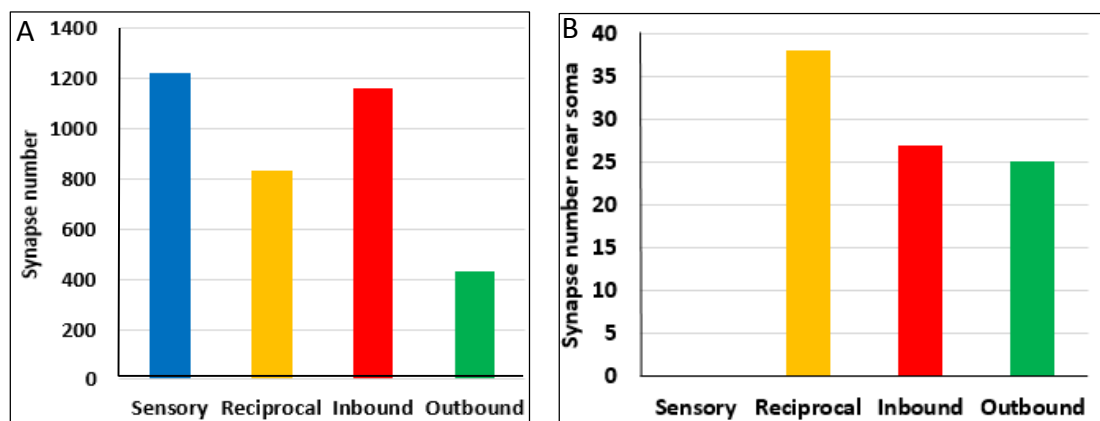


Fig. 29: Synapse type numbers of mitral cell 1483.

(A) Synapses numbers in mitral cell 1483. Majority of the synapses are sensory and inbound. Followed by reciprocal and outbound. (B) Synapses near the soma of mitral cell 1483. Sensory synapses were absent.

Results

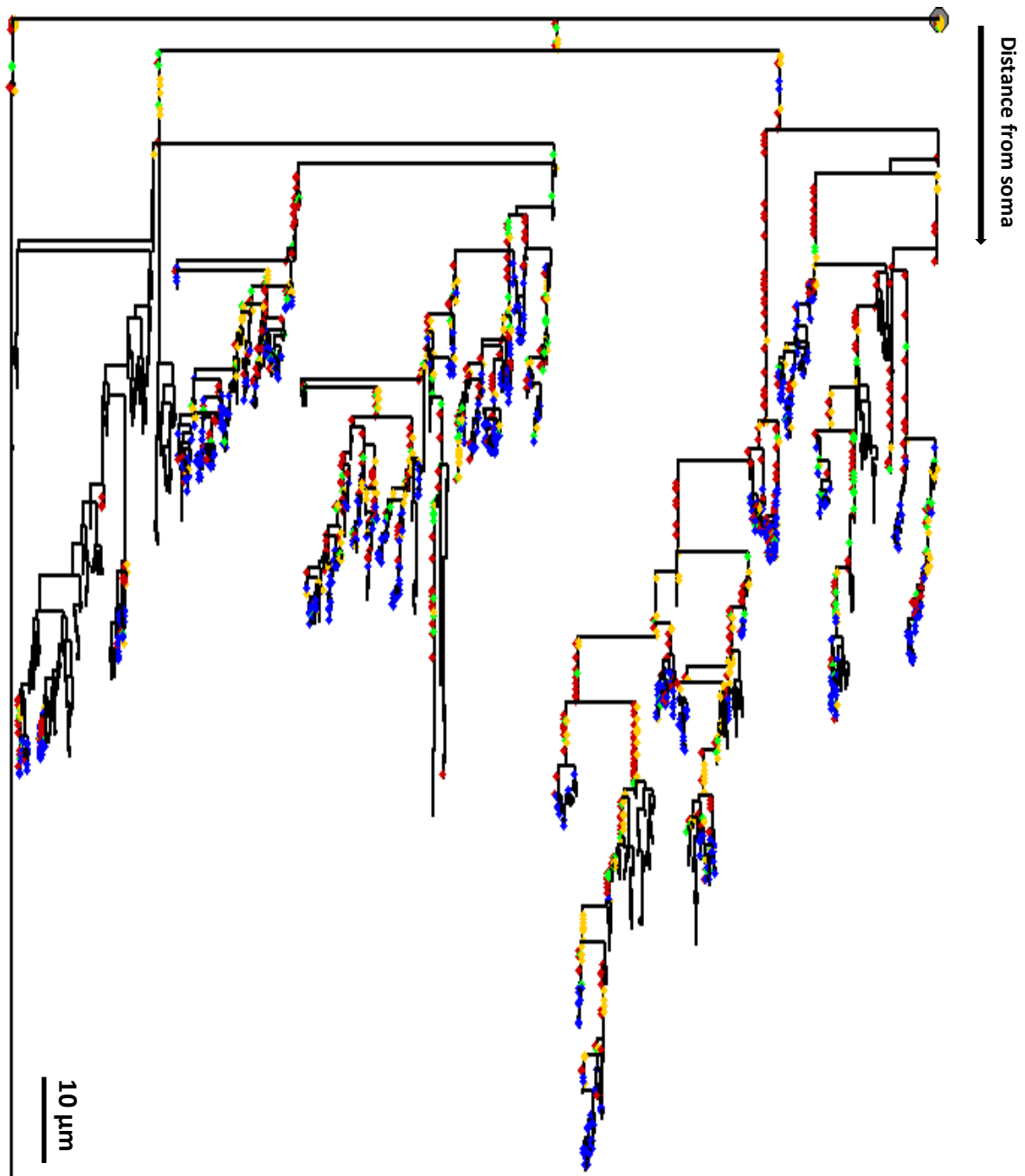


Fig. 30: 2D dendrogram.

Distribution of synapses in MC1483 shown in a 2D layout. Each small colored dot represents a synapse type. Sensory (blue), Reciprocal (yellow), Inbound (red) and outbound (green) synapses are distinguished. The horizontal axis shows the distance from the soma and the vertical axis separates different branches.

Synapse distribution (Mitral cell 1477)

Synapse detection was completed for the third mitral cell. After its complete skeleton reconstruction the total tracing length was 2.32 mm. The number of synapses labelled in the entire mitral cell were 2497. Out of the four synapses classes the majority of synapses labelled were inbound synapses (1017, 41%) and reciprocal synapses (828, 33%). The number of sensory synapses labelled were (427, 17%) and the number of outbound synapses labelled were (225, 9%) (Fig. 31 A).

Consistent with earlier synapse identification results, here as well we observe strong compartmentalization of sensory synapses (shown in blue) on the distal most dendritic branches of the mitral cell (Fig. 32). Inbound, outbound and reciprocal synapses showed no obvious compartmentalization. Synapses identification near the soma of MC 1477 was done as well. Around the soma, reciprocal and inbound synapses were the most abundant followed by outbound synapses. No sensory synapses were found near the soma (Fig. 31 B).

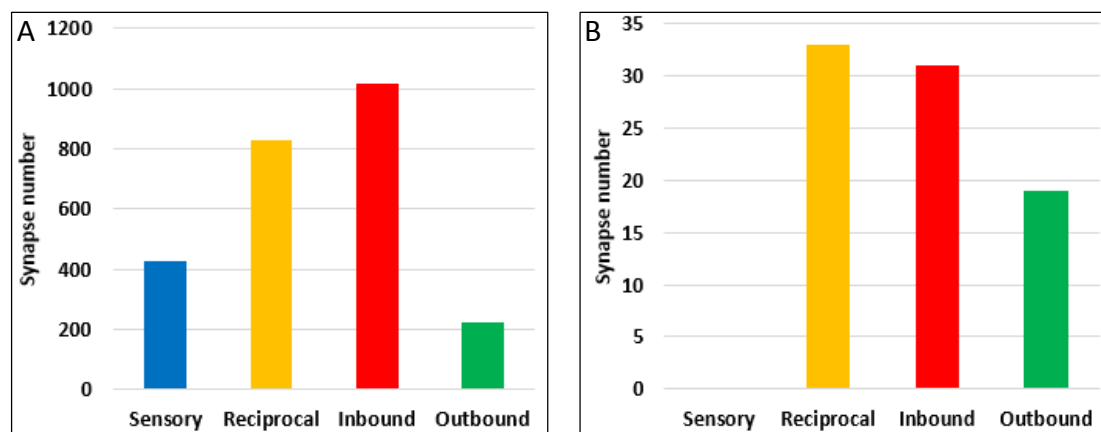


Fig. 31: Synapse distribution of MC 1477.

(A) Synapses numbers in mitral cell 1477. Majority of the synapses are inbound and reciprocal followed by sensory and outbound. (B) Synapses near the soma of mitral cell 1477. Sensory synapses were absent.

Results



Fig 32. 2D dendrogram.

Distribution of synapses in MC1477 shown in a 2D layout. Each small colored dot represents a synapse type. Sensory (blue), Reciprocal (yellow), Inbound (red) and outbound (green) synapses are distinguished. The horizontal axis shows the distance from the soma and the vertical axis separates different branches.

Results

The total number of synapses labelled in all the three fully traced mitral cells was 10732 (3577 ± 853 mean \pm S. D.). Of those, 29% were sensory synapses, 28% were reciprocal synapses, 31% were inbound synapses, and 12% were outbound synapses (Fig. 33). The fraction of reciprocal synapses, differs substantially from neuron to neuron, ranging from 23% to 33%. However, the mean value of 28.66 ± 5.13 (mean \pm S.D.) gives a coarse estimate that can be used for comparison with theoretical models.

The “variance-balanced state” (VBS) model predicts that for a robust VBS to occur, a substantial fraction of synapses (approximately >20 %) between mitral cells and OB interneurons should be reciprocal. This reciprocal synapses fraction takes into account all reciprocal synapses irrespective of which interneuron population they belong to. This number is normalized by the total number of synapses, excluding sensory synapses. This yields a 32% fraction of reciprocal synapses (Fig. 34), in agreement with predictions of the theoretical VBS model.

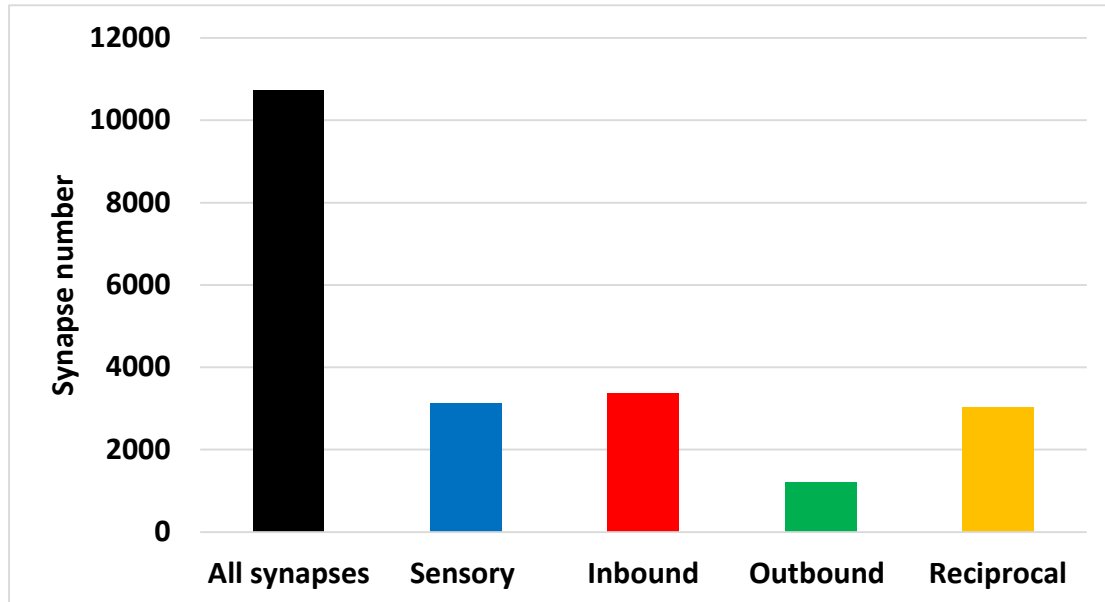


Fig. 33: Final synapse numbers.

(A) Total number of sensory synapses (3128, 29%), reciprocal synapses (3038, 28%), inbound synapses (3358, 31%), outbound synapses (1208, 12%).

Results

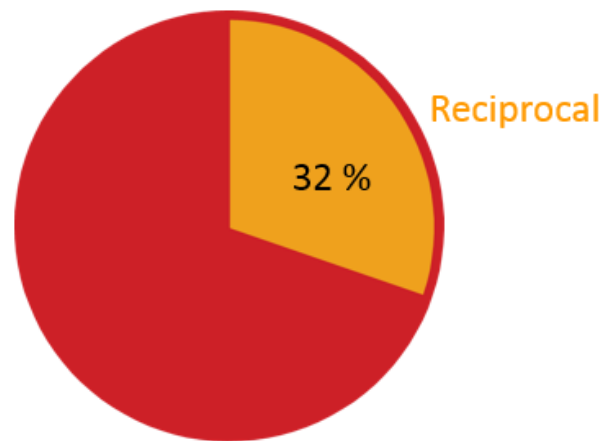


Fig. 34: Fraction of reciprocal synapses in VBS model.

The fraction of reciprocal synapses is 32%. Here the total number of synapses is 7662. This synapse number includes all network input synapses to the mitral cell except sensory synapses.

DISCUSSION

4.1 Reconstruction of neuronal morphology and synapses in volumetric EM data

Acquisition of large volumetric electron microscopy data and further reconstruction of neuronal morphology and their synapses for connectivity mapping is a major goal in neuroscience. We acquired a large EM dataset from the adult zebrafish olfactory bulb and reconstructed a subset of the neurons in this volume. The reconstruction of all neurons in the stack would require an enormous amount of manual labor and is far beyond the scope of this study. However, the reconstruction of individual neurons and the annotation of their synapses was feasible. This allowed us to address fundamental questions of reciprocal connectivity between mitral cells and interneurons in the OB.

The reconstruction of neurons and the annotation of their synapses requires a resolution of approximately 10 – 30 nanometers throughout large volumes of tissue. We have been able to maintain a high resolution (9 nm pixel size in xy and 25 nm in z) throughout the acquired dataset. New methods that involve conductive embedding of the tissue samples, dramatically reduced charging. This approach was essential for the acquisition of a large dataset and improved image quality (Wanner et. al. submitted). The large volume of the dataset and its high image quality allowed us to reconstruct the arbors and synapses of three mitral cells. Such detailed reconstructions of mitral cells and labeling of their synapses have so far not been achieved in any other brain area/species with the exception of *C. elegans*, where connections were reconstructed from serial electron microscopic images through decades of manual labor (White et al., 1986).

4.2 Mitral cells receive direct input from olfactory sensory axons

Olfactory information is transmitted from the olfactory sensory neurons to the mitral cells either directly or via interneurons. Recent studies suggest that an excitatory interneuron type called external tufted cell (ET cell), present in the glomerular layer, receives direct sensory

synaptic input and then transmits it to the mitral cell (Shiple et al., 2004; Schoppa et al., 2012). Based on recent physiological results it has been proposed that mitral cells do not receive direct input from sensory neurons, but that their excitatory input is transmitted exclusively through the disynaptic pathway via ET cells. Other studies, however, indicated that at least a subset of synapses of sensory neurons directly target mitral cells (Shiple et al., 2004). An olfactory bulb circuitry with ET cells in between olfactory sensory neurons and mitral cells could potentially allow for more flexible processing of sensory information because the activity of output neurons is not directly driven by their inputs (De Saint Jan et al., 2009; Najac et al., 2011; Schoppa et al., 2012). For example, ET cells could temporally integrate inputs, suppress weak inputs by thresholding, perform other non-linear operations, or serve as target for neuromodulatory inputs. In addition, ET cells could be involved in transmitting information across glomeruli via excitatory pathways while other inter-glomerular interneurons are inhibitory.

Studies proposing that mitral cells do not receive direct sensory input used physiological methods. Recordings were performed from the ET cell and mitral cell while stimulating axons of olfactory sensory neurons in brain slices (Schoppa et al., 2012). However, these physiological studies do not directly resolve connectivity, since a detailed anatomical mapping of synapses is required to ultimately identify the synaptic partners of sensory axons.

We reconstructed mitral cells completely, mapped their synapses, and classified them into different categories. We found that each mitral cell received a large number of direct synaptic inputs from olfactory sensory neurons. Of all the synapses (10917 synapses in total) we labeled in three mitral cells, a considerable fraction (28%, i.e. 3138 synapses) were sensory synapses. In all mitral cells, sensory input was found preferentially on the distal dendrites. Although an indirect connection between sensory neurons and MC via ET cells cannot be ruled out, the large fraction of sensory synapses on MC indicates a major role of these direct contacts. The hypothesis that there are no or only few direct inputs from ORN to MC can therefore be ruled out, and it is likely that the large number of direct sensory synapses on MC has important

physiological effects. Our results therefore indicate that the activity of mitral cells is strongly determined by their sensory inputs.

4.3 Two photon calcium imaging reveals dense granule cell responses

Consistent with a previous study (Yaksi et al., 2007), our results from two photon imaging revealed that a large fraction of neurons in the GCL of the adult OB responds to any given odor. Odor stimuli included individual amino acids at intermediate concentration, which are relatively weak stimuli. This result cannot be explained by strong odor stimulation. The majority of neurons in the GCL are most likely granule cells, implying that granule cell activity patterns evoked by odor stimulation are dense. The large number of responsive granule cells suggests that granule cells may have a strong impact on OB output.

Two theoretical studies have recently proposed different functions of granule cells in odor processing. One study proposes that reciprocally connected granule cells form sparse overcomplete representations of odors that are removed from mitral cell activity patterns and decorrelate OB output (Koulakov and Rinberg, 2011). A central prediction of this study is that granule cell activity patterns are very sparse. However, our data directly demonstrate that odor-evoked granule cell activity is dense.

Another theoretical study came to a conclusion that is different from the study mentioned above (Wiechert, 2015). This study concluded that reciprocally connected granule cells do not decorrelate or otherwise reorganize OB output patterns. Instead, reciprocally connected granule cells are predicted to downscale activity patterns, resulting in contrast normalization. This study does not predict sparse granule cell activity patterns. Therefore our data do not support conclusions of the first study but are consistent with predictions of the second study.

4.4 Reciprocal synapses show weak compartmentalization

Unlike sensory synapses, which show strong compartmentalization on the distal dendrites, reciprocal synapses do not seem to be strongly compartmentalized. In all the mitral cells we

traced, we see substantial numbers of broadly distributed reciprocal synapses present in each mitral cell. However, at least in some mitral cells, reciprocal synapses may have a tendency to be concentrated near branch points.

Reciprocal synapses are present around the soma as well as along the dendritic branches of mitral cells. We also observe that reciprocal synapses vary in size. Reciprocal synapses around the mitral cell soma are smaller in size compared to the ones near the mitral cell dendrites. In principle these different subpopulations of reciprocal synapses could originate from different types of interneurons. This question can now be addressed by tracing neurons from the reciprocal synapses.

4.5 Reciprocal connectivity may support variance balancing

The computational consequences of reciprocal connectivity were examined in a recent theoretical model. This work demonstrates that reciprocal synapses can support a variance-balanced state (VBS) that achieves efficient contrast normalization (Wiechert, 2015). The model predicts that for a robust VBS to occur, a substantial fraction of synapses (approximately >20 %) between mitral cells and OB interneurons should be reciprocal. Moreover, mitral cells should receive substantial excitatory input to reach a balanced state. We have already shown that the MC indeed receive a large number of direct sensory input that could provide the necessary excitatory drive. Consistent with this hypothesis, mitral cells have high spontaneous firing rates and constantly receive excitatory and inhibitory inputs (Friedrich and Laurent, 2004). It has, however, been unknown whether the fraction of reciprocal synapses in the network is sufficiently high to support a balanced state (Hirata 1964, Rall et al., 1966; Rall and Shepherd, 1968; Price and Powell, 1970). To address this question, we directly quantified the number of reciprocal synapses in mitral cells.

Here, we find based on our pooled synapse detection data from three mitral cells that the fraction of reciprocal synapses is 32%. This fraction of reciprocal synapses takes into account all reciprocal synapses, irrespective of the interneuron population to which they belong. The computational study by Wiechert (Wiechert, 2015), shows how the variance of the output

pattern (MC activity) relates to the variance of the input pattern (sensory neuron activity) when the degree of reciprocity of the network is changed. In the model, the variance of the output pattern is normalized efficiently when the fraction of reciprocal synapses is higher than ~20%. This result was robust even when the strengths of individual synapses were assumed to be heterogeneous. Our findings are therefore consistent with the hypothesis that reciprocal connectivity in the OB supports a variance-balanced state that results in contrast normalization.

4.6 Limitations of the study and outlook

Tracing and synapse detection reliability

Tracing of mitral cells in the adult olfactory bulb was performed by a single person. Although this person has visited most branches multiple times, it is still possible that some branches are incorrect or missing. However, the main results of this study are statistical in nature, and no major differences in synapse distribution have been observed between different branches. It is therefore unlikely that any missing branches would have a strong impact on the result. Wrong branches are unlikely to make major contributions to the reconstructions because they are typically straightforward to detect, for example by incorrect connections to more than one soma. It is therefore unlikely that tracing errors resulted in major errors.

In order to quantify the tracing precision more rigorously and also to detect false positively traced branches, the full tracing would need to be verified multiple times. Ideally multiple tracers should trace each neuronal skeleton and then the skeletons should be compared to detect mismatch points (Wanner et al., submitted).

Similarly, the accuracy and completeness of synapse detection may be further increased by combining independent annotations of multiple tracers. Synapse detection during the first round of tracing on three mitral cells revealed the number to be 9362. After tracing the branches found during the second round from three mitral cells, the total synapse number increased to 10917. Hence, it is possible that not all synapses have been detected. Assuming that synapses have been missed stochastically, it is unlikely that a small fraction of missed synapses would have a substantial impact on the statistical results.

Synapse classification could also be further improved. Presently, synapses are assigned to four different classes. In principle, it is possible to define more sub-classes. This information could then be further used to refine models of the circuits and to re-analyze possible clustering of synaptic sub-types.

Reconstruction of olfactory sensory neurons and postsynaptic partners

Quantitative data on synaptic connectivity between sensory neurons and OB neurons was obtained from reconstructions of sensory axons. However, these results are preliminary because the number of reconstructed axons was small. Since we have traced many olfactory sensory neurons completely and also identified and labeled all their synapses, we see sensory neurons make relatively few synapses (15 on average). It is therefore realistic to fully trace all their postsynaptic partners starting from these individual synapses. This would allow to determine the identity of other postsynaptic neurons apart from mitral cells and to address the question whether this set of neurons also includes ET cells.

The zebrafish glomerular layer contains approximately 140 distinct glomeruli and a region containing additional, small glomerular structures that have not been delineated precisely. Subsets of these glomeruli are large and unambiguously identifiable between individuals (Braubach et al., 2012). Moreover, anatomically and molecularly defined clusters of glomeruli can be found consistently in different individuals. Reconstruction of these sensory neurons would also delineate the structure of glomeruli in the adult olfactory bulb more clearly.

Another interesting future direction is to trace neurons postsynaptic to sister mitral cells. This provides the opportunity to determine whether sister mitral cells receive correlated input also from the OB network. If so, sister mitral cells would be likely to represent redundant output channels of the OB. Such architecture could increase the “safety factor” in odor representations. Alternatively, sister mitral cells could receive different inputs from the network and therefore convey non-redundant information. Such architecture could enhance the bandwidth of information transmission from the OB to higher brain areas.

Reconstruction of interneurons

Computations such as pattern decorrelation depend on network interactions between mitral cells (Tabor et al., 2004). Mitral cells connected to different glomeruli do not make direct synaptic contacts (Pinching and Powell, 1971; Price and Powell, 1970; White, 1972). Rather, most inter-glomerular interactions between mitral cells are mediated via interneurons and are inhibitory in nature. Many synaptic contacts between mitral cells and interneurons (particularly granule cells) are made between dendrites and are reciprocal in nature, i.e., an excitatory mitral cell-to-interneuron synapse occurs in close proximity to an inhibitory interneuron-to-mitral cell synapse between the same neurons (Isaacson and Strowbridge, 1998; Urban and Sakmann, 2002). It is therefore thought that interneurons, particularly granule cells, mediate mutual lateral inhibition between mitral cells. Besides this striking symmetry of synaptic contacts at fine spatial scales, it is unknown whether connectivity between mitral cells and interneurons exhibits non-random structure at larger scales. In other words, the topology of connections in the OB, which is represented by the neuronal connectivity matrix, is largely unknown. Recent evidence indicates that connectivity is sparse and that connection probability decreases with distance (Egger and Urban, 2006; Fantana et al., 2008; Wiechert et al., 2010). However, these studies do not reveal the connectivity matrix because they provide only first-order statistical information on connection probability.

In order to better understand the reciprocal circuit that involves the mitral cells, it would be helpful to reconstruct the arborization of the synaptic partners involved. These are most likely predominantly granule cells and also periglomerular cells. The precise reciprocal connectivity would allow refining current models that assume stochastic connectivity between mitral cells and interneurons for reciprocal synapses. This could be done with the reciprocal synapses or inbound synapses of traced mitral cells as starting points. We see a broad distribution of reciprocal synapses along the branches of the mitral cells and weak compartmentalization at the branch points.

Choosing areas with a cluster of reciprocal synapses and tracing these interneurons, possibly granule cells, would give an idea how MC and GC are connected. The number of reciprocal

synapses is large in each of the mitral cells we reconstructed. Hence to trace all of them would require enormous labor. Therefore focusing on a subset of reciprocal synapses and reconstructing them completely would be possible.

Physiological recordings combined with dense reconstructions

Ultimately, understanding of a neuronal circuit requires not only the detailed connectivity, but also the physiological behavior of the circuit. To access how functional response properties of individual neurons and neuronal computations are shaped by interactions with other neurons, it will be important to measure functional response properties and connectivity matrices of large numbers of neurons in the same specimens. The physiology of the olfactory bulb in zebrafish is already partly understood (Niessing et al., 2010; Friedrich et al., 2001), but our understanding could be further enhanced by combining functional studies with complementary dense circuit reconstruction as has been done in other studies (Briggman et al., 2011).

For example, it has been observed that mitral cells abruptly change their firing response when the fish is exposed to gradually changing odor stimuli (Niessing et al., 2010). This switching behavior cannot be explained using a theoretical model that is based on random connectivity (Wiechert et al., 2010), but could likely be achieved by a network with non-random connectivity. A dense connectivity reconstruction can provide an approach to search for non-random connectivity features that could explain the abrupt transitions in network states. More specifically, such network behavior could be produced by preferred or anti-preferred connectivity among ensembles of neurons with similar response properties. Similar connectivity rules could also account for computations in other brain areas and have been proposed to be fundamental motifs of neuronal circuit architecture. Testing such hypotheses requires exhaustive analysis of the connectivity among neurons, together with a physiological characterization of their response properties.

REFERENCES

- Abraham, N. M., Egger, V., Shimshek, D. R., Renden, R., Fukunaga, I., Sprengel, R., ... Kuner, T. (2010). Synaptic Inhibition in the Olfactory Bulb Accelerates Odor Discrimination in Mice. *Neuron*, *65*(3), 399–411. doi:10.1016/j.neuron.2010.01.009
- Ache, B. W., & Young, J. M. (2005). Olfaction: Diverse Species, Conserved Principles. *Neuron*, *48*(3), 417–430. doi:10.1016/j.neuron.2005.10.022
- Adrian, E.D., 1950. The electrical activity of the mammalian olfactory bulb. *Electroencephalography and clinical neurophysiology*, *2*(1), pp.377-388.
- Alioto, T. S., & Ngai, J. (2005). The odorant receptor repertoire of teleost fish. *BMC Genomics*, *6*, 173. doi:10.1186/1471-2164-6-173
- Almarestani, L., Waters, S. M., Krause, J. E., Bennett, G. J., & Ribeiro-da-Silva, a. (20074). Morphological characterization of spinal cord dorsal horn lamina I neurons projecting to the parabrachial nucleus in the rat. *The Journal of Comparative Neurology*, *504*(3), 287–297. doi:10.1002/cne
- Andres, K. H. (1965). Der Feinbau des Bulbus olfactorius der Ratte unter besonderer Berücksichtigung der synaptischen Verbindungen. *Z. Zellforsch. mikrosk. Anat.* *65*, 530-560.
- Aungst, J. L., Heyward, P. M., Puche, a C., Karnup, S. V, Hayar, a, Szabo, G., & Shipley, M. T. (2003). Centre-surround inhibition among olfactory bulb glomeruli. *Nature*, *426*(6967), 623–629. doi:10.1038/nature02185
- Braubach, O. R., Fine, A., & Croll, R. P. (2012). Distribution and functional organization of glomeruli in the olfactory bulbs of zebrafish (*Danio rerio*). *The Journal of Comparative Neurology*, *520*(11), 2317–2339. doi:10.1002/cne.23075
- Brennan, P. a., & Keverne, E. B. (1997). Neural mechanisms of mammalian olfactory learning. *Progress in Neurobiology*, *51*(4), 457–481. doi:10.1016/S0301-0082(96)00069-X
- Briggman, K. L., & Bock, D. D. (2012). Volume electron microscopy for neuronal circuit reconstruction. *Current Opinion in Neurobiology*, *22*(1), 154–161. doi:10.1016/j.conb.2011.10.022
- Briggman, K. L., & Denk, W. (2006). Towards neural circuit reconstruction with volume electron microscopy techniques. *Current Opinion in Neurobiology*, *16*(5), 562–570. doi:10.1016/j.conb.2006.08.010
- Briggman, K. L., Helmstaedter, M., & Denk, W. (2011). Wiring specificity in the direction-selectivity circuit of the retina. *Nature*, *471*(7337), 183–188. doi:10.1038/nature09818

References

- Brustein, E., Marandi, N., Kovalchuk, Y., Drapeau, P., & Konnerth, a. (2003). "In vivo" monitoring of neuronal network activity in zebrafish by two-photon Ca(2+) imaging. *Pflügers Archiv : European Journal of Physiology*, 446(6), 766–73. doi:10.1007/s00424-003-1138-4
- Buck, L. B. (2000). The molecular architecture of odor and pheromone sensing in mammals. *Cell*, 100, 611–618. doi:10.1016/S0092-8674(00)80698-4
- Bundschuh, S. T., Zhu, P., Scharer, Y.-P. Z., & Friedrich, R. W. (2012). Dopaminergic Modulation of Mitral Cells and Odor Responses in the Zebrafish Olfactory Bulb. *Journal of Neuroscience*, 32(20), 6830–6840. doi:10.1523/JNEUROSCI.6026-11.2012
- Canalón, P. Degeneration and regeneration of olfactory cells induced by ZnSO₄ and other chemicals. *Tissue Cell* 14, 717–733 (1982).
- Chen, W. R., Xiong, W., & Shepherd, G. M. (2000). Analysis of relations between NMDA receptors and GABA release at olfactory bulb reciprocal synapses. *Neuron*, 25(3), 625–633. doi:10.1016/S0896-6273(00)81065-X
- Davies, S. N., Lester, R. A., Reymann, K. G., & Collingridge, G. L. (1989). Temporally distinct pre- and post-synaptic mechanisms maintain long-term potentiation. *Nature*, 338(6215), 500–503. doi:10.1038/338500a0
- De Saint Jan, D., Hirnet, D., Westbrook, G. L., & Charpak, S. (2009). External Tufted Cells Drive the Output of Olfactory Bulb Glomeruli. *Journal of Neuroscience*, 29(7), 2043–2052. doi:10.1523/JNEUROSCI.5317-08.2009
- Denk, W., & Horstmann, H. (2004). Serial Block-Face Scanning Electron Microscopy to Reconstruct Three-Dimensional Tissue Nanostructure. *PLoS Biology*, 2(11), e329. doi:10.1371/journal.pbio.0020329
- Denk, W., Strickler, J. H., Webb, W. W., Series, N., & Apr, N. (2008). Two-Photon Laser Scanning Fluorescence Microscopy, 248(4951), 73–76. doi:10.1126/science.2321027
- Denk, W., Strickler, J.H. and Webb, W.W., 1990. Two-photon laser scanning fluorescence microscopy. *Science*, 248(4951), pp.73-76.
- Dowling, J.E. and Boycott, B.B., 1966. Organization of the primate retina: electron microscopy. *Proceedings of the Royal Society of London B: Biological Sciences*, 166(1002), pp.80-111.
- Edwards, J. G. & Michel, W. C. Odor-stimulated glutamatergic neurotransmission in the zebrafish olfactory bulb. *J. Comp. Neurol.* 454, 294–309 (2002).

References

- Egger, V., & Urban, N. N. (2006). Dynamic connectivity in the mitral cell-granule cell microcircuit. *Seminars in Cell and Developmental Biology*, *17*(4), 424–432. doi:10.1016/j.semcdb.2006.04.006
- Egger, V., Svoboda, K., & Mainen, Z. F. (2003). Cellular/Molecular Mechanisms of Lateral Inhibition in the Olfactory Bulb: Efficiency and Modulation of Spike-Evoked Calcium Influx into Granule Cells, *23*(20), 7551–7558.
- Engeszer, R. E., Barbiano, L. A. DA, Ryan, M. J., & Parichy, D. M. (2007). Timing and plasticity of shoaling behaviour in the zebrafish, *Danio rerio*. *Animal Behaviour*, *74*(5), 1269–1275. doi:10.1016/j.anbehav.2007.01.032
- Eyre, M., Finklea, B., Nusser, Z., & Antal, M. (2006). External tufted cells in the main olfactory bulb form two distinct subpopulations. *The European Journal of Neuroscience*, *24*(4), 1124–36. doi:10.1111/j.1460-9568.2006.04988.x
- Fantana, A. L., Soucy, E. R., & Meister, M. (2008). Rat Olfactory Bulb Mitral Cells Receive Sparse Glomerular Inputs. *Neuron*, *59*(5), 802–814. doi:10.1016/j.neuron.2008.07.039
- Franks, K. M., & Isaacson, J. S. (2005). Synapse-Specific Downregulation of NMDA Receptors by Early Experience: A Critical Period for Plasticity of Sensory Input to Olfactory Cortex. *Neuron*, *47*(1), 101–114. doi:10.1016/j.neuron.2005.05.024
- Friedrich, R. W. (2001). Dynamic Optimization of Odor Representations by Slow Temporal Patterning of Mitral Cell Activity. *Science*, *291*(5505), 889–894. doi:10.1126/science.291.5505.889
- Friedrich, R. W., & Korsching, S. I. (1997). Combinatorial and Chemotopic Odorant Coding in the Zebrafish Olfactory Bulb Visualized by Optical Imaging. *Neuron*, *18*(5), 737–752. doi:10.1016/S0896-6273(00)80314-1
- Friedrich, R. W., Jacobson, G. a., & Zhu, P. (2010). Circuit Neuroscience in Zebrafish. *Current Biology*, *20*(8), R371–R381. doi:10.1016/j.cub.2010.02.039
- Friedrich, R. W., Yaksi, E., Judkewitz, B., & Wiechert, M. T. (2009). Processing of odor representations by neuronal circuits in the olfactory bulb. *Annals of the New York Academy of Sciences*, *1170*, 293–297. doi:10.1111/j.1749-6632.2009.04010.x
- Fuller, C. L., & Byrd, C. A. (2005). Ruffed cells identified in the adult zebrafish olfactory bulb. *Neuroscience Letters*, *379*(3), 190–4. doi:10.1016/j.neulet.2004.12.062
- Fuller, C. L., Yettaw, H. K., & Byrd, C. A. (2006) Mitral cells in the olfactory bulb of adult zebrafish (*Danio rerio*): morphology and distribution. *J Comp Neurol*. 2006 Nov 10; *499*(2):218-30.

References

- Gire, D. H., Franks, K. M., Zak, J. D., Tanaka, K. F., Whitesell, J. D., Mulligan, a. a., ... Schoppa, N. E. (2012). Mitral Cells in the Olfactory Bulb Are Mainly Excited through a Multistep Signaling Path. *Journal of Neuroscience*, *32*(9), 2964–2975. doi:10.1523/JNEUROSCI.5580-11.2012
- Gire, D. H., Restrepo, D., Sejnowski, T. J., Greer, C., De Carlos, J. A., & Lopez-Mascaraque, L. (2013). Temporal Processing in the Olfactory System: Can We See a Smell? *Neuron*, *78*(3), 416–432. doi:10.1016/j.neuron.2013.04.033
- Golgi, C., 1875. Sulla fina struttura dei bulbi olfattorii. Tipografia di Stefano Calderini.
- Göldner, F. H. & Wolff, J. R. Dendro-dendritic synapses in the suprachiasmatic nucleus of the rat hypothalamus. *J. Neurocytol.* *3*, 245–250 (1974).
- Haberly, L. B. (2001). Parallel-distributed Processing in Olfactory Cortex: New Insights from Morphological and Physiological Analysis of Neuronal Circuitry. *Chemical Senses*, *26* (5), 551–576. doi:10.1093/chemse/26.5.551
- Halabisky, B., Friedman, D., Radojicic, M., & Strowbridge, B. W. (2000). Calcium influx through NMDA receptors directly evokes GABA release in olfactory bulb granule cells. *The Journal of Neuroscience*, *20*(13), 5124–5134. doi:20/13/5124 [pii]
- Hálasz, N., and Greer, C.A. (1993). Terminal arborizations of olfactory nerve fibers in the glomeruli of the olfactory bulb. *J. Comp. Neurol.* *337*, 307-316.
- Hansen, A., & Zielinski, B. S. (2005). Diversity in the olfactory epithelium of bony fishes: Development, lamellar arrangement, sensory neuron cell types and transduction components. *Journal of Neurocytology*, *34*(3-5), 183–208. doi:10.1007/s11068-005-8353-1
- Hayar, A. (2004a). External Tufted Cells: A Major Excitatory Element That Coordinates Glomerular Activity. *Journal of Neuroscience*, *24*(30), 6676–6685. doi:10.1523/JNEUROSCI.1367-04.2004
- Hayar, A. (2004b). Olfactory Bulb Glomeruli: External Tufted Cells Intrinsically Burst at Theta Frequency and Are Entrained by Patterned Olfactory Input. *Journal of Neuroscience*, *24*(5), 1190–1199. doi:10.1523/JNEUROSCI.4714-03.2004
- Helmchen, F., & Denk, W. (2005). Deep tissue two-photon microscopy. *Nature Methods*, *2*(12), 932–940. doi:10.1038/nmeth818
- Helmstaedter, M. (2013). Cellular-resolution connectomics: challenges of dense neural circuit reconstruction. *Nature Methods*, *10*(6), 501–507. doi:10.1038/nmeth.2476

References

- Helmstaedter, M., Briggman, K. L., & Denk, W. (2011). High-accuracy neurite reconstruction for high-throughput neuroanatomy. *Nature Neuroscience*, *14*(8), 1081–1088. doi:10.1038/nn.2868
- Helmstaedter, M., Briggman, K. L., Turaga, S. C., Jain, V., Seung, H. S., & Denk, W. (2013). Connectomic reconstruction of the inner plexiform layer in the mouse retina. *Nature*, *500*(7461), 168–74. doi:10.1038/nature12346
- Higashijima, S., Masino, M. a, Mandel, G., & Fetcho, J. R. (2003). Imaging neuronal activity during zebrafish behavior with a genetically encoded calcium indicator. *Journal of Neurophysiology*, *90*(6), 3986–3997. doi:10.1152/jn.00576.2003
- Hildebrand, J. G., & Shepherd, G. M. (1997). MECHANISMS OF OLFACTORY DISCRIMINATION:Converging Evidence for Common Principles Across Phyla. *Annual Review of Neuroscience*, *20*(1), 595–631. doi:10.1146/annurev.neuro.20.1.595
- Hinds, J. W. (1968a). Autoradiographic study of histogenesis in the mouse olfactory bulb. I. Time of origin of neurons and neuroglia. *The Journal of Comparative Neurology*, *134*(3), 287–304. doi:10.1002/cne.901340304
- Hinds, J. W. (1968b). Autoradiographic study of histogenesis in the mouse olfactory bulb: Cell proliferation and migration. *The Journal of Comparative Neurology*, *134*(3), 305–322. doi:10.1002/cne.901340305
- Hirata, Y., 1964. Some observations on the fine structure of the synapses in the olfactory bulb of the mouse, with particular reference to the atypical synaptic configurations. *Archivum histologicum Japonicum= Nihon soshikigaku kiroku*, *24*, pp.293-302.
- Isaacson, J. S., & Strowbridge, B. W. (1998). Olfactory reciprocal synapses: Dendritic signaling in the CNS. *Neuron*, *20*, 749–761. doi:10.1016/S0896-6273(00)81013-2
- Jahr, C. E., & Nicoll, R. a. (1980). Dendrodendritic inhibition: demonstration with intracellular recording. *Science (New York, N.Y.)*, *207*(4438), 1473–1475. doi:10.1126/science.7361098
- Julliard, A. K., Saucier, D., & Astic, L. (1996). Time-course of apoptosis in the olfactory epithelium of rainbow trout exposed to a low copper level. *Tissue & Cell*, *28*(3), 367–377. doi:10.1016/S0040-8166(96)80023-1
- Kashiwadani, H., Sasaki, Y. F., Uchida, N., & Mori, K. (1999). Synchronized oscillatory discharges of mitral/tufted cells with different molecular receptive ranges in the rabbit olfactory bulb. *Journal of Neurophysiology*, *82*(4), 1786–1792. doi:10.1016/S0168-0102(98)82274-8

References

- Kim, J. S., Greene, M. J., Zlateski, A., Lee, K., Richardson, M., Turaga, S. C., ... Seung, H. S. (2014). Space-time wiring specificity supports direction selectivity in the retina. *Nature*, *509*(7500), 331–6. doi:10.1038/nature13240
- Kiyokage, E., Pan, Y.Z., Shao, Z., Kobayashi, K., Szabo, G., Yanagawa, Y., Obata, K., Okano, H., Toida, K., Puche, A.C., and Shipley, M.T. (2010). Molecular identity of periglomerular and short axon cells. *J. Neurosci.* *30*, 1185-1196.
- Kleinfeld, D., Bharioke, a., Blinder, P., Bock, D. D., Briggman, K. L., Chklovskii, D. B., ... Sakmann, B. (2011). Large-Scale Automated Histology in the Pursuit of Connectomes. *Journal of Neuroscience*, *31*(45), 16125–16138. doi:10.1523/JNEUROSCI.4077-11.2011
- Knott, G., Marchman, H., Wall, D., & Lich, B. (2008). Serial Section Scanning Electron Microscopy of Adult Brain Tissue Using Focused Ion Beam Milling. *Journal of Neuroscience*, *28*(12), 2959–2964. doi:10.1523/JNEUROSCI.3189-07.2008
- Kosaka, K., Toida, K., Aika, Y., & Kosaka, T. (1998). How simple is the organization of the olfactory glomerulus?: The heterogeneity of so-called periglomerular cells. *Neuroscience Research*, *30*(2), 101–110. doi:10.1016/S0168-0102(98)00002-9
- Kosaka, K., and Kosaka, T. (2005). Synaptic organization of the glomerulus in the main olfactory bulb: compartments of the glomerulus and heterogeneity of the periglomerular cells. *Anat. Sci. Int.* *80*, 80–90. doi:10.1111/j.1447- 073x.2005.00092.x
- Koulakov, A. A., & Rinberg, D. (2011). Sparse Incomplete Representations: A Potential Role of Olfactory Granule Cells. *Neuron*, *72*(1), 124–136. doi:10.1016/j.neuron.2011.07.031
- Kyle, J. H. & Ghani, N. Mercury concentrations in canned and fresh fish and its accumulation in a population of port moresby residents. *Sci. Total Environ.* *26*, 157–162 (1983).
- L.E. Iverson, M.A. Tanouye, H.A. Lester, N. Davidson, B. Rudy A-type potassium channels expressed from Shaker locus cDNA *Proc. Natl. Acad. Sci. USA*, *85* (1988), pp. 5723–5727
- Laframboise, A. J., Ren, X., Chang, S., Dubuc, R. & Zielinski, B. S. Olfactory sensory neurons in the sea lamprey display polymorphisms. *Neurosci. Lett.* *414*, 277–281 (2007).
- Laurent, G., Stopfer, M., Friedrich, R. W., Rabinovich, M. I., Volkovskii, A., & Abarbanel, H. D. I. (2001). ODOR ENCODING AS AN ACTIVE , DYNAMICAL PROCESS : Experiments , Computation ,
- Li, J., Mack, J.A., Souren, M., Yaksi, E., Higashijima, S.I., Mione, M., Fetcho, J.R. and Friedrich, R.W., 2005. Early development of functional spatial maps in the zebrafish olfactory bulb. *The Journal of neuroscience*, *25*(24), pp.5784-5795.

References

- Lindsay, S. M., & Vogt, R. G. (2004). Behavioral responses of newly hatched zebrafish (*Danio rerio*) to amino acid chemostimulants. *Chemical Senses*, *29*(2), 93–100. doi:10.1093/chemse/bjh009
- Liu, N., Xu, F., Marengo, L., Hyder, F., Miller, P., & Shepherd, G. (2004). Informatics approaches to functional MRI odor mapping of the rodent olfactory bulb. *Neuroinformatics*, *2*(1), 3–18. doi:10.1385/ni:2:1:003
- Lund, R. D. (1969). Synaptic patterns of the superficial layers of the superior colliculus of the rat. *The Journal of Comparative Neurology*, *135*(2), 179–207. doi:10.1002/cne.901350205
- Macrides, F., & Schneider, S. P. (1982). Laminar organization of mitral and tufted cells in the main olfactory bulb of the adult hamster. *The Journal of Comparative Neurology*, *208*(4), 419–30. doi:10.1002/cne.902080410
- Mathieson, W. B., & Maler, L. (1988). Morphological and electrophysiological properties of a novel in vitro preparation: the electrosensory lateral line lobe brain slice. *Journal of Comparative Physiology. A, Sensory, Neural, and Behavioral Physiology*, *163*(4), 489–506. doi:10.1007/BF00604903
- Mathieu, C. (1999). the Beam-Gas and Signal-Gas Interactions in the Variable Pressure Scanning Electron Microscope. *Scanning Microscopy*, *13*(1), 23–41.
- Matsunami, H., Montmayeur, J. P., & Buck, L. B. (2000). A family of candidate taste receptors in human and mouse. *Nature*, *404*(6778), 601–4. doi:10.1038/35007072
- Merkle, F.T., Fuentealba, L. C., Sanders, T. A., Magno, L., Kessar, N., and Alvarez Buyla, A. (2014). Adult neural stem cells in distinct microdomains generate previously unknown interneuron types. *Nat. Neurosci.* *17*, 207–214. doi: 10.1038/nn.3610
- Michel, W. C., & Lubomudrov, L. M. (1995). Specificity and sensitivity of the olfactory organ of the zebrafish, *Danio rerio*. *Journal of Comparative Physiology. A, Sensory, Neural, and Behavioral Physiology*, *177*(2), 191–199. doi:10.1007/BF00225098
- Mikula, S., Binding, J., & Denk, W. (2012). Staining and embedding the whole mouse brain for electron microscopy. *Nature Methods*, *9*(12), 1198–1201. doi:10.1038/nmeth.2213
- Miyawaki, a, Llopis, J., Heim, R., McCaffery, J. M., Adams, J. a, Ikura, M., & Tsien, R. Y. (1997). Fluorescent indicators for Ca²⁺ based on green fluorescent proteins and calmodulin. *Nature*, *388*(6645), 882–887. doi:10.1038/42264
- Mombaerts, P. (1999a). Molecular biology of odorant receptors in vertebrates. *Annual Review of Neuroscience*, *22*, 487–509. doi:10.1146/annurev.neuro.22.1.487

References

- Mombaerts, P. (1999b). Seven-transmembrane proteins as odorant and chemosensory receptors. *Science (New York, N.Y.)*, 286(5440), 707–711. doi:10.1126/science.286.5440.707
- Mori, K. (1987). Membrane and synaptic properties of identified neurons in the olfactory bulb. *Prog. Neurobiol.* 29, 275–320. doi:10.1016/0301-0082(87)90024-4
- Mori, K., Kishi, K., & Ojima, H. (1983). Distribution of dendrites of mitral, displaced mitral, tufted, and granule cells in the rabbit olfactory bulb. *The Journal of Comparative Neurology*, 219(3), 339–55. doi:10.1002/cne.902190308
- Mori, K., Kishi, K., and Ojima, H. (1983). Distribution of dendrites of mitral, displaced mitral, tufted and granule cells in the rabbit olfactory bulb. *J. Comp. Neurol.* 219, 339–355. doi:10.1002/cne.902190308
- Mori, K., Nagao, H., & Yoshihara, Y. (1999). The olfactory bulb: coding and processing of odor molecule information. *Science (New York, N.Y.)*, 286(5440), 711–5. doi:10.1126/science.286.5440.711
- Mueller, T., Vernier, P., & Wullimann, M. F. (2004). The adult central nervous cholinergic system of a neurogenetic model animal, the zebrafish *Danio rerio*. *Brain Research*, 1011(2), 156–169. doi:10.1016/j.brainres.2004.02.073
- Murphy, G. J., Darcy, D. P., & Isaacson, J. S. (2005). Intraglomerular inhibition: signaling mechanisms of an olfactory microcircuit. *Nature Neuroscience*, 8(3), 354–364. doi:10.1038/nn1403
- Nagayama, S., Homma, R., & Imamura, F. (2014). Neuronal organization of olfactory bulb circuits. *Frontiers in Neural Circuits*, 8(September), 1–19. doi:10.3389/fncir.2014.00098
- Najac, M., De Saint Jan, D., Reguero, L., Grandes, P., & Charpak, S. (2011). Monosynaptic and Polysynaptic Feed-Forward Inputs to Mitral Cells from Olfactory Sensory Neurons. *Journal of Neuroscience*, 31(24), 8722–8729. doi:10.1523/JNEUROSCI.0527-11.2011
- Naritsuka, H., Sakai, K., Hashikawa, T., Mori, K., and Yamaguchi, M. (2009). Perisomatic targeting granule cells in the mouse olfactory bulb. *J. Comp. Neurol.* 515, 409–426. doi:10.1002/cne.22063
- Nicoll, R.A., 1969. Inhibitory mechanisms in the rabbit olfactory bulb: dendrodendritic mechanisms. *Brain research*, 14(1), pp.157-172.
- Niessing, J., & Friedrich, R. W. (2010). Olfactory pattern classification by discrete neuronal network states. *Nature*, 465(7294), 47–52. doi:10.1038/nature08961

References

- Nowycky, M. C., Mori, K., & Shepherd, G. M. (1981). GABAergic mechanisms of dendrodendritic synapses in isolated turtle olfactory bulb. *Journal of Neurophysiology (Bethesda)*, 46(3), 639–648. Retrieved from <Go to ISI>://ZOOREC:ZOOR11800040365
- Orona, E., Scott, J.W., and Rainer, E. C. (1983). Different granule cell populations innervate superficial and deep regions of the external plexiform layer in rat olfactory bulb. *J. Comp. Neurol.* 217, 227–237. doi:10.1002/cne.902170209
- Pallotto, M., Watkins, P.V., Fubara, B., Singer, J.H., Briggman, K.L. Extracellular space preservation aids the connectomic analysis of neural circuits. *Elife*. 2015 Dec 9;4. pii: e08206. doi: 10.7554/eLife.08206
- Paré, D., Shink, E., Gaudreau, H., Destexhe, A. and Lang, E.J., 1998. Impact of spontaneous synaptic activity on the resting properties of cat neocortical pyramidal neurons in vivo. *Journal of neurophysiology*, 79(3), pp.1450-1460.
- Parrish-Aungst, S., Shipley, M.T., Erdelyi, F., Szabo, G. and Puche, A.C., 2007. Quantitative analysis of neuronal diversity in the mouse olfactory bulb. *Journal of Comparative Neurology*, 501(6), pp.825-836.
- Phillips, C.G., Powell, T.P.S. and Shepherd, G.M., 1963. Responses of mitral cells to stimulation of the lateral olfactory tract in the rabbit. *The Journal of physiology*, 168(1), p.65.
- Pinching, a J., & Powell, T. P. (1971a). The neuron types of the glomerular layer of the olfactory bulb. *Journal of Cell Science*, 9(2), 305–345. doi:10.3389/fncir.2014.00098
- Pinching, a J., & Powell, T. P. (1971b). The neuropil of the periglomerular region of the olfactory bulb. *Journal of Cell Science*, 9, 379–409.
- Pinching, a J., & Powell, T. P. (1971c). Ultrastructural features of transneuronal cell degeneration in the olfactory system. *Journal of Cell Science*, 8(1), 253–87. Retrieved from <http://www.ncbi.nlm.nih.gov/pubmed/4101588>
- Pologruto, T. a, Sabatini, B. L., & Svoboda, K. (2003). ScanImage: flexible software for operating laser scanning microscopes. *Biomedical Engineering Online*, 2, 13. doi:10.1186/1475-925X-2-13
- Price, J. L., & Powell, T. P. (1970). The synaptology of the granule cells of the olfactory bulb. *Journal of Cell Science*, 7, 125–155.
- Price, J. L., & Powell, T. P. S. (1970). The Mitral and Short Axon Cells of the Olfactory Bulb. *Journal of Cell Science*, 7(3), 631–651. Retrieved from <http://jcs.biologists.org/content/7/3/631> \n<http://jcs.biologists.org/content/7/3/631.full.p>

References

- df\nhttp://jcs.biologists.org/content/7/3/631.short\nhttp://www.ncbi.nlm.nih.gov/pubmed/5492279
- Price, J. L., & Sprich, W. W. (1975). Observations on the lateral olfactory tract of the rat. *J Comp Neurol*, 162(3), 321–336. doi:10.1002/cne.901620304
- Rall, W., & Shepherd, G. M. (1968). Theoretical reconstruction of field potentials and dendrodendritic synaptic interactions in olfactory bulb. *Journal of Neurophysiology*, 31, 884–915.
- Rall, W., Shepherd, G. M., Reese, T. S., & Brightman, M. W. (1966). Dendrodendritic synaptic pathway for inhibition in the olfactory bulb. *Experimental Neurology*, 14(1), 44–56. doi:10.1016/0014-4886(66)90023-9
- Ramón y Cajal S (1880) El protoplasma. La Clínica. Semanario de Medicina, Cirujía y Farmacia 153: 299, 154:306-308, 155:313-314. Reprinted in: Discurso de doctorado y trabajos de juventud. MerchánPérez A (ed). Universidad Europea-CEES Ediciones, Madrid, 2001
- Ramón y Cajal, S. (1911). Histologie du systeme nerveux de l'homme et des vertebres. 11. Trans. By L. Azoulay. Paris: Maloine
- Rodriguez, I., Feinstein, P., & Mombaerts, P. (1999). Variable patterns of axonal projections of sensory neurons in the mouse vomeronasal system. *Cell*, 97(2), 199–208. doi:10.1016/S0092-8674(00)80730-8
- Rossum, M. Van. (2004). Neural Computation, (February). doi:10.1201/9781420050646.pta
- Rubin, B. D., & Katz, L. C. (1999). Optical Imaging of Odorant Representations in the Mammalian Olfactory Bulb. *Neuron*, 23(3), 499–511. doi:10.1016/S0896-6273(00)80803-X
- Schneider SP, Macrides F (1978) Laminar distributions of interneurons in the main olfactory bulb of the adult hamster. *Brain Res Bull* 3:73– 82
- Schoppa, N. E. (2006). Synchronization of Olfactory Bulb Mitral Cells by Precisely Timed Inhibitory Inputs. *Neuron*, 49(2), 271–283. doi:10.1016/j.neuron.2005.11.038
- Schoppa, N. E., & Urban, N. N. (2003). Dendritic processing within olfactory bulb circuits. *Trends in Neurosciences*, 26(9), 501–506. doi:10.1016/S0166-2236(03)00228-5
- Schoppa, N. E., Kinzie, J. M., Sahara, Y., Segerson, T. P., & Westbrook, G. L. (1998). Dendrodendritic inhibition in the olfactory bulb is driven by NMDA receptors. *The Journal of Neuroscience : The Official Journal of the Society for Neuroscience*, 18(17), 6790–802. Retrieved from <http://www.ncbi.nlm.nih.gov/pubmed/9712650>

References

- Shepherd, G. M. (1963). August 1962), 65–88. Society, T. R., Society, R., & Sciences, B. (n.d.). Downloaded from <http://rspb.royalsocietypublishing.org/>
- Spence, R., Gerlach, G., Lawrence, C., & Smith, C. (2008). The behaviour and ecology of the zebrafish, *Danio rerio*. *Biol Rev Camb Philos Soc*, 83(1), 13–34. doi:10.1111/j.1469-185X.2007.00030.x
- Srubek, G. (2014). Distinct Profiles of Myelin Distribution, 319(APRIL), 319–324. doi:10.1126/science.1249766
- Stosiek, C., Garaschuk, O., Holthoff, K., & Konnerth, A. (2003). In vivo two-photon calcium imaging of neuronal networks. *Proceedings of the National Academy of Sciences of the United States of America*, 100(12), 7319–7324. doi:10.1073/pnas.1232232100
- Suter, B. (2010). Ephus: multipurpose data acquisition software for neuroscience experiments. *Frontiers in Neural Circuits*, 4(August), 1–12. doi:10.3389/fncir.2010.00100
- Tabor, R. (2004). Processing of Odor Mixtures in the Zebrafish Olfactory Bulb. *Journal of Neuroscience*, 24(29), 6611–6620. doi:10.1523/JNEUROSCI.1834-04.2004
- Taigman, Y., Yang, M., Ranzato, M.A. and Wolf, L., 2014. Deepface: Closing the gap to human-level performance in face verification. In Proceedings of the IEEE Conference on Computer Vision and Pattern Recognition (pp. 1701-1708).
- Tapia, J.C., Kasthuri, N., Hayworth, K.J., Schalek, R., Lichtman, J.W., Smith, S.J. and Buchanan, J., 2012. High-contrast en bloc staining of neuronal tissue for field emission scanning electron microscopy. *Nature protocols*, 7(2), pp.193-206
- Titze, B., & Denk, W. (2013). Automated in-chamber specimen coating for serial block-face electron microscopy. *Journal of Microscopy*, 250(2), 101–110. doi:10.1111/jmi.12023
- Toida, K., Kosaka, K., Heizmann, C. W., & Kosaka, T. (1998). Chemically defined neuron groups and their subpopulations in the glomerular layer of the rat main olfactory bulb: III. Structural features of calbindin D28K-immunoreactive neurons. *Journal of Comparative Neurology*, 392(October 1997), 179–198. doi:10.1002/(SICI)1096-9861(19980309)392:2<179::AID-CNE3>3.0.CO;2-#
- Urban, N. N., & Sakmann, B. (2002). Reciprocal intraglomerular excitation and intra- and interglomerular lateral inhibition between mouse olfactory bulb mitral cells. *The Journal of Physiology*, 542(Pt 2), 355–367. doi:10.1113/jphysiol.2001.013491
- Vinje, W. E., Gallant, J. L. (2000). Sparse coding and decorrelation in primary visual cortex during natural vision. *Science*, 2000 Feb 18; 287(5456):1273-6.

References

- Wachowiak, M., & Cohen, L. B. (2001). Representation of Odorants by Receptor Neuron Input to the Mouse Olfactory Bulb. *Neuron*, 32(4), 723–735. doi:10.1016/S0896-6273(01)00506-2
- Wanner, A. A., Genoud, C., Masudi, T., Siksou, L., Friedrich W. R., (2016) Inter-glomerular network organization of the zebrafish olfactory bulb revealed by dense EM-based reconstruction (SUBMITTED)
- Wellis, B. Y. D. P., & Kauer, J. S. (1993). Salamander Olfactory Bulb. *Physiology*, 315–339.
- White, J. G., Southgate, E., Thomson, J. N., & Brenner, S. (1986). The Mind of a Worm. *Philosophical Transactions of the Royal Society B: Biological Sciences*, 314(1165), 1–340. Retrieved from http://www.wormatlas.org/MoW_built0.92/MoW.html
- Wiechert, M. T., Judkewitz, B., Riecke, H., & Friedrich, R. W. (2010). Mechanisms of pattern decorrelation by recurrent neuronal circuits. *Nature Neuroscience*, 13(8), 1003–1010. doi:10.1038/nn.2591
- Wiechert, M.T. (2015). Reciprocal synapses: How network structure determines computation. Presented at the KITP Meeting: Deconstruction the Sense of Smell. <http://online.kitp.ucsb.edu/online/smell15/wiechert/>
- Wullimann, M.F., Rupp, B. & Reichert, H. 1996. Neuroanatomy of the Zebrafish Brain: a Topological Atlas.
- Yaksi, E., & Friedrich, R. W. (2006). Reconstruction of firing rate changes across neuronal populations by temporally deconvolved Ca²⁺ imaging. *Nature Methods*, 3(5), 377–383. doi:10.1038/nmeth874
- Yaksi, E., Judkewitz, B., & Friedrich, R. W. (2007). Topological reorganization of odor representations in the olfactory bulb. *PLoS Biology*, 5(7), e178. doi:10.1371/journal.pbio.0050178
- Yaksi, E., von Saint Paul, F., Niessing, J., Bundschuh, S. T., & Friedrich, R. W. (2009). Transformation of odor representations in target areas of the olfactory bulb. *Nature Neuroscience*, 12(4), 474–482. doi:10.1038/nn.2288
- Yokoi, M., Mori, K., & Nakanishi, S. (1995). Refinement of odor molecule tuning by dendrodendritic synaptic inhibition in the olfactory bulb. *Proceedings of the National Academy of Sciences of the United States of America*, 92(8), 3371–3375. doi:10.1073/pnas.92.8.3371

References

- Zhu, P. X., Frank, T., & Friedrich, R. W. (2013). Equalization of odor representations by a network of electrically coupled inhibitory interneurons. *Nature Neuroscience*, *16*(11), 1678–1686. doi:10.1038/nn.3528
- Zhu, P., Fajardo, O., Shum, J., Zhang Schärer, Y.-P., & Friedrich, R. W. (2012). High-resolution optical control of spatiotemporal neuronal activity patterns in zebrafish using a digital micromirror device. *Nature Protocols*, *7*(7), 1410–1425. doi:10.1038/nprot.2012.072

TAFHEEM MASUDI, PhD.

Email: tafheem.masudi@outlook.com

Phone: +41-786832722

Address: Basel, Switzerland

Nationality: Indian

Birth date: 8th Jan 1985

Marital status: Married



Education

- June 2011 – Mar 2016: Doctor of Philosophy (Ph.D.) in Neurobiology and Neurosciences. Friedrich Miescher Institute for Biomedical Research, University of Basel.
Research supervisor: Prof. Rainer Friedrich.
Thesis title: “Connectivity motifs underlying neuronal computations in the adult olfactory bulb”.
- Jan 2009 – Dec 2010: Research Assistant, Developmental Neurobiology. National Centre for Biological Sciences, TIFR, Bangalore, India.
Research supervisor: Prof. K VijayRagavan, Late Prof. Veronica Rodrigues.
- May 2006 – Aug 2008: Master’s in Biotechnology, Bangalore University, India. First rank.
- Mar 2003 – Mar 2006: Bachelor’s in Biology, Chemistry. Kashmir University, India. First class.

Publications

- Reciprocal synapses: How network structure determines computation. (Manuscript in preparation).
- Dense EM-based reconstruction of the interglomerular projectome in the zebrafish olfactory bulb. Adrian Wanner, Christel Genoud, **Tafheem Masudi**, Léa Siksou & Rainer W Friedrich. *Nat. Neurosci*, June 2016.
- Different DVGlut enhancer elements label distinct subpopulations of motor neurons, mediating specific aspects of locomotor behavior in Drosophila melanogaster. Venkatesh Onteddu, **Tafheem Masudi**, Syed Sakeena, Darren Williams, K VijayRaghavan. (Manuscript in revision).

Posters

- ‘Imaging, structure & function in zebrafish’, Brain Conference, Paris, 4-7 Dec 2014.
- 8th FENS Forum of Neuroscience, Barcelona, 14-18 July 2012.
- International EMBO Global Exchange Lecture Course July 2010, NCBS.
- Harvard-NCBS Optogenetics conference, July 6-20, 2009.

Research Experience

PhD Researcher, FMI Basel (June 2011 – Mar 2016). Prof. Rainer Friedrich group.

Aim of the project: To study the function of reciprocal synapse connectivity in zebrafish olfactory bulb.

Teaching assistant, University of Basel (July. 2013 – Dec. 2013)

Teaching biology to Bachelor students.

Research Assistant, NCBS Bangalore (Jan 2009 – Dec 2010). Prof. K VijayRaghavan group.

Aim of the project 1: Study the regulation of vesicular glutamate transporter and motor neuron organization and development in *Drosophila* larvae.

Aim of the project 2: Study the role of glia at the neuromuscular junction in *Drosophila* larvae.

Teaching assistant, National Centre for Biological Sciences, (2010).

Teaching assistant in the International EMBO Global Exchange Lecture Course 2010, NCBS.

Teaching assistant at WHO-TDR GLP Training Workshop for Academia, 2010, NCBS Bangalore.

Trained and mentored associates for master's student projects, microsurgical and behavior protocols.

Master's in Biotechnology, Bangalore University, Thesis project.

Aim of the project: Studying the role of bursicon during *Drosophila* development.

Research expertise

- **Microscopy:** Apotome microscopy, confocal microscopy, two photon microscopy, serial block face electron microscopy.
- **Image processing, Image analysis:** Matlab, Image J, Fiji, Scanimage, Pymagor, Amira, Ilastik.
- **Animal model system:** *Drosophila*, Zebrafish.
- **Microsurgeries:** *Drosophila* NMJ surgery, *Drosophila* brain surgery. *Drosophila* time-dependent experiments, tissue collection, genetics and handling. *Zebrafish* brain surgery, *Zebrafish* time-dependent experiments, tissue collection, genetics and handling.
- **Behavioral assays:** Developed *Drosophila* larval locomotory behaviour assay. Learnt *Drosophila* adult locomotory behavior. *Zebrafish* adult aggression, locomotion, anxiety, courtship behaviors.
- **Molecular Biology:** Electrophoresis-Agarose, native PAGE, SDS-PAGE, PCR, Immunohistochemistry.

Achievements and Memberships

- Awarded PhD Fellowship, Friedrich Miescher Institute for Biomedical Research, 2011.
- Awarded PhD Fellowship, École polytechnique fédérale de Lausanne EPFL, 2011.
- Awarded PhD Fellowship, The Research Institute of Molecular Pathology (IMP) Vienna, 2011.
- Awarded PhD Fellowship, Linköping University. Department of Clinical Medicine, 2011.
- Indian Institute of Science, Bangalore, Visiting Junior Research Fellow, 2010.
- Masters in Biotechnology, University topper, 1st among 90 other students.
- Best Outgoing Student of the Year, Bangalore University, 2008.
- 1st place for Scientific Model and Poster Presentation, Bangalore University, 2007.
- Swiss Society of Neuroscience, student member.
- Federation of European Neuroscience Societies (FENS), student member.
- Certification in Introductory Course in Laboratory Animal Science, (category B FELASA accredited).